INVESTIGATION ON THE SWELLING MECHANICS OF HYDROGEL TISSUE EXPANDERS USING A SKIN-MIMICKING APPARATUS

Park Maneepairoj

St Edmund Hall

Submitted for the degree of Masters in Science by Research in the Department of Materials, University of Oxford

Michaelmas Term, 2013

สำหรับคุณพ่อและคุณแม่ที่รัก

dedicated to

my father
PAITOON MANEEPAIROJ

and

my mother
VIPA MANEEPAIROJ

Table of Contents

Acknowledgements

I would like to take this opportunity to thank those people who greatly helped me during the course of my research.

Firstly, I would like to thank my supervisor, Dr. Jan T. Czernuszka for his support, ideas, encouragement, and most of all his guidance. I am extremely grateful for allowing me to think independently and giving me the creative freedom to direct my own research. It was a privilege to be part of his team and to be his student. Thank you for the motivation which was necessary for me to push forward.

Secondly I would like to thank the Biomaterials group members. It is an honour to be part of an amazing team. Special thanks to Zamri Radzi, Hannah Lee, Quan Du, Qi Chen, Maryam Tamaddon, and Kerem Bayakceken for being part of my wonderful experience. I would like to also thank Laurie Walton at the mechanical workshop for his contributions in making my rig design possible.

I would like to thank my family for all the support and prayers. Thank you so much for your love and for the meaningful conversations over the telephone. To my mom and dad, thank you for being my teachers in life and the best role models. I am grateful without words for the support that has leaded me to what has been a fantastic chapter of my life.

Last but not least, I would like to thank the almighty God for his presence gave me wisdom and strength. Thank you for leading me in my everyday life and please continue to show me the way[†].

List of Figures and Tables

List of Symbols and Abbreviations

A	Surface Area
a_n	Positive root of Bessel function
C_{VP}	Concentration of vinyl pyrrolidone
C_w	Solvent concentration
D	Diffusion coefficient
DSC	Differential scanning calorimetry
DTA	Differential thermal analyser
E	Elastic Modulus
ε	Elastic Strain
F	Swelling Force
FDA	U.S. Food and Drug Administration
M_c	Molecular weight between cross-links
M_t	Mass of solvent uptake at time t
M_∞	Mass of the solvent uptake at equilibrium
m_s	Swollen mass
m_0	Dry mass
n	Diffusion exponent
P	Swelling pressure
PMMA	poly(methylmethacrylate)
PVP	poly(N-vinylpyrrolidone)
p	Elastic contractility
π	Osmotic pressure

Q_m	Mass swelling ratio
Q_V	Volume swelling ratio
R or *r*	Radius
RT	Room temperature
ρ	Density
S	Slant height
σ	Stress
σ_{crit}	Critical Stress
σ_E	Stress due to elastic modulus
σ_τ	Stress in relationship with solute diffusion
TGA	Thermogravimetric analyser
T_g	Glass transitional temperature
UV	Ultraviolet Radiation
U_e	Immediate distension
U_v	Delayed distension
U_r	Immediate retraction
U_f	Final deformation
U_e	Immediate distension
V_s	Swollen volume
V_0	Dry volume
VP/MMA	poly(vinyl-pyrrolidone) poly(methyl-methacrylate)
v_e	Effective cross-linking density

Abstract

The concept of self-expanding hydrogel tissue expanders has opened a new pathway to the treatment of soft tissue defects. Traditionally designed to expand the skin, modifications to the swelling behaviour of these devices may lead to various new-found applications. Properties of poly(vinylpyrrolidone) /poly(methyl-methacrylate) (VP/MMA) hydrogel system such as the degree, rate, force generation, and anisotropic behaviour of swelling were investigated in this study as part of a preliminary understanding of the hydrogel material.

The swelling of hydrogel network is the balance between two main driving forces: 1) the relaxation of the gel network and 2) the osmotic diffusion of solvent via gel hydrophilicity. A direct relationship between the elastic modulus and the swelling pressure was found by measuring the swelling force over the hydration period. Despite reduction in the overall swelling ratio, gels with a larger modulus were observed to have a larger corresponding force generation. This is due to the straining of gels with higher cross-linking density. The results showed a maximum stress of 64.0 ± 3.2 kPa and 30.8 ± 1.5 kPa for 90:10 wt% and 99:1 wt% VP/MMA, respectively.

Specially modified anisotropic swelling gels were shown to have larger stress generation along the axis of directional swelling (~70-80 kPa). Limitation factors to the anisotropic modification are materialistic and geometrical. Shape-memory characteristics were found to be reduced at high compression ratio as a result of plastic deformation. Gels with slenderness ratio above 2.5

were evaluated to be susceptible to device slippage/buckling. These results provide useful design limitations for self-expanding tissue expanders.

The overall goal in creating a new testing system for self-swelling tissue expanders was achieved.A skin-mimicking apparatus was specially built to highlight the amount of skin expansion and simulate surface topography. Strain contours along the expanded skin were also plotted to represent skin tension. Prior to this study,these measurements were only possible under *in vivo* animal testing. The advantage in having this device is to support the prevention of related animal testing.

Chapter 1: Introduction

1.1 Introduction

Tissue expansion has become a significant technique in surgical treatment of soft tissue defects for both children and adults. For years, tissue expanders have provided us a solution for the socially damaging effects of skin defects, severe scarring and deformed skin [1]. The use of the traditional silicone balloon expander is however accompanied by the inconvenience of having to be manually expanded over numerous visits to the hospital. In addition, the bulkiness of the device and the discontinuous expansion nature of the treatment have caused high risk of medical complications [2]. For this reason, the use of osmotically swelling hydrogels was introduced as an alternative device where expansion is induced via absorption of body fluids [1, 3].

Recently, surgeons have a choice between the use of a manually inflated silicone balloon expander and a self-inflating osmotic tissue expander. There is an inclination towards the use of self-inflating tissue expander as their use seems to be more economical for healthcare providers [3]. The increased popularity of the device and the potential of the self-swelling system have propelled developments of the tissue expander into wider range of applications. This includes the expansion of other soft tissues not just the dermis but also palate and mucosa [5].

To obtain regulatory approval, a new medical device has to obtain a CE mark (in the Europe).One of the steps in the process is the use of an animal model. The use of animals as a comparative model to the human body has been successful but yet it is often considered as cruel or unacceptable [4]. In addition, the level of control needed in order to use laboratory

animals has made these tests expensive and the procedures troublesome. This brings us to the development of a standard apparatus for testing hydrogel tissue expanders.

The aim of this study is to design a testing apparatus which can reduce the use of animals by mimicking the biomechanics of the human skin. In order to achieve this goal, the mechanical behaviour of skin and the swelling mechanics of the poly(vinylpyrrolidone)/poly(methyl-methacrylate) (VP/MMA) hydrogel expanders were investigated to complete the understanding of tissue expansion. With considerations of this information, the apparatus was designed to simulate *in vivo* conditions and for observation of the expanding skin area through the use of a synthetic material.

This thesis is separated into 3 main sections. The next chapter is a literature review on the history of tissue expansion and the mechanical characterization of the human skin tissue. The swelling behaviour of hydrogels with specific interest in the swelling force will be investigated in Chapter 3 and the design of the skin mimicking apparatus together with the results taken from the skin-mimicking setup will be analysed in Chapter 4.

1.2 Chapter References

1) Marcus J, Horan DB, Robinson JK. Tissue expansion: Past, Present, and future. Journal of the American Academy of Dermatology. 23:5, 1990

2) Manders EK, Schenden MJ, Furrey JA, Hetzler PT, Davis TS, and Graham WP. Soft-tissue Expansion: Concepts and Complications. The Milton S. Hershey Medical Center of the Penn. State, 1984

3) Austad ED and Rose GL. A self-inflating tissue expander. Plast. Reconstr Surg. 70:588-93, 1982

4) Radzi Z. Development of Self-Inflating Anisotropic Tissue Expanders for Clinical Applications. PhD Thesis, University of Oxford, Oxfordshire, United Kingdom, 2012

Chapter 2: Literature Review

2.1 Overview

The mechanical behaviour of soft tissues - or more specifically discussed in this literature review as the mechanical behaviour of dermal skin, is a field yet to be fully understood given that the skin is a highly complex material. To date, the development of synthetic materials for prostheses has advanced successfully into orthopaedic surgery and dentistry with the help of understanding between mechanical compatibility of the implant and the location of its application[41]. Investigating the mechanical behaviour of human skin must then be seen as a crucial step towards the integration of soft tissue replacements for reconstructive surgery.

The tissue expander is an example of a biomedical device that will benefit from the understanding of the human skin. During tissue expansion, skin growth is induced through the stress generation from the expander which correspondently stretches the skin and subsequently promotenew tissue formation. As the functioning mechanism of the expander is wholly related to the ability to deform skin, it is important in the design criteria that the amount of generated stress is compatible with the tissue it is to expand. To date, the release of new expander technology has been rapid as the demand of cosmetic and reconstructive surgery surges. Understanding the mechanical behaviour of skin tissue will support the improvement and development of these novel devices.

The aim of this literature review is to compile and analyse the tests that were done in the past to investigate the mechanical properties of skin. The first part of this chapter gives an overview on the past, present, and future of tissue expansion. The second part focuses on the general structure of skin and a compilation of methods in characterising its mechanical behaviour. In

the final section, an overall summary to the investigation will be made and possible improvements to this field of research will be introduced.

2.2 Tissue Expansion

In cutaneous wound closure, the surgeon's goal is to return the skin to its preoperative function and appearance; maintaining the skin's contour, texture, and colour. This is a relatively straightforward process when the wound is small. However, in larger wounds or wounds near the margins of the lip, nose, or eyelid, there is difficulty in wound closure as it may result in permanent deformity from creating an unnatural skin tension [1]. The use of local skin grafts is usually used in these situations but often results in incoherency of skin type. For this reason, the method of tissue expansion was introduced.

Tissue expansion is a natural process. A simple example of tissue expansion is the abdominal wall enlargement of a pregnant woman in response to a growing uterus. The response from the body is expansion of surrounding skin while the skin maintains normal quality and thickness [1]. This adaptivity of human skin tissue to loading occurs naturally during pregnancy and has also been exploited by several cultures for aesthetic and religious purposes [8]. This includes enlarging the lower lip with large plates or by using rings to enhance linear growth of one's neck.

The idea of tissue expansion as a medical process works by stimulating the growth of new skin adjacent to the area of the defect. Rather than to remove skin graft from another area of the body, which means having two different surgical procedures, the use of tissue expander will

only require surgery at one area. In addition, the contour, colour and texture of the replaced skin is usually well matched with the surrounding skin under the tissue expansion process as natural skin graft is grown next to the skin defect [2-4]. Overall, this makes tissue expansion a superior clinical procedure.

2.2.1 Silicone Balloon Tissue Expander

The first tissue expander designed for medical use was an inflatable balloon introduced by Neumann (1957) [5]. The expander consists of a deflated medical grade silicone balloon and an injection port that can be implanted and then inflated under the skin through multiple injections of saline solution. As the balloon expands, the overlying skin will be simultaneously stretched to reach up to 2 to 3 times its initial dimensions [6]. The expander is then removed so that the extra skin can then be pulled over to replace the skin defect – a clinical 'flap'[9].

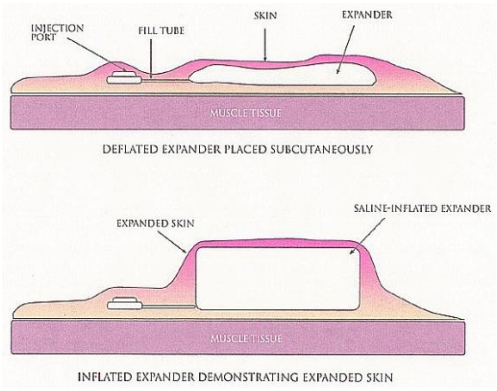

Figure 2.01: Schematic diagram of traditional balloon expander placed under the skin. Adopted from ref. [6]

The operative process involves selecting the right size of expander. The base diameter is chosen to be approximately the same size as the skin defect while the incision should be as small as practically possible and perpendicularly aligned to the direction of expansion in order

to minimise tension on the incision [7].The skin expansion process is performed by injecting normal saline (sterile solution of NaCl) into the tissue expander until the skin becomes visibly taut.

The patient will need regular visits for injection of additional fluid into the expander. Typical addition of fluid for each visit is about 10-12% of the existing volume. From 130 patients treated with tissue expansion, the average time of flap development was 3 to 6 weeks [6]. According to Radovan, this expander can be applied for the development of flaps in almost any area of the body [6]. This includes the scalp, face, neck, trunk, and both upper and lower extremities. Tissue expanders are also widely used in breast reconstruction after mastectomy [8].

Figure 2.02: Balloon Tissue Expanders in various shapes. [12]

2.2.2 Medical Complications with the balloon expander

A paper by Manders et al. documented complications encountered in a series of 35 patients aged between 3 and 82 years undergoing a total of 41 expansions [10]. Minor complications include pain during injection, seroma formation, persistence of dog-ears, and widening of scars [10]. Major complications, on the other hand, will interrupt the reconstructive program to the

extent that they can prevent the desired result. According to Manders et al., there are four major complications; infection, expander exposure, implants failure, and induced ischemia [56]. These complications are summarised in Table 2.03.

Table 2.03: Complications with using balloon expanders from ref.[10]

Complications	Symptom/Description
Pain	Pain is usually the result of tenseness which lasts between 8-12 hours after expansion. To deal with this complication, few millimetres of saline can be withdrawn to reduce pain while schedule injection is most appropriate in morning hours so that the discomfort will reduce within the day. Patterns showed that pain experienced from expansion is greatest on the forehead while it is less painful on scalp or for breast reconstruction.
Seroma	As the body automatically forms encapsulating tissue over foreign objects, the gap between the capsule and the expander membrane can store small amount of fluid. A problem may arise during saline injection as the fluid inside the cavity will be under pressure. The needle hole provides the outlet of this fluid but also creating accessible route for contaminating organism from the needle.
Dog-ears/ widening of scars	The development of a flap in the form of 'dog-ears' can occur when expanded skin is gathered at its leading edge. This flap formation is normal after tissue expansion and usually accepted as many will disappear or become smaller. Another common complication is the widening of scars after surgery.
Infection	There were case studies of patients that developed bacterial or other types of infection. This can lead to the need of expander removal.
Implant Exposure	Dehiscence of the incision, erosion of an envelope fold, or manipulation by psychotic patient can lead to expander exposure. With envelope folds wearing through the overlying soft tissue, the expansion must be terminated.
Implant Failure	Fault at the remote port connector or fault during assembly. Failure can also occur when envelope is perforated by needle. Case study shows that implant failure is mostly due to physician error [10].
Ischemia	Induced ischemia results from vigorous inflation of the expander. Such expansion can compress overlying tissue to the point that the supply of blood is stopped.

Complications can sometimes appear subjective and are not always due to any fault in device design. However, the silicone balloon expander itself is not practical or economical due to the requirement of many visits to the hospital. As highlighted in table 2.03 expansion in large steps can lead to severe pain while the use of needle injection can lead to infections or implant failure. A solution to these many problems was the development of self-inflating tissue expander.

2.2.3 Self-inflating Tissue Expanders

Self-inflating tissue expanders were first introduced by Austad and Rose (1982) as a semi-permeable membrane shell containing hypertonic sodium chloride [1]. Once implanted, these devices would swell osmotically and concomitantly expand the skin without the need of an injection port or manual inflation. This is advantageous particularly for young children, while the risk of infection is greatly reduced as there is not a need for regular punctures [11]. However in practice, the expander was flawed because of slow expansion times (8-14 weeks) and the high risk in exposing hypertonic saline inside the body during leakage or membrane rupture [8]. These were the reasons why the use of self-inflating expanders was abandoned.

The idea of osmotically driven expanders was however revived by Wiese et al. in 1993 by using hydrogels [12]. Hydrogels are generally rubber-like materials consisting of a cross-linked polymer network and an aqueous matrix. Compared to all the previous designs, the tissue expander introduced by Wiese et al. is a solid body with an initially rigid structure. The ability to swell without dissolving and to retain its large volume increase makes hydrogels suitable candidate materials for tissue expansion.

The swelling property or hydrophilicity of a hydrogel is due to the presence of ionic residues such as hydroxylic (-OH), carboxylic (-COOH), amidic (-CONH), and sulphuric ($-SO_3H$) end groups [13]. The maximum volume expansion will depends on concentration, degree of ionization, and ionization equilibrium.

Figure 2.04: Schematic of hydrogel chains showing relaxation of hydrophilic regions when in contact with water.Ref. [13]

During expansion, the hydrogel will maintain its overall geometry by swelling equally in all directions. This is due to the insoluble network which is partially hydrophobic. Once in contact with water, the two types of polymers which are initially in random mixture would rearrange to support a more thermodynamically favourable structure (figure 2.04). Hydrogel materials can be classified on the basis of different polymer properties; their preparation method, types of cross-linking between chains, composition and crystallinity [13]. With so many ways and compositions to synthesize these hydrogels, there is the potential in creating tissue expanders with various functions. Important features of the hydrogel will be discussed in the next chapter.

A paper by Obdeijn et al. reported a three-year clinical experience with a commercial hydrogel tissue expander (OSMED gmbh, Hartheim, Germany) [11]. The implant consists of a dehydrated hydrogel in a silicone envelope where the function of the silicone membrane is to regulate final swelling volume and to reduce device fracture. The surgical technique is to create a subcutaneous pocket next to the skin defect, under local anaesthesia [11]. The expander is then left to self-expand for 6-8 weeks. The OSMED gel is left *in situ* for another 4-12 weeks before removal and final soft tissue reconstruction [11].

Figure 2.05: Anhydrous (left) and expanded (right) OSMED self-inflating expander. From Ref. [14]

2.2.4 Medical complications with the hydrogel expander

A study of 9 patients with 20 hydrogel implants revealed 6 complications [11]. One of the expanders failed to inflate because of filling with blood. [11]. Infection and ischemia were also observed in some cases and there was a problem with expander migration. [11]. Ronert et al. published a more positive experience with OSMED showing 88.8% success with only 3 failures in 26 implants [19]. The paper concluded that the implant is fast, safe and reliable. But, Cunha et al. revealed a significant increase in major complications when the implant is used around the head and neck areas [17].

Although these expanders have significant advantages, there are still limitations to their applications especially in sensitive skin areas. The main disadvantage agreed by most papers is its uncontrollable swelling behaviour and that the device immediately starts to swell once implanted [11, 16, 17]. In the case of pain or ischemia, the device cannot be stopped or slowed down due to constant water uptake. This is different from the traditional balloon expander where expansion is manually controlled [18, 19]. From the complications experienced, it is clear that a typical hydrogel expander lacks the controlling mechanism to achieve the wanted function.

Swan [9] and Radzi [10] have designed a way to control the expansion of poly(vinyl-pyrrolidone)/poly(methyl-methacrylate) (VP/MMA) The Ideal behaviour would incorporate a time delay before swelling can occur to give a time gap for healing of surgical wounds. The delay can then be followed by a constant swell rate that is suitable for skin growth while not causing ischemia, irritation or pain. To date we were able to obtain this delay by two

techniques; 1) by coating the hydrogel with a semi-permeable silicone membrane [20] and 2) by addition of a biodegradable interpenetrating network within the hydrogel [21]. Both methods proved to be effective ways in delaying the swelling of VP/MMA hydrogels.

2.2.5 Anisotropically swelling gels

The development of self-expanding tissue expanders has made it possible to expand soft tissues at more specific locations due to the absence of a bulky, often large, filling port. Ideally, the anhydrous gels can be cut into any particular shape and used to expand skin around smaller defects or more delicate areas.Swan et al. explainedhowever that some applications will be limited due to the gel's isotropic swelling behaviour [9]. Due to this limitation, anisotropic swelling gels were introduced with particular interest on repairing the mucosal tissue for cleft palate [85]. This anisotropy of VP/MMA gels can be achieved through careful heat treatment and compression of the dry gel [9]. This creates an anisotropic swelling behaviour where the swelling direction can be controlled.

With the anisotropic swelling, the use of tissue expanders for reconstructive surgery has reached a new milestone, and developed into a much more versatile surgical tool. From such manipulation of the hydrogel, it is important to investigate how this compression affects the device's swelling rate as well as the possibility of increased swelling force. And to explain this behaviour, swelling force measurements and water transport analysis will be covered in Chapter 3.

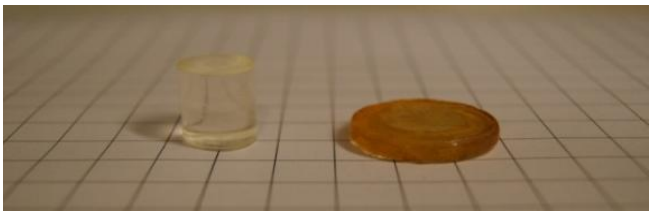

Figure 2.06: Uncompressed and compressed VP/MMA hydrogels of the same volume. The discolouring of the compressed gel is due to heat treatment.

Wiese et al. showed that the hydrogels exhibited viscoelastic behaviour that was composition and water content dependent [13]. In the same study, the swelling pressure was measured using a special chamber shown in figure 2.07. The hydrogel cylinders were sealed within the expansion chamber and the pressure was taken from the hydrostatic pressure as the hydrogel expands through a latex diaphragm.

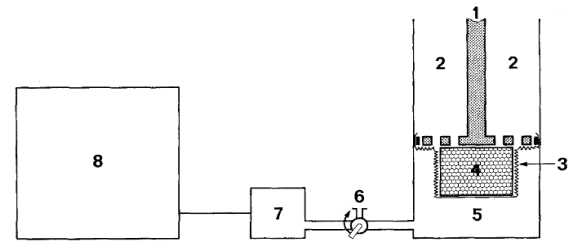

Figure 2.07: Schematic drawing of the pressure registration chamber developed by KG Wiese. (1) perforated piston with peripheral rubber sealing and lockable piston rod, 2) chamber with Na-Cl solution, 3) water-proof membrane, 4) gel cylinder sample, 5) measuring chamber, 6) triple way stopcock, 7) pressure transducer, and 8) a recording system. Adopted from ref. [27]

The pressure was measured over 72 hours with a maximum of 31.3 kPa [13]. A similar apparatus was used by Swan et al. for the anisotropic expanders where the maximum swelling pressure was 68.8 kPa for 90:10 wt% VP/MMA and 94.6 kPa for 99:1 wt% VP/MMA [9]. Both studies showed that the maximum swelling pressures were dependent on gel composition and the final swelling degree. The use of the measuring chamber is however an indirect method of measuring the swelling pressure due to the pressure being exerted from an expanding membrane. The use of this chamber is not commercially recognized and difficult to replicate.

Similar attempts to measure the swelling force were also investigated with particular interest on drug release of hydrogels. Again these authors failed to show a numerical representation of their findings [28, 29]. In this study, we will explore an alternative method in measuring the magnitude of swelling force which is different from the methods described above. From here the swelling force over expander area will be labelled as 'the swelling stress '.

To date, there is still a lack of quantitative data to characterise the swelling stresses generated from gel expansion [9, 13, 27]. This severe lack has led to dangerous complications that have been discussed in section 2.2.4. The swelling stress, swelling rate, and maximum swelling ratio of the device are crucial information for selecting the appropriate hydrogel material. A goal of this research is to be able to characterise these properties and build a better understanding of the osmotically swelling gels.

2.3 Mechanical Properties of Skin

Before we can fully develop a new tissue expander, it is necessary to understand the structure and function of skin. The human skin is the largest organ in the integumentary system [30]. As it is the outer covering of the body, the main function of skin is to act as an anatomical protection against pathogens and damage from the external environment. The skin is also responsible for regulating heat, water content, sensation, and excretion/absorption of materials [31]. To perform these functions, it is important for the skin to maintain its mechanical stability as well as flexibility. Mechanical properties of our skin can vary considerably as it depends on body site, age, race, sex, UV exposure, use of skincare products and nutritional status [5].The natural balance of skin can be affected by diseases, trauma, medical or cosmetic treatments. Following

the onset of these conditions, it is essential to set a reference to the characteristics of what is considered ‘normal skin’.

The skin is a heterogeneous tissue composed of three main layers, called the epidermis, dermis and hypodermis(see fig.2.08)[30]. The epidermis is the outermost layer of the skin which is waterproof and serves as a protective covering to the body. As it has no blood vessels, the epidermis is nourished by diffusion from blood capillaries within the dermis layer [32]. The epidermis can be divided into 5 different sub layers which are, from the most superficial inwards; stratum corneum, stratum lucidum, stratum granulosum, stratum spinosum, and stratum basale. The formation of skin cells is by mitosis at the stratum basale. After cell mitosis the keratinocytes will move outward to the surface changing their shape along each layer as shown in figure 2.08. The stratum corneum on the surface consists of 20-30 layers of flat-shaped cells.

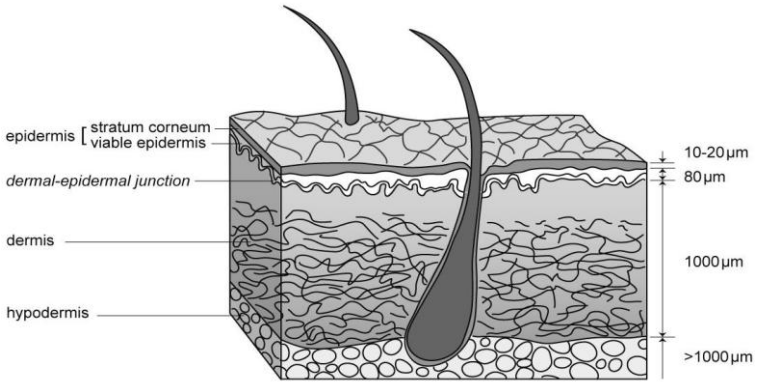

Figure 2.08: Schematic representation of the skin different layers. Adopted from ref.[33]

Below the epidermis is the dermis layer. The dermis is the thickest layer in the skin and is composed of connective tissue consisting of fibrous proteins such as collagen and elastin. The dermis also has nerve endings to provide the sense of heat and touch. The dermis can be divided into two areas called the papillary region and the reticular region [34]. The papillary

region provides connection to the epidermis while the much thicker reticular region is made of dense collagen and elastic fibres. These densely weaved fibres in the reticular region are the main contributors to the strength of skin [35].

Finally the hypodermis (also known as subcutaneous fat) lies underneath the dermis. The hypodermis acts as a connector between the skin and the underlying bone and muscle as well as a place for storage of fat [34]. This fat makes the hypodermis a fibrofatty layer which aids homeostasis by insulating the body from heat loss. Unlike the other skin layers, the thickness of the hypodermis will significantly vary with age, sex, ethnical background and body-mass index of each individual [36]. Although the skin contains microstructures like blood vessels, lymph vessels, nerve endings, sweat glands and hair follicles, the low influence on the mechanical properties mean they can be neglected in comparison to the bulk mechanical behaviour.

2.3.1 Skin Components and General Mechanical Behaviour of Skin

The human skin is a heterogeneous, anisotropic, and non-linear viscoelastic material [30, 32]. Considerable effort has been made in quantifying the mechanical characteristics of the overall skin composite but the task has been shown in the literature to be extremely challenging. To date, most research has been carried out by testing the skin *in vivo* and has been focused on characterising the Young Modulus of the dermis layer as it is generally thought to govern the strength of skin[37]. This was supported by similarities between the skin's overall biomechanical properties with the properties of the collagen-based dermal layer [38]. However, Wildnauer et al. showed the importance of loading magnitude [39]. The epidermis contribution on the skin's stiffness is known to dominate when the applied stress is low.

To understand the mechanical behaviour of any given material, it is often useful to know its composition and microstructure. This is also the case for skin tissue. In general, connective tissues such as the skin are made of a fibrous framework containing collagen and elastin fibres. The framework of these two main compositions is uniquely constructed with different geometry and the morphology for each different type of connective tissue [40]. The amount of collagen and elastin is then one of the most important features that can be use to characterise the strength of skin.

2.3.10 Collagen

Collagen is a group of naturally occurring proteins usually found in the connective tissues of mammals, such as in tendons, ligaments, skin, cartilage and bone. Collagen fibrils in skin are composed of types I, II, and III collagen which come in both wide and narrow forms [40]. Collagen in skin and tendon can be as large as several hundred nanometres in diameter [41]. On a smaller scale, a collagen molecule is a subunit of a larger collagen aggregate, and each collagen molecule is made up of three polypeptide strands called alpha chains. Each of these alpha chains possesses conformation of a left-handed helix where three of these helices are twisted together to form a quaternary protein structure strongly hold together by hydrogen bonds and covalent crosslinking. Collagen fibres naturally align parallel to the skin's surface and take up about 70% of the fat-free dry weight of the dermis [39]. Its strength is approximately 1.5-3.5 MPa, a strain to failure typically 5-6%, and a Young's modulus of between 0.1-1.0 GPa [42].

2.3.11 Elastin

Elastin is an important protein in connective tissues which provides tissues in the body the ability to retain their initial shape after small deformations. The fibre is composed of the proteins fibrin and elastin made of simple amino acids such as glycine, alanine, valine, and proline. The protein molecules form together an insoluble and cross-linked (through covalent di-sulphide linkages) array creating a random coil conformation. In contrast to collagen, the amount of elastin in skin is less than 1% of the dry weight [43]. Withinthe dermis, elastin fibres form a delicate network between the collagen fibres. They are far less stiff than collagen and can go through elastic deformation up to very high strains. Oxlund et al. showed the role of elastin in the mechanical properties of skin by degrading the elastin fibres from rat skin samples [44]. The study showed that the absence of elastin is only apparent at insignificantly low stress ($\sigma < 40$ mNmm^{-2}) and deformation ($\varepsilon < 4.0\%$) [44].

2.3.2 Stress-strain Relationships

The non-linear elasticity of skin can be expressed through a typical stress-strain curve obtained from a uniaxial tensile test. This curve typically shows three main regions (figure 2.09). The first region is called 'initial deformation' and is where large strain can be done under small stresses. At this stage of deformation, the elastin fibres are responsible for the deformation response. The modulus at this region was measured to be 0.10 MPa [31]. The high flexibility of the skin at these strain values enables easy movement of underlying muscles.

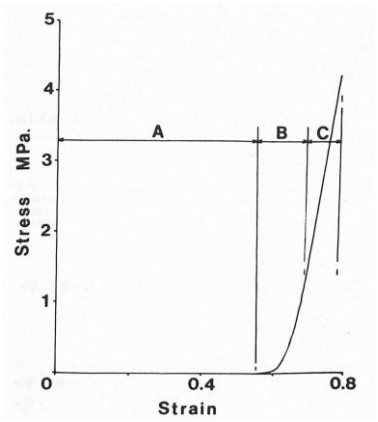

Figure 2.09: Stress-strain curve for human skin shown 3 regions. A) initial deformation, B) intermediate deformation, and C) near maximal deformation. The skin was taken from abdomen of a 45-year old woman. Adopted from ref .[66]

The second region is called the 'intermediate deformation'. At this region, the stiffness of the skin rapidly increases as the fibres begin to align along the direction of stress. Lastly, the final region is called the 'near maximal deformation'. At this point, the fibres are fully aligned giving a constant maximal stiffness [66]. Although the elastin and collagen fibres are considered to show linear elastic behaviour individually, the shape of the curve does not suggest a linear elastic material.

Visco-elastic behaviour of the skin was observed in regions 'B' and 'C' of the typical stress-strain curve (figure 2.09). Viscoelasticity is the property of materials that showed both elastic and viscous characteristics when deformed. In other words, the material will respond with dependence of time such that applying a slow increase of stress gives a viscous characteristic and a rapid increase of stress gives a more elastic behaviour. This property of the skin was closely investigated by Dunn and Silver [37]. The paper explained that the collagen fibrils in skin are more randomly arranged than in other tissues and can orient along the applied stress. This is associated with the rearrangement of the interfibrillar matrix containing water and what is called 'ground substance', a viscous liquid within connective tissues, comprising proteoglycans, glycoproteins, and hyaluronic acid. When subjected to consecutive load cycles, it was evident

that skin shows stress-relaxation under constant strain and creep under constant stress. Wilkes at al. explained that the time-dependant behaviour is due to the viscous resistance by the 'ground substance'. The removal of this ground substance from connective tissues resulted in a decrease in strength, stiffness and time dependant characteristics [46]. Thus, the movement of water (either free or bound to these hydrophilic compounds) imparts the viscoelasticity.

The paper by Dunn and Sliver stated that collagen fibres are free to orient along any direction and showed from their tensile test results that the mechanical properties of skin was independent of the specimen orientation [37]. This was however because their experiments were done *in vitro*. The skin is in fact, anisotropic in its natural condition as it is subjected to directional pre-stress *in vivo*. The fact that the skin is in a state of pre-tension *in vivo* was shown from the increased thickness of the dermis layer after the skin was removed from the body [38]. This indicated that there was a recoiling of the fibres. According to Wilkes et al., this pre-stress is strong enough to pull the elastin fibre network [37]. This seems to coincide with other studies about the function of elastin under small loads. The paper by De Jong studied the pre-tension of the skin *in vivo* on the human forearm by using a compressive load [47]. They claimed that the magnitude of the pre-tension is equivalent to the compressive force required to form wrinkles. The pre-tension stress was measured to be 0.024 MPa along the fibres and 0.0093 MPa across the fibres [47].

The direction of these pre-stresses is the reason why the skin is considered anisotropic. Within the skin, collagen fibres show preferential direction of extensibility which can be seen through what is called Langer's lines. The Langer's lines were first introduced by Karl Langer as he punctured the skin with a circular-shaped tip [48]. The resulting punctures in the skin showed

ellipsoid shapes rather than the shape of the circular tip which suggest that the skin is under some stress. These directions of stresses were mapped on a human model shown in figure 2.10.

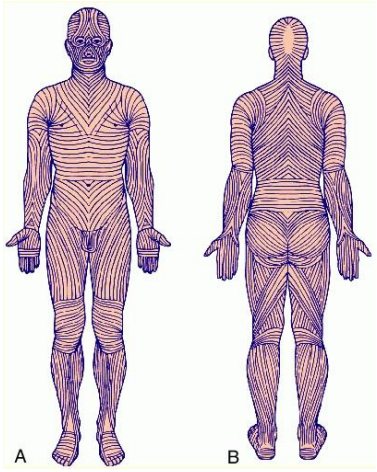

Figure 2.10: Langer's lines mapped on human body A) front B) back [50]

The presence of these lines showed that elastin and collagen fibres are more stretched in some directions than others. This means that the skin's extensibility is lower and the stiffness is higher along the Langer's lines [49]. Because of this anisotropic character of the skin, the direction of stretching in testing the mechanical properties is an important factor that cannot be neglected during experiments.

2.3.3 The Mechanical Experiments on the Skin in Vivo and in Vitro

Mechanical characteristics of the complex skin structure such as the modulus of elasticity can be measured on the outer surface (*in vivo*). Although these *in vivo* tests will not ideally characterise the contribution of all layers in the skin, it is considered harmless to the test subject and is much more convenient to process. This convenience comes with the limit of not

permanently damaging the skin and hence limited evidence to the plastic behaviour and the nature of its failure. The main advantage of these tests is that data is obtained from real-life conditions.

2.3.3.1 Tensile Testing

Most of the tests used in defining the mechanical properties of skin were based on conventional tensile testing [50-53].Two main modes of tensile tests have been used to evaluate skin mechanics. These two modes are uniaxial and biaxial. According Kenedi et al, these two tests yield the same deformation pattern while the more important factor is the dependency upon the Langer's Lines [51, 54]. As a result, it is better to focus on uniaxial tensile tests as it is the commonest and simplest method. Figure 2.11 shows a typical set-up of the *in vivo* tensile test.

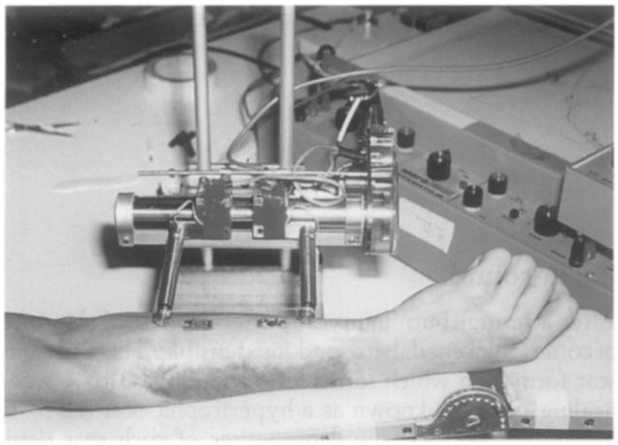

Figure 2.11: An extensometer for applying a constant stretching rate to the skin using two brass tabs secured to the forearm with double-sided adhesive tape [50].

The main problem with *in vivo* tensile testing is the difficulty in getting the length and width of the skin strip for accurate calculation. The modulus range of skin measured using *in vivo* tensile tests is between 4.6-20 MPa [60].

2.3.3.2 Torsion Test

One of the successful methods in measuring the extensibility of skin is by using torsion. This was first used by Vlasblom (1967)[56]. The torsional moment is transmitted to the skin by a disc [39]. The torsion technique is known to give two key advantages [59]. The first advantage is that the stress is applied parallel to the skin's surface such that we can reduce the physical contribution of the hypodermis and the underlying muscles. Secondly, the anisotropic character of skin is minimised due to the multidirectional stress applied. The apparatus set-up of the torsional test is shown in figure 2.12.The modulus range of skin measured using *in vivo* torsion tests is between 0.42-1.32 MPa [57, 59, 74-5].

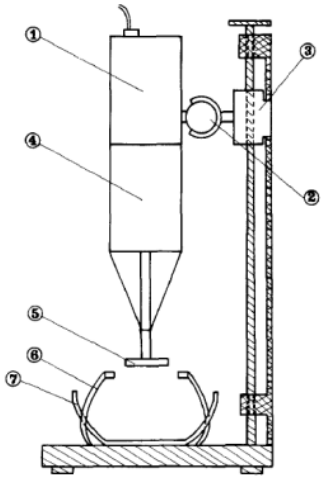

Figure 2.12: Diagram of the torsion testing apparatus by Leveque 1) rotational detector; 2)and 3) apparatus frame; 4) torque motor: 5) disc; 6) guard ring; 7) cradle [39].

2.3.3.3 Suction test

Measuring the mechanical behaviour of skin through the suction method involves the measurement of skin elevation through a circular aperture [83]. This technique has two commercially available instruments which is advantageous in terms of reproducibility of the

results [46]. Once the suction device is installed, the probe can be easily placed on the skin for testing. The method is most useful for comparing the mechanical behaviour between different anatomical regions.

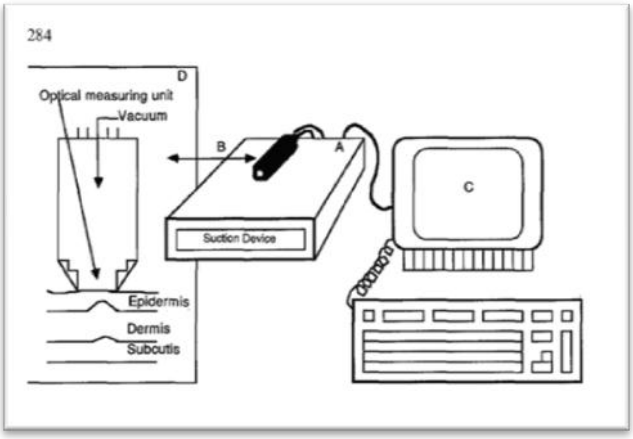

Figure 2.13: Diagram of a suction test apparatus [46].

The measured elastic modulus from suction test showed significantly lower values compared to the ones reported by other authors [39, 40, 42]. More supporting studies will be needed to document that the testing system is truly valid in achieving the intrinsic parameters for the skin's mechanical behaviour. The modulus range of skin measured using *in vivo* suction tests is between 0.11-0.27 MPa [64, 75].

2.3.3.4 Indentometry test

Indentation testing is carried out by using a rigid indenter to apply a certain force or deformation onto the skin. Deformation of the skin is measured through a linear displacement transducer attached to the loading beam [61-63].

In the past, indentation tests used for assessment of skin's *in vivo* biomechanics focused on measuring the deformation of skin through displacement of the indenter. However, this value

is not necessarily the actual deformed thickness as measurement cannot be done within the skin. Zheng and Mak tested the mechanical properties of soft tissues by integrating the ultrasound system into the common indentation apparatus [62]. With this method, deformation of different tissue layers could be measured in real-time. Validation of the system was by comparing the test results on porcine tissue with the results from a tensile test [62]. The advantage of this method is its ability to analyse different contributions from the fat layer and muscle layer while accurately measuring the actual deformation of the tissue. The modulus range of skin measured using indentrometry tests is between 1.09-2.52 kPa [61].

2.3.3.5 In vitro Experiments

Testing the skin *in vitro* is a much preferred method when it comes to understanding the contribution of each histological layer. This is because each layer of the skin can be isolated physically and then tested. The other advantage in doing experiments *in vitro* compared to *in vivo* is the ability to study the skin up to its ultimate tensile strength: it is useful to know the mechanical capacity of skin as it goes through permanent deformation. This understanding of the plastic behaviour can then be brought to use in designing new medical devices such as the hydrogel tissue expander or even a guideline for fabricating a tissue engineering scaffold.

The concern with *in vitro* methods is the inevitable loss of the skin's natural condition once the skin is harvested from the body. As natural conditions are disrupted, it is difficult to say if the results from *in vitro* tests are comparable to what will occur in a human body. The *in vitro* test of human skin graft is a straight forward process as the skin is no longer attached to the body.

Although simple to perform, the main drawback of the method is the limited availability of skin grafts [40].

Unlike the abundance in methods designed to test the mechanical behaviour of skin *in vivo*, uniaxial tensile testing is the only common experiment for testing skin *in vitro*. Prior to the experiment, skin tissues at the specific area of interest are obtained from donors at autopsy. The intact skin grafts are then cleaned and fixed. The methods of storage and the processing of these samples may alter the properties, but is rarely specified [40].

2.4 Discussion

The abundance of methods and technical devices that are found in the literatures creates a wide diversity in experimental conditions. Together with the complex material behaviour of skin, coming up with a conclusion about the mechanical properties of skin is a challenging task. The data obtained are often descriptive and are mainly based on self-derived parameters that are dependent on the unique experimental conditions [64]. Nevertheless, these results are useful in terms of explaining the characteristics of skin with variation in age, gender, and test site.

Daly et al. described the changes in mechanical properties with age [65]. Daly observed that the magnitude of the initial elastic deformation region (region 'A' in fig. 2.09) decreases with increasing age while the UTS did not change. The shifting of the graph in figure 2.15 suggests that the stiffness of collagen fibres does not change with age as the strength of the skin remains fairly constant but that the gradual destruction of elastin with increasing age is the

main cause[65]. When elastin was enzymatically removed from the tissue composite the curves shifted in the direction observed [65]. However, the change in configuration of the collagen fibres was also discussed in some papers as the main contributor of this change [57, 66].

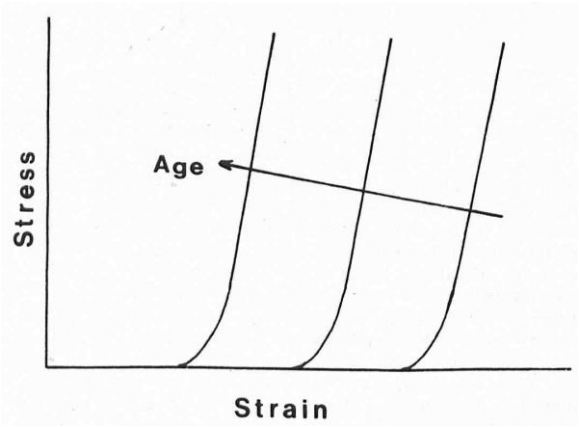

Figure 2.15: The effect of age on uniaxial tensile properties of skin [65]

By using the torsion technique with an ultrasound device, Escoffier et al. was able to investigate the age-related mechanical properties of skin in detail [57]. By testing on the ventral forearm of 123 healthy volunteers with a good age distribution, the results show that the skin maintains its thickness and extensibility up to age 70 while the skin's elasticity and recovery capacity decrease at a much earlier age [57]. In contrast to Daly's approach in explaining the loss of elasticity, Escoffier explained that the decrease in thickness and extensibility can be due to contraction of the skin as large amount of space in the fibre network disappears from the dermis. With increase in age, the skin tends to be stiffer from increased interactions of the fibrous network with intermolecular and intramolecular cross-linking of collagen [68]. The recovery capacity or the creep relaxation is also decreased due to decrease of the viscous liquid characterised by glycolaminoglycans [65]. This loss of dermal hydration was also thought to be the reason for the aged appearance of skin [69]. Whatever the cause, the main point was made that there are age-related mechanical changes that will increase the stiffness of skin. [59].

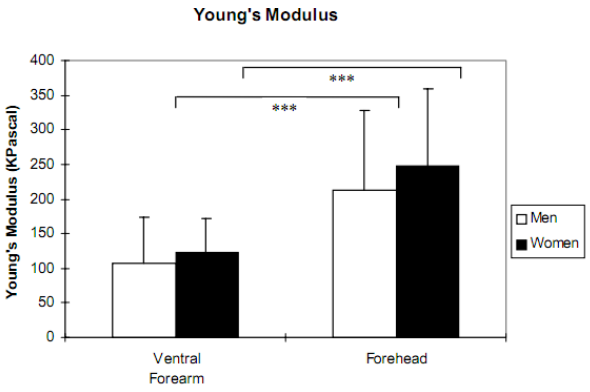

Figure 2.16: Graph comparing Young's modulus between ventral forearm and forehead sites separating male and female results [72].

Pierard and Lapiere discussed the difference in mechanical properties with relation to gender [71]. This variation between the mechanical properties is said to be because of differences in architecture of the fibrous framework. The sex-dependent variations in the thickness and mechanical properties was also later analysed by Diridollou et al. [72]. By using the suction method described in section 2.3, the thickness and the Young's Modulus were compared between the male and female human skin. The result showed no difference in thickness between male and female ventral forearm but showed that male's forehead skin is generally about 13% thicker than of female forehead skin [72].

Figure 2.16 compares the Young's modulus of male and female skin at two anatomical sites. The graph shows slightly greater Young's modulus from female skin at both forehead and forearm. This contradicts Pierard and Lapiere as this suggests that the extensibility of skin is larger in men than in women. The higher modulus of female skin was also noted in papers by Grahame [73] and Agache [74]. Figure 2.16 also suggests that the Young's Modulus of our

forehead skin is about twice the value taken from the ventral forearm [72]. This highlighted the importance of skin anisotropy, structure and thickness at different body areas.

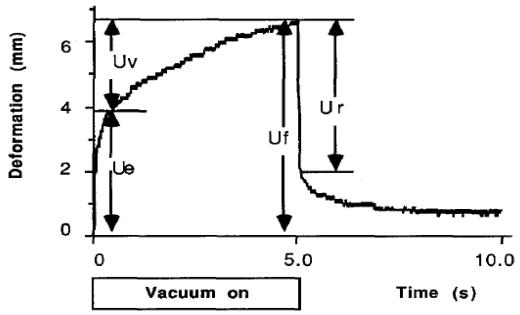

Figure 2.17: Skin deformation plotted as a function of time – The plot shows the measured parameters: *Ue* (immediate distension), *Uv* (delayed distension), *Ur* (immediate retraction), and *Uf* (final deformation). The skin showed visoelastic behaviour where some permanent deformation is shown after release in load- this is due to the purely viscous component [66].

Although it is evident that the mechanical characteristics of skin differ with age and sex, some regions of the skin will be more variable to difference in age and sex while skin from places such as the postauricula is said to show no significant variations [66]. Cua et al. discussed the creep-relaxation properties of skin at 11 different anatomical regions. These regions were compared by two relative parameters independent of skin thickness: the ratio between the viscoelastic properties and immediate distension (*Uv/Ue*) and the ratio between immediate retraction and the total distension (*Ur/Uf*) (figure 2.17). The latter parameter represents the skin's ability to recover to its initial position [66].

Table 2.18: *Uv/Ur* and *Ur/Uf* calculated when 500 mbar of pressure was applied for 5-seconds and then relaxed for 5-seconds. * Regions with significant difference between the age groups. Adopted from ref. [66]

Region	Uv/Ue		Ur/Uf	
	Young	Old	Young	Old
Forehead	0.56 ± 0.07	0.61 ± 0.07	0.72 ± 0.04	0.66 ± 0.05
Postauricular	0.49 ± 0.07	0.46 ± 0.07	0.76 ± 0.04	0.65 ± 0.06
Upper arm	0.43 ± 0.05	0.42 ± 0.05	0.92 ± 0.01	0.84 ± 0.04
Volar forearm	0.59 ± 0.02	0.55 ± 0.05	0.88 ± 0.02*	0.77 ± 0.03
Dorsal forearm	0.46 ± 0.04*	0.64 ± 0.05	0.77 ± 0.05*	0.64 ± 0.04
Palm	0.49 ± 0.05	0.53 ± 0.04	0.66 ± 0.03*	0.53 ± 0.02
Abdomen	0.27 ± 0.04*	0.49 ± 0.07	0.91 ± 0.02	0.87 ± 0.03
Thigh	0.34 ± 0.02	0.44 ± 0.03	0.92 ± 0.01	0.88 ± 0.03
Ankle	0.42 ± 0.04	0.52 ± 0.05	0.78 ± 0.02*	0.62 ± 0.02
Upper back	0.50 ± 0.03*	0.65 ± 0.06	0.91 ± 0.02*	0.81 ± 0.02
Lower back	0.38 ± 0.03*	0.54 ± 0.06	0.90 ± 0.02	0.86 ± 0.04

Ur/Uf in table 2.18 can be associated with the skin's elastic properties. The thigh and upper arm showed highest elasticity while the palm is the least elastic out of all the 11 tested areas [28]. The information from the paper might not be numerically significant but it is useful to know the elastic variation of skin at different areas. The amount of methods and technical devices that are used in the literature together made a collection of unique experimental conditions. It is always important to perform experiments with good quality samples in a well-controlled environment. There is a need for researchers to focus on one parameter that can universally characterise the skin. In my opinion this parameter should be the Young's modulus. Accurate measurements have to be made while a correct model to determine the modulus will need to be developed. Compilation of the moduli measured through a number of *in vivo* experiments is shown in table 2.19.

The scarce amount of data reflects the difficulty in quantifying the Young's modulus as complicated models have to be made. As table 2.19 shows, the measured Young's modulus can vary by a factor of 10^3 depending on the technique used. An explanation of this large difference in moduli is mainly due to how the skin is deformed during each procedure.

Table 2.19: Summary of the Young's modulus obtained for skin tissue at different anatomical regions.

Method	Young's Modulus (MPa)	Test Region	Source
Tensile	E= 20	Calf (parallel)	Manschot and Brakkee [60]
	E= 4.6	Calf (perpendicular)	Manschot and Brakkee [60]
Torsion	E= 0.42-0.85	Dorsal forearm	Agache et al. [74]
	E= 1.12	Ventral forearm	Escoffier [57]
	E= 1.32	Ventral forearm	Leveque et al. [59]
Suction	E= 0.13-0.26	Various sites	Barel et al. [75]
	E= 0.11-0.16	Forearm	Diridollou et al. [46]
	E= 0.21-0.27	Forehead	Diridollou et al. [46]
Indentometry	E=1.99-2.52 x 10^{-3}	Thigh (young male)	Bader and Bowker [61]
	E=1.51-1.79 x 10^{-3}	Forearm (young male)	Bader and Bowker [61]
	E=1.09-1.29 x 10^{-3}	Forearm (young female)	Bader and Bowker [61]
	E=1.11-1.51 x 10^{-3}	Forearm (aged female)	Bader and Bowker [61]

The moduli obtained from indentation method are much lower than the ones obtained from tensile, torsion, or suction tests. This may beexplained by the limited indentation distance before reaching the subcutaneous tissues. Because of this low strain, the stiffer collagen fibres were not fully stretched nor aligned.Instead, the matrix of the dermis and the underlying tissues were the only contributors to these relatively low moduli.

Despite the effort in measuring the effective dimensions and being the most precise in methodology, the modulus of 20 MPa and 4.6 MPa, depending on orientation, obtained from Manschot and Brakkee using the tensile testing method is higher than the other values [60]. The higher modulus from the test may be due to the coming together of the surrounding skin when the selected section is pulled. This results in an increased amount of deformed material which is in the form of densely packed collagen. In addition, the modulus from tensile testing is also dependent upon the direction of Langer's line.

As the values in the table 2.19 do not show a comprehensive trend, there is still a search for a mechanical model that can be commonly accepted among physicians. By neglecting the moduli measured with indentation and tensile methods, the modulus of skin measured through torsion and suction methods isbetween0.11 – 1.32 MPa [46, 57, 59, 75]. This range of modulus was also accepted in more recent papers [77].

In vitro testing, on the other hand, is different from the non-invasive *in vivo* tests as the skin's plastic behaviour can be observed while each skin layer can also be separated for investigation. This is incredibly useful information for plastic surgery particularly for the use of tissue

expanders. As expansion of skin is needed to perform the reconstructive surgery, the skin will need to be deformed to increase the skin area. Knowing the skin's extensibility and the limit to when it will fail is crucial as stretching the skin too rapidly can cause serious damage to the patient's skin. There are records of numerous *in vitro* experiments that were done in the past. Unfortunately, most of them were not well documented and often unclear whether the dermis or the total skin was tested.

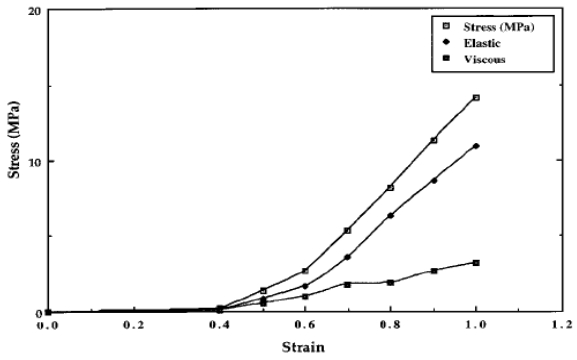

Figure 2.20: Stress-stain curve for human skin graft. Total stress is plotted with unfilled squares. Elastic and Viscous parts were plotted separately. Ref.[31]

Figure 2.20 shows the stress-strain curve obtained through *in vitro* tensile testing by Silver et. al[31]. The modulus at low strain (below 0.4) was calculated to be 0.1MPa while the slope shifts to 18.8MPa at higher strains (above 0.6) [31]. A similar stress-strain curve for skin was also obtained by Daly and Odland [45]. Both papers agreed that the initial portion of the curve involves stretching of the elastin fibres while the collagen fibrils and fibres are still folded. Collagen fibre contribution will then dominate at subsequent skin deformation with molecular stretching and slippage [31].

2.5 Chapter Summary

The human skin is a heterogenous, anisotropic, and viscoelastic tissue with variations between individuals.[79]. Because of its complex structure and the influence by external factors, skin has been proved difficult to characterise.

Tensile, torsional, suction, and indentation tests have been performed *in vivo* to measure the strength of skin and the results from these literatures have been discussed. An age-related mechanical property of skin was investigated and the skin's elasticity and recovery capacity is said to decrease with age [57, 76]. It seems that that female skin generally has a slightly higher modulus than male skin [73, 74]. Test site variation was also discussed where the skin was tested at 11 regions [66].

Young's modulus of the skin was obtained by many authors and the results can vary by a factor of more than 10^3. This large variation in the calculated modulus is because the skin behaves differently with the type and rate of deformation applied. In conclusion, the Young's modulus of skin is suggested to be around 0.1 – 1.32 MPa. Future work must focus on developing a standard testing apparatus so that the modulus of skin can be generalised.

2.6 Chapter 2 references

1) Austad ED and Rose GL. A self-inflating tissue expander. Plast. Reconstr Surg. 70:588-93, 1982

2) LoGiudice J and AK Gosain. Pediatric tissue expansion: indications and complications. J. of craniofacial surgery, 14(6): 866-872, 2003

3) Carneiro R and Dichiara J. A protocol for tissue expansion in upper extremity reconstruction. Journal of Hand Surgery, 16 (1):147-151, 1991

4) Hallock GG. Safety of clinical overinflation of tissue expanders. Plastic and Reconstructive Surgery, 96(1):153-157, 1995

5) Neumann GC. The expansion of an area of skin by progressive distension of a subcutaneous balloon; use of the method for securing for subtotal reconstruction of the ear. Plast Reconstr Surg. 19: 124-30, 1982

6) Radovan C. Tissue Expansion in Soft-tissue Reconstruction. Tissue Expansion and Reconstruction. 74:4, 1983

7) Radovan C. Breast reconstruction after mastectomy using the temporary expander. Plast. Reconstr. Surg. 69: 195, 1982

8) Marcus J, Horan DB, Robinson JK. Tissue expansion: Past, Present, and future. Journal of the American Academy of Dermatology. 23:5, 1990

9) Swan MC, Bucknall DG, Goodacre TEE, Czernuszka JT. Synthesis and properties of a novel anisotropic self-inflating hydrogel tissue expander. Acta Biomaterialia. 7:1126-32, 2011

10) Manders EK, Schenden MJ, Furrey JA, Hetzler PT, Davis TS, and Graham WP. Soft-tissue Expansion: Concepts and Complications. The Milton S. Hershey Medical Center of the Penn. State, 1984

11) Borzacchiello A and Ambrosio L. Structure- Property Relationships in Hydrogels. Springer-Verlag Italia, 2009

12) Johnson & Johnson Medical 2013. http://www.mentormedical.co.uk/tissue-expanders.php ,accessed 1 November 2010.

13) Wiese KG, Heinemann DEH, Ostermeier D, and Peters JH. Biomaterial Properties and biocompatibility in cell culture of a novel self-inflating hydrogel tissue expander. John Wiley & Sons, 2000

14) Berge SJ. Tissue expansion using osmotically active hydrogel systems for direct closure of the donor defect of the radial forearm flap. Plastic and Reconstructive Surgery, 108(1):1-5, 2001

16) Obdeijn MC, Nicolai JA, Werker PMN. The osmotic tissue expander: a three-year clinical experience. J Plast Reconstr Aesthet Surg , 62: 1219-22, 2009

17) Cunha MS, Nakamoto HA, Herson MR. Tissue expander complications in plastic surgery: a 10-year experience. Rev Hosp Clin Fac Med Sao Paulo, 57:93, 2002

18) Kobus KF. Cleft palate repair with the use of osmotic expanders: a preliminary report. Journal of Plastic, Reconstructive and Aesthetic Surgery, 60(4):414-421, 2007

19) Ronert MA, Hofheinz H, Manassa E. The beginning of a new era in tissue expansion: self-filling osmotic tissue expander- four year clinical experience. Plast Reconstr Surg. 114:1025-31, 2004

20) Radzi Z. Development of Self-Inflating Anisotropic Tissue Expanders for Clinical Applications. PhD Thesis, University of Oxford, Oxfordshire, United Kingdom, 2012

21) Lee JH. Development of an anisotropic swelling hydrogel for tissue expansion: Control over the degree, rate and direction of hydrogel swelling. PhD Thesis, Georgia Institute of Technology, Atlanta, GA, United States, 2008

22) Von See C. Bone augmentation after soft-tissue expansion using hydrogel expanders: effects on microcirculation and osseointegration. Clinical Oral Implants Research, 21(8): 842-847, 2012

23) Von See C, Micro-computed tomography and histologic evaluation of the interface of hydrogel expander and underlying bone: influence of pressure distributors on bone resorption. Journal of oral and maxillofacial surgery, 68(9):2179-2184, 2010

24) Abrahamsson P. Periosteal expansion of rabbit mandible with an osmotic self-inflatable expander. Scandinavian Journal of Plastic and Reconstructive Surgery and Hand Surgery, 43(3):121-125, 2009

25) Abrahamsson P. Onlay bone grafting of the mandible after periosteal expansion with an osmotic tissue expander: An experimental study in rabbits. Clinical Oral Implants Research, 21(12):1404-1410 , 2010

26) Abrahamsson P. Intra-oral soft tissue expansion and volume stability of onlay bone grafts. Swedish dental journal. Supplement, 211: 11-66, 2011

27) Wiese KG. Osmotically induced tissue expansion with hydrogels: A new dimension in tissue expansion? A preliminary report. Journal of Cranio-Maxillo-Facial Surgery, 21(7):309-313, 1993

28) Peppas NA and Colombo P, Development of disintegration forces during water penetration in porous pharmaceutical systems. J. Control Release, 10;245-250, 1989

29) Catellanni P, Predella A, Bellotti A and Colombo P. Tablet water uptake and disintegration force measurements. Int. J. of Pharm. 51: 63-66, 1989

30) Kenedi RM, Gibson T, Evans JH, and Barbenel JC. Tissue Mechanics. Phys. Med. Biol. 20(5):699, 1975

31) Silver FH, Freeman JW, and DeVore D. Viscoelastic properties of human skin and processed dermis. Skin Research and Technology; 7: 18-23, 2001

32) Proksch E, Brandner JM, Jensen JM.The skin: an indispensable barrier. Exp Dermatol. 17(12):1063-72, 2008

33) Manschot JFM. The Mechanical Properties of Human Skin In vivo. Ph.D. thesis, Catholic University of Nijimegen, 1985.

34) Madison K. Barrier function of the skin: "la raison d'être" of the epidermis. J Invest Dermatol. 121(2):231-41, 2003

35) Norlan L. Skin Barrier Structure and Function: The Single Gel Phase Model. J. Invest. Dermatol. 177(4): 830-836, 2001

36) Connor, Steven: *The book of skin*, Cornell University Press, 176, 2003

37) Dunn MG and Silver FH. Viscoelastic Behaviour of Human Connective Tissue: Relative Contribution of Viscous and Elastic Components. Connective Tissue res. 12:59-70, 1983

38) Wilkes GL, Brown IA, and Wildnauer RH. The biomechanical properties of skin. Critical Reviews in Bioengineering. 453-495, 1973

39) Wildnauer RH, Bothwell JW, and Douglass AH. Stratum Corneum biomechanical properties – influence of relative humidity on normal and extracted human stratum corneum. The journal of Investigative Dermatology, 56: 72-78, 1971

40) Basaran O, Ozdemir H., Kut A, Sahin FI, Deniz M, Sakallioglu EA, and Haberal MA. Effects of different preservation solutions on skin graft epidermal cell viability and graft performance in a rat model. Burns, 32(4), 423-429, 2006

41) Marks R. Mechanical Properties of the Skin. In: Physiology, biochemistry, and molecular biology of the skin. Oxford University Press, Oxford, 1991

42 Finlay B. Scanning electron microscopy of the human dermis under uni-axial strain. Biomedical Engineering. 4:322-327, 1969

43) Rantala-Ryhanen S, Ryhanen L, Nowak FV, Uitto J. Proteinases in Human Polymorphoneuclear Leukocytes. European Journal of Biochemistry. 134 (1); 129-137, 1983

44) Oxlund H, Manschott J, and Viidik A. The Role of Elastin in the Mechanical Properties of Skin. J. Biomechanics. 21(3):213-218, 1988

45) Daly CH and Odland GF. Age-Related Changes in the Mechanical Properties of Human skin. The Journal of Investigating Dermatology 73:84-87, 1979

46) Diridollou S, Patat F, and Gens F. In vivo model of the mechanical properties of the human skin under suction. Skin Research and Technology. 6; 214-221, 2000

47) De Jong LAM and Douven LFA. Pre-tension and anisotropy in skin. Nat.Lab. Unclassified Report NL-UR 023/95. Phillips Research Laboratories, 1996

48) Langer K. On the anatomy and physiology of the skin. I. The cleavability of the cutis. British Journal of Plastic Surgery. 31(1): 3-8, 1978

49) Geerligs M. Skin Layer Mechanics. PhD Thesis, TU Eindhoven, Eindhoven, The Netherlands, 2009

50) Burton JL and Cunliffe WJ. Subcutaneous Fat. In: Champion, R.H., Burrington, J.L., Ebling, F.J.G. (editors), Textbook of Dermatology, 5th edition. Blackwell Scientific Publications, New York, 1992

51) Clark JA, Cheng JCY, and Leung KS. Mechanical Properties of normal skin and hypertrophic scars. Burns. 22(6):443-446, 1996

52) Kenedi RM, Gibson T, and Daly CH. Bioengineering Studies of the Human Skin. Biomechanics and related bioengineering topics. Pergamon, Oxford, 1965

53) Manschot JFM and Brakkee AJM. The Measurement and Modelling of the Mechanical Properties of Human Skin In Vivo – I The Measurement. J. Biomechanics. 19(7):511-515, 1986

54) Lanir Y and Fung YC. Two-dimensional Mechanical Properties of Rabbit Skin. II. Experimental Results. J Biomechanics 7:171-182, 1974

55) Daly CH. The Biomechanical Characteristics of Human Skin. PhD Thesis, University of Strathclyde, Glasgow, Scotland 1966

56) Barbenel JC and Evans JH. The time-dependent mechanical properties of skin. J of Invest. Dermatol. 69: 318-320, 1977

57) Escoffier C, Pharm M, De Rigal J. Age-Related Mechanical Properties of Human Skin: An In Vivo Study. Investigative Dermatology, 1989

58) Pierard GE, Tassoudji N, and Franchimont C. Influence of the Test Area on the Mechanical Properties of Skin. J of Dermatol. 191:9-15, 1995

59) Leveque JL, de Regal J, Agache PG, and Monneur C. Influence of Ageing on the in Vivo Extensibility of Human Skin at a Low Stress. Arch Dermatol Res 1980 269, 127-135

60) Manschot JFM and Brakkee AJM. The Measurement and Modelling of the Mechanical Properties of Human Skin In Vivo – II The Model. J. Biomechanics. 19(7):517-521, 1986

61) Bader DL and Bowker P. Mechanical characteristics of skin and underlying tissues in vivo. Biomaterials. 4:1-8, 1983

62) Zheng YP and Mak AFT. An ultrasound indentation system for biomechanical properties assessment of soft tissues in-vivo. IEEE Transactions on Biomedical Engineering. 43:912-918, 1996

63) Hayes WC, Keer LM, Herrmann G, and Mockross LF. A mathematical analysis for indentation tests of articular cartilage. Journal of Biomechanics 5: 541-51, 1972

64) Sanders R. Torsional Elasticity of Human Skin in vivo. Pfliigers Arch. 342:255-260, 1973

66) Cua AB, Wilhelm KP, and Maibach HI. Elastic properties of human skin: relation to age, sex, and anatomical region. Arch Dermatol Res. 282:283-288, 1990

67) Minns RJ, Soden PD, and Jackson DS. The role of the fibrous components and the ground substance in the mechanical properties of biological tissues: a preliminary investigation. Journal of Biomechanics, 6: 153-165, 1973

68) Lavker RM, Zheng P, Dong G. Aged Skin: a study by light, transmission electron, and scanning electron microscopy. J. of Invest. Dermatol. 88; 44-51, 1987

69) Lovell CR, Smolenski KA, Duance VC, Light ND, Young S, Dyson M. Type I and III Collagen content and fibre distribution in normal human skin during aging. J. Dermatology. 117; 419-428, 1987

70) Uitto JJ, JazioMJ, Olsen DR. Molecular mechanisms of cutaneous aging. J. Am Acad Dermatol 21; 614-622, 1989

71) Pierard GE and Lapiere M. Physiopathological Variations in the Mechanical Properties of Skin. Arch. Derm. Res. 260: 231-239, 1977

72) Diridollou, Black D, Lagarde JM, and Gall Y. Sex- and site- dependent variations in the thickness and mechanical properties of human skin in vivo. International Journal of Cosmetic Science, 22; 421-435, 2000

73) Grahame R and Holt PJL. The influence of aging on the in vivo elasticity of human skin. Gerontologia, 15; 121-139, 1969

74) Agache PG, Monneur C, Leveque JL, and De Rigal J. Mechanical Properties and Young's Modulus of Human Skin In Vivo. Arch Dermatol Res. 269:221-231, 1980

75) Barel AO, Courage W, and Clary P. Suction method for measurement of skin mechanical properties: The Cutometer. Handbook of Non-Invasive Methods and the skin. Boca Raton, CRC Press, 1995.

76) Fazio MJ, Olsen DR, Uitto JJ. Skin Aging: lessons from cutis laxa and elastoderma. Cutis. 43; 437-444, 1989

77) Hendrik FM. Mechanical behavior of human epidermal and dermal layers in vivo. PhD Thesis, Universiteitsdrukkerij TU Eindhoven, Eindhoven, The Netherlands, 2005

78) Mechanic GL, Katz EP, Henmi M, Noyes C, Yamauchi, M. Locus of a histidine-based, stable trifunctional, helix to helix collagen crosslink: stereospecific collagen structure of type I skin fibrils. Biochemistry, 26: 3500–3509, 2000

79) Michael GD and Frederick HS. Viscoelastic Behavior of Human Connective Tissues: Relative Contribution of Viscous and Elastic Components. Connective Tissue Research. 12:59-70, 1983

80) Jansen LH and Rottier PB. Elasticity of human skin related to age. Dermatologica 115:106-111, 1957

81) Jansen LH and Rottier PB. Some mechanical properties of human abdominal skin measured in excised strips. Dermatologica 117:65-83, 1958

82) Gammal S, Auer T, Hoffman K, Altmeyer P, Passman C, and Ermert H. High resolution ultrasound of the human epidermis. In: Serup, J. and Jemec, G.B.E. (eds.) Handbook of Non-Invasive Methods and the skin. Boca Raton, CRC Press, 1995.

83) Gniadecka M and Serup J. Suction chamber method for measurement of the mechanical properties: The Dermaflex. Handbook of Non-Invasive Methods and the skin. Boca Raton, CRC Press, 1995.

84) Kastelic J, Galeski A, and Baer E. The Multicomposite Structure of Tendon. Connective tissue res. 6:11-23, 1978

85) Bucknall D, Czernuszka J, Goodacre T, Meakins J, and MC Swan. A self-inflating anisotropic composition. Methods of manufacturing said composition and uses thereof. Patent File: WO2007080391 A2. January 9, 2007

Chapter 3: Swelling Force Measurements

3.1 Introduction

The use of a hydrogel expander is a recently developed method in providing extra skin for surgical procedures. Its use is an innovative approach to treat congenital facial disorder and trauma victims with extensive scars and burns. As mentioned in Chapter 2, these self-inflating expanders are improvements to the traditional silicone balloon expanders as it offers continuous expansion. In addition, their use can potentially open up new lines of medical expanders where swelling behaviour can be manipulated. This means that it should be possible to expand the skin or other soft tissues in more delicate areas of the facial region. With a solid body, the gels can be manufactured into any size and shape while the swelling characteristics can be tailored to fit its designated application. Apart from its known biocompatibility and ability to absorb large amount of water, little has been investigated on one of the most important property for a tissue expander to function; the swelling force opposing the skin tension.

Hydrogels generally consist of 2 components: the insoluble polymer network which maintains the structure, and the aqueous component which varies from dry gel (xerogel) to fully swollen [1]. The hydrogel network is usually a co-polymer between a hydrophilic and a hydrophobic component. The water uptake from the hydrophilic sections causes the swelling of gel while the overall structural is hold together by the cross-linked hydrophobic network [2]. During the swelling process, the diffused solution will act as a plasticizer to the polymer network, decreasing overall mechanical properties, lowering the glass transition temperature, and consequently increasing chain mobility [3].

At the moment of transition from glassy to rubbery state the polymer gel is naturally subjected to internal stress along the glass-gel boundary [3]. This stress is compressive at the glassy region and tensile at the gel-like region (fig. 3.10). The mixture of these stresses is responsible for deformity of the original shape [3]. Due to this constant change in structure and composition, it is often difficult to characterise these gels using standard material characterization methods. The property of gels is greatly affected by the amount of solvent it holds.

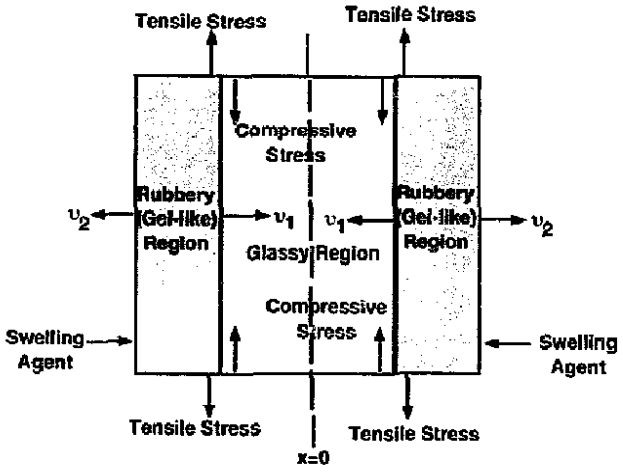

Figure 3.10: Diagram showing stress regions within a swelling hydrogel. υ_1 and $\upsilon_2$shows the movement of each boundary. Ref. [3]

The amount of swelling of a particular gel can be measured from the mass swelling ratio or volume swelling ratio denoted as Q_m and Q_V respectively.

$$Q_m = \frac{m_s}{m_0} \text{and} Q_v = \frac{V_s}{V_0} \qquad \text{Eq. 3.11}$$

where $\boldsymbol{Q}$ is the swelling ratio, $\boldsymbol{m_s}$ is the mass of swollen gel, $\boldsymbol{m_0}$ is the mass of xerogel, $\boldsymbol{V_s}$ is the volume of swollen gel, and $\boldsymbol{V_0}$ is the volume of xerogel. The equilibrium swelling ratio is important as it shows the maximum expanding capability of an expander in a controlled environment. As it is an intrinsic property, the swelling ratio is independent of geometry or

size. Although a high swelling ratio is favoured for a good tissue expanding device, the ratio does not guarantee that the material will swell with adequate pressure to overcome skin tension.

The swelling of hydrogels has been investigated by many authors [1-5].The driving force for swelling is the mixing of solvent into the polymer network to reduce the free energy. In general, this osmotic pressure (π) inside the gel distends the network and is opposed by elastic contractility (p) of the stretched chain [1]. Resulting swelling pressure, P, created by the gel can then be shown as:

$$P = \pi - p \qquad \text{Eq. 3.12}$$

This swelling pressure is described as the pressure exerted by the gel when swelling is constrained. At equilibrium, the swelling pressure is zero and hence, $\pi = p$. According to Khare and Peppas, the magnitude of swelling pressure is dependent upon the type of polymer, the degree of cross-linking, temperature, polymer-solvent interactions, degree of ionisation, and other environmental conditions [4]. The mechanical properties of these gels will affect the magnitude of elastic contractility while the ionic and structural properties contribute to the osmotic pressure.

To date, a fair amount of work has been dedicated to understanding the swelling rate of hydrogels and to control the initially fast swelling rate such that the swelling time suits surgical purposes [5, 6]. However, it is of the same importance that the swelling pressure of hydrogel tissue expanders is quantified before they become clinically used. A successful tissue expander device will need to produce enough swelling pressure to stretch and promote new healthy skin. One of these modifications to the hydrogel is the introduction of anisotropic swelling through

compression under heat treatment. This modification to the gel creates devices that can ideally expand in one direction, increasing the swelling in one dimension from 3 times to 15 times in length [5].

By having a more effective device, the initial size of these gels can be reduced and hence smaller incisions needed to place them. The anisotropic behaviour of these modified gels will lead to new applications such as treating cleft palate and syndactyly. Understanding the mechanics behind the swelling force is a key to whether or not these novel gels can achieve their goals. In this chapter, the swelling force of methyl-methacrylate and N-vinyl-pyrrolidone (VP/MMA) copolymer has been measured. The behaviour of isotropic and anisotropic swelling gels will be also investigated and discussed.

3.2.1 Poly(N-vinylpyrrolidone)/(methylmethacrylate) hyrogels

A copolymer of poly(N-vinylpyrrolidone) (PVP) and poly(methylmethacrylate) (PMMA) (Polymeric Ltd, Longfield, UK) was used as the starting material. VP/MMA is a copolymer between hydrophilic (PVP) and hydrophobic (PMMA) material consisting of a three-dimensional cross-linked network that can hold relatively large amount of water [7]. Synthetic hydrogel materials like VP/MMA (figure 3.20) have been widely known to be biocompatible for numerous medical applications [9, 10].

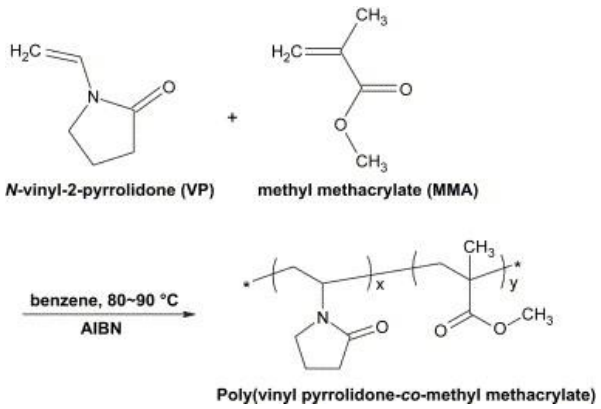

Figure 3.20: VP/MMA co-polymerization and chemical structure [9]

PVP and PMMA polymers are individually established as clinically safe [7-10]. PVP is used in hair and body products due to its good water solubility and is also commonly used as a binder for tablet-form drugs [9]. PMMA on the other hand is used as bone cement during knee and hip prosthesis implantation [10]. It is also used as hard contact lenses and replacement intraocular lenses. The ratio between VP and MMA is important in acquiring the desired gel property. Gels with a higher PVP ratio tend to swell more while the amount of PMMA is crucial for structural stability [5, 6].

In this study, five different compositions from 90-99% VP (weight ratio) were investigated (Table 3.20). Dry samples were machined using a mechanical lathe (XYZ 1440, XYZ Machine Tools, UK) at 220 rpm to the desired diameter and height. The samples were later polished with P600 grit paper to remove machining marks.

Table 3.21: VP/MMA compositions used in experiments

VP:MMA Weight% Ratio
90:10
93:7
95:5
97:3
99:1

3.2.2 Swelling behaviour of hydrogels

Swelling behaviour of hydrogels is typically observed by hydrating dry gels in aqueous solutions at controlled temperatures until fully swollen at some equilibrium value [3, 5, 6]. In this case, the hydrogel is hydrated in distilled water at room temperature (24^{o}C). The mass and volume change can then be monitored with swelling time. The swelling process can be quantified through mass and volume swelling ratio (Equation 3.11). The samples were taken out of solution and any remaining surface water was removed using filter paper. The expanded height and diameter of gels were then measured using a digital calliper (Absolute Digimatic Caliper, Mitutoyo, Japan) and weighed on a balance (ABS Analytical Balance, Kern Scale Tehnic, UK). The solution was changed with fresh solution after each measurement. Swelling rate was observed from plots of increasing swelling ratio over hydrating time. The swell rate of five different gel compositions was observed.

3.2.3 Water transport in a cylinder

The kinetics of swelling is a complicated phenomenon which has three successive steps [11].

1. The diffusion of water molecules into the polymer system
2. The relaxation of the hydrated polymer chains (chain disentanglements)
3. The expansion of the polymer network in the surrounding solution

As for hydrogels with a cylindrical shape

1. Swelling of the gel in the radial direction with cusp-like patterns on the surface
2. Shrinking of the gel in the radial direction and swelling in the axial direction
3. Re-swelling of the gel and disappearance of the pattern

Diffusion of water into the matrix begins from the transport of solvent into the swollen matrix and subsequently the diffusion of solvent from the swollen matrix into the unswollen matrix. To exhibit Fickian behaviour, the rate-determining step has to be the diffusion of the solvent into the swollen matrix where there is a linear relationship between water uptake and square root of time. If the advancement of the solvent passing the swollen-unswollen boundary is slower than the solvent-swollen boundary then the system is regarded as 'non-Fickian' [11]. Volume and mass increase is the result from diffusion of water into a hydrogel. The water transport can be characterised by Fick's second law or by more advanced models of anomalous diffusion. One method to describe water transport in polymers is via the power law [12].

$$\frac{M_t}{M_\infty} = kt^n \qquad \text{Eq.3.22}$$

Where $\mathbf{M_t}$ is the mass of solvent uptake at time **t**, M_∞ is the mass of the solvent uptake at equilibrium, **k** is a constant and **n** is the diffusion exponent.

The mechanism can be characterised through the diffusion exponent **n.** At n=0.5 the water transport is controlled by the chemical exponential gradient of which little or no volume variation occurs during the transport. This is known as Case I diffusion. For the process where the diffusion exponent n=1, the volume variation is proportional to time. This suggests that the water transport is controlled by Case II diffusion where stress relaxation is the driving force of the volume increase. The swelling of hydrogels is however likely to be a mixture of the two processes. This intermediate case is called anomalous diffusion (0.5<n<1) [13]. The diffusion exponent 'n' can be determined using log-log plots from results of mass measurements over time.

The most common method of extracting the diffusion coefficient of gels is by hydrating polymer sheets of known thickness and using log-log plots of the power law (Eq.3.22) [5, 6, 14]. On the other hand, the diffusion of water into cylindrical hydrogels can be characterised through a model where concentration is a function of radius and time. For this we consider the gel to be a long cylinder in which diffusion is everywhere radial [15]. Fick's second law of diffusion equation for this is:

$$\frac{\partial C}{\partial t} = \frac{1}{r}\frac{\partial}{\partial r}\left(rD\frac{\partial C}{\partial r}\right) \qquad \text{Eq.3.23}$$

By methods of partial differentiation and applying the boundary conditions such that the surface concentration is constant, the model is simplified [15]:

$$\frac{C-C_1}{C_1-C_0} = 1 - \frac{2}{r}\sum_{i=0}^{\infty} \exp\left[-Da_n^2 t \frac{J_0(a\alpha_i)}{J_1(r\alpha_i)}\right] \qquad \text{Eq.3.24}$$

where ***D*** is the diffusion coefficient, ***C*** is the water concentration, C_1 is the initial water concentration in the polymer, C_0 is the water concentration at the surface of the polymer, $J_0(x)$ and $J_1(x)$ are Bessel functions of zero and first order, respectively, α_i values are from the positive roots of these Bessel functions, ***a*** is the radius, and ***r*** is the radial coordinate such that $0 < r < a$.

Changing the equation to fit with mass of water transported into the polymer gives [15]:

$$\frac{M_t}{M_\infty} = 1 - \sum_{i=0}^{\infty} \frac{4}{a^2\alpha_i^2} \exp(-D\alpha_i^2 t) \qquad \text{Eq.3.25}$$

M_t is the mass of solvent uptake at time **t**, α_i is from the solution of $J_0(a\alpha_i) = 0$, and M_∞ is the mass of the solvent uptake at equilibrium

Table 3.26: First five roots for the Bessel function of zero order

n	$J_0(x)$
1	2.4048
2	5.5201
3	8.6537
4	11.7915
5	14.9309

Although these models are made for cylindrical samples of infinite length, results have been shown to be comparable with results from those obtained by diffusion through polymer sheets [16, 17]. The diffusion coefficient of 90:10, 95:5, and 99:1 VP/MMA samples were measured by hydrating long cylindrical samples of 5.77 mm diameter and 40.00mm length. The values of the diffusion coefficient were obtained using the model up to the first hundred roots of the Bessel function.

3.2.4 Mechanical Testing

The compressive Young's moduli of gels were measured using a dynamic mechanical analyser (DMA 7e Perkin Elmer). The load transmitted to the sample is generated by a force motor using repelling magnetic fields while linear displacement is measured by a linear variable differential transformer. Samples of different hydrated times were loaded using the static compression mode at 500mN/min to 5000mN. Samples of 90-99 wt% were machined to cylinders5.77mm in diameter and 6.00 mm in height. From dry gels (xerogels) to fully swollen gels, the elastic modulus can be determined through analysis of the stress-strain curve with measured Poisson's ratio of 0.5. Surface water was removed from samples using filter paper. Height and diameter of swollen gels were measured using digital callipers [±0.01 mm]. Three tests were carried out for each composition of which each gel is hydrated for a maximum of 48hours.

3.2.5 Force measurement setup

The swelling force was measured using a 300N load cell (SMA miniature S-type, Interface Measurements Ltd.) attached on a load frame of a Instron Model 3360 Dual Column. Dry samples were placed under a fixed plate. Distilled water was filled into the sample holder up to compression plate height. The force reading was zeroed after addition of solvent to begin swelling force reading. The uniaxial force was measured by the swelling of gel against the fixed plate. Swelling force data of the hydrated polymer was collected every 10 seconds for 48 hours at room temperature. A diagram of the apparatus set up is shown in figure 3.27. Swelling force is measured for different compression plate displacements, initial sample volumes, and compositions.

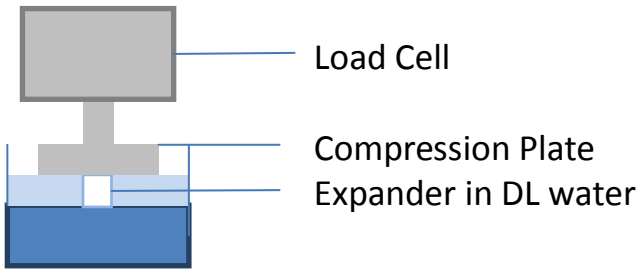

Fig 3.27: Swelling force measurement set-up

3.2.6 Introduction of anisotropic swelling

The unmodified swelling characteristic of a hydrogel is to expand in all directions while maintaining its initial geometry (isotropic).Processing of anisotropic swelling gels involves heating of xerogels marginally below its glass transitional temperature(T_g) in a thermostatically controlled hydraulic press (Specac Ltd., Slough, UK) [5]. The gels were heated for 60 minutes before being slowly compressed at 100MPa to the wanted thickness. The gels were held at

temperature for a further 30mins before the heater is switched off. The compressed gel is allowed to cool for 4 hours to room temperature before being removed and stored in an airtight container.

3.2.8 Thermal properties of VP/MMA

It is important to know the thermal properties of our gels prior to the anisotropic processing so that we do not permanently deform the sample but instead create a shape memory gel. This can be done by heating the gel up to its rubbery state. At this state the gel is in between a hard solid and a viscous material. This is a character of a polymer at its glass transition temperature (T_g).

Many characteristic properties of copolymeric gels tend to be intermediate between the two polymers and will be related by the composition. The T_g is one of those properties in which the rule of mixtures can be applied. The effect of copolymer composition on T_g can be described using the Flory-Fox [18] or the Gordon-Taylor equation [19, 20]. Both methods have been shown to be accurate in predictions of T_g for different poly(vinyl-pyrrolidone)/hydroxylethyl methacrylate (VP/HEMA) ratios. T_g of cross-linked PVP (T_g=185-190°C [45]) and atactic PMMA polymers (T_g=101-108°C [43]) were taken from literature.

$$\frac{1}{T_g^{FF}} = \frac{w_1}{T_{g,1}} + \frac{w_2}{T_{g,2}} \qquad \text{Eq 3.28}$$

Flory-Fox equation

$$T_g^{GT} = \frac{w_1 T_{g,1} + k w_2 T_{g,2}}{w_1 + k w_2}, k = \frac{\rho_1 T_{g,1}}{\rho_2 T_{g,2}} \qquad \text{Eq 3.29}$$

Gordon-Taylor equation

where w_i are the weight fractions, T_{gi} are glass transition temperatures and ρ_i are the densities of the two components (ρ_{PVP} = *1.25 g/cm^3 [45]* and ρ_{PMMA}=*1.17-1.20 g/cm^3 [43]*). The T_g of gels with different VP/MMA ratios were calculated using both the Flory-Fox and Gordon-Taylor equations.

The thermal properties of 5 different VP/MMA samples were then characterised using thermogravimetric/differential thermal analyser (TG/DTA) and differential scanning calorimetry (DSC). Changes in mass of the sample with temperature were tested using a PerkinElmer Pyris Diamond TG/DTA from 0^{o}C to 600^{o}C to monitor its thermal stability.The DSC scans of the copolymer samplers were obtained on a PerkinElmer Diamond DSC instrument from 0^{o}C to 300^o at a scanning rate of 100^{o}C/min. Glass transition temperatures (T_g) were obtained from DSC graphs.

3.3 Results and discussion

A favourable property of hydrogels is their ability to swell when in contact with a thermodynamically compatible solvent. From the moment of contact, swelling begins with solvent molecules attaching on to the hydrogel surface and penetrating into the network. With the surface absorbing water, the meshes of the network will expand and allow more solvent to penetrate deeper into the material. The glassy unsolvated core and the expanded rubbery polymer are separated with a moving boundary. This boundary can be seen in the early stages of hydrated VP/MMA samples (fig. 3.30).

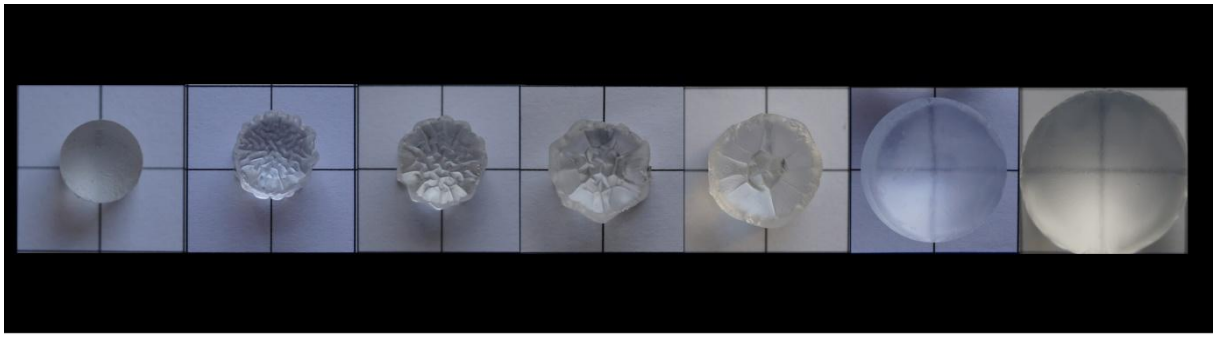

Figure 3.30: The transition from dry to fully swollen gel. From left: Dry gel, after 15 min., 30 min., 60 min., 3 hours, 24 hours, and 48 hours.

Cusp-like patterns and uneven swelling on the surface of the gels were observed during the intermediate swelling phases. This temporary deformation in geometry is due to the rapid relaxation on the surface which forms a stress boundary between gel-like material and a glassy core. This is apparent in the cylindrical shaped samples as folds on sharp corners and necking along the length. Dependent upon the gel composition, the VP/MMA hydrogel can expand from the initial size by 2-3 times in height and diameter. At equilibrium, the swollen gel returns to its original geometry as the internal stresses are homogenized.

3.3.1 Swelling Ratio

The mass and volume swelling ratio were calculated and plotted against time (fig. 3.31-2). The swelling of the gels showed rapid swelling phase at short times (0-120 minutes) and a decreasing swelling rate until an equilibrium is reached. Mass swelling ratio (Q_m) for 90:10 VP/MMA at fully swollen state is 7.6 while the maximum volume swelling ratio (Q_v) is 8.7. Swelling of gels with more hydrophilic components such as samples 95:5 and 99:1 VP/MMA showed higher equilibrium swelling ratios (fig. 3.32). The water uptake is greatly enhanced while time to reach equilibrium is increased. This change is seen in figure 3.26 where maximum Q_m is 9.8 and 12.3 for 95:5 and 99:1 VP/MMA respectively. Maximum Q_v for 95:5 VP/MMA is

measured to be 11.4 and for 99:1 VP/MMA it is 14.1. The equilibrium mass and volume swelling ratio showed that copolymeric VP/MMA hydrogels with 90-99 wt% VP are likely to have a useful swelling capacity for tissue expansion [5, 6].

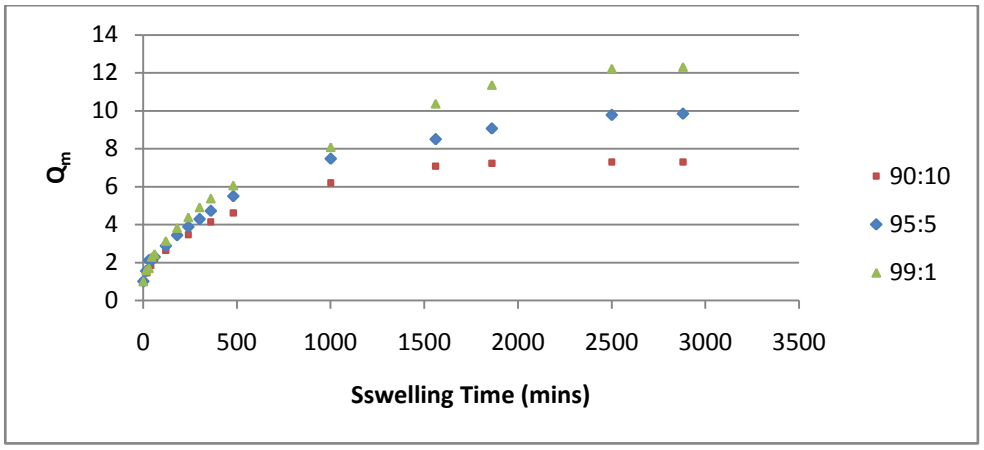

3.31: Mass swelling ratio of 90:10, 95:5, and 99:1 VP/MMA hydrogels against swelling time

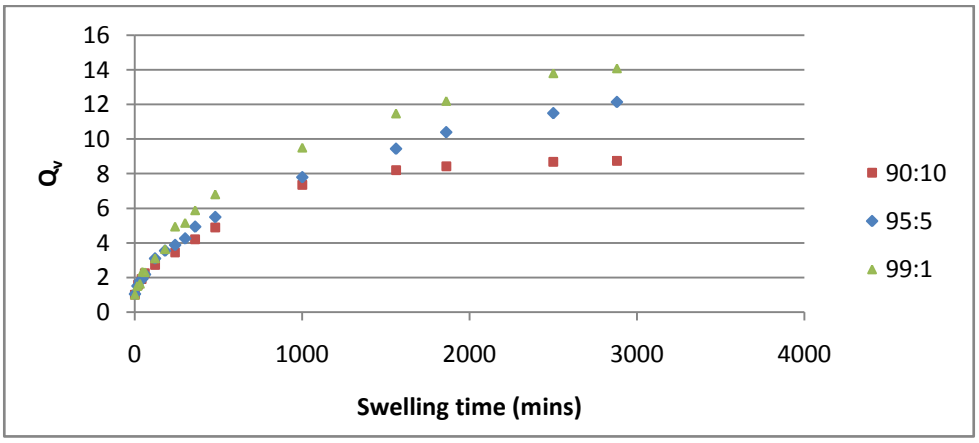

Figure 3.32: Volume swelling ratio of 90:10, 95:5, and 99:1 VP/MMA hydrogels against swelling time.

The measured mass and volume swelling ratios showed apparent differences where measured Q_v is greater than Q_m for all swollen gels. As seen in the two plots, the difference between the two ratios becomes larger as the gel approaches its maximal swelling capacity. This observation suggests that the density of the hydrogel, being the mass over volume, is continuously reducing as swelling progress. This is expected as the increasing component within the swollen gel is

water. However it is to note that there is a reaction between the water absorbed and gel network that can also reduce the overall density.

The gel samples used in our experiments are composed of 90-99 wt% hydrophilic VP. Once in contact with water, the hydrophilic sites of the polymer network will form strong hydrogen bonds with the water molecules creating a uniformly distributed layer. These water molecules which have restricted mobility are also called bound or non-freezing water [42]. The reduced density shown in high swelling hydrogels could be due to the repelling force between the oxygen atoms of the bound water and the oxygen of free water. The opposing forces between the different 'states' of water then create more widely separated molecules with lesser bulk density compared to that of a purely unbound water. While this is also an explanation for the decrease in density of the material, another reason is that there was apparent leaching out of gel material into the solvent. This is possibly due to flaws from synthesis which resulted in unreacted low-molecular-weight polymers.

3.3.2 Solvent Diffusion in Hydrogel

When used in biomedical applications one of the most important features of the hydrogel is the swelling rate. As seen in the swelling ratio against time graphs (figure 3.31-2), the rate of swelling is rapid during the initial stages (2-3 hours) before slowing down to approach a saturation point. The rapid swelling which sees each hydrogel samples expand to near its maximum swelling ratio over short times is however undesirable for tissue expanders.

The swelling behaviour of the 90:10 VP/MMA gel hydrated in distilled water can be expressed by its diffusion coefficient (D). Using the Power Law (Eq. 3.22), the diffusion exponent (n) for the material was calculated using log plot of the initial linear portion of the swelling curve (see fig. 3.33). The diffusion exponent was calculated to be 0.57 which is near to that considered to be Fickian Diffusion. This value suggests that the mode of water transport is driven by the diffusion of solute into the polymer matrix. This however will change as swelling continues. At greater times, the diffusion exponent showed an intermediate value between 0.5 and 1.0 which suggests that the water transport is driven by both the concentration gradient and stress relaxation. The transition from a Case I diffusion to anomalous diffusion is due to the change in structure and composition of the hydrogel as it absorbs water; creating a network with a mixture of free and bound water. The change in diffusion nature was also explained by Gehrke et al. that deviation from Fickian diffusion will occur once the glassy core disappears [29]. Figure 3.34 shows the differences between Case I, Case II, and anomalous diffusion.

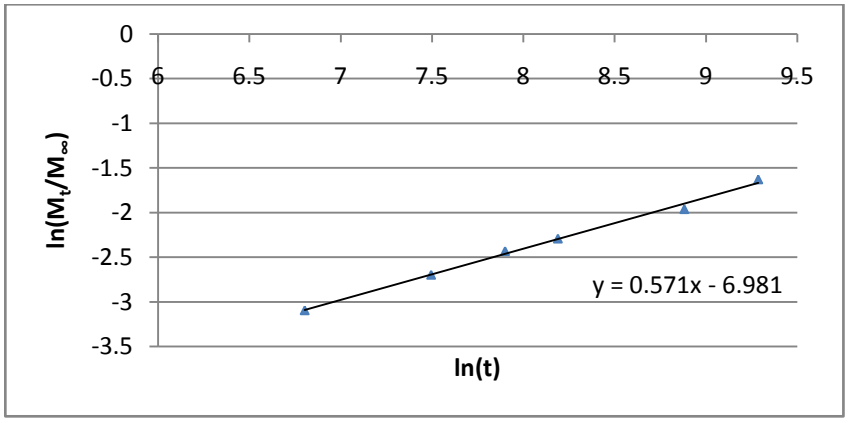

Figure 3.33: Plot representing **$\ln(M_t/M_\infty) = n \ln(t) + \ln(k)$** (Power Law Eq 3.22). The data was taken within the first 3 hours of hydration.

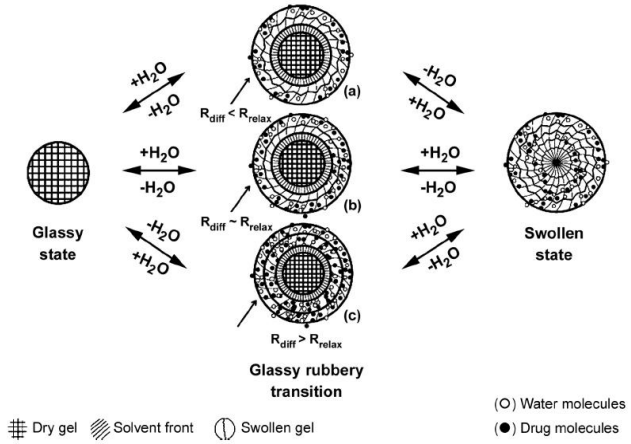

Figure 3.34: The mechanisms of diffusion a) when swelling is mostly relaxation controlled b) relaxation and chemical gradient controlled c) mostly chemical exponential gradient controlled. Adopted from Ref [28]

The diffusion coefficients (D) of 90:10, 95:5, and 99:1 VP/MMA samples in distilled water were calculated using Fick's second law by taking the increase in concentration as a function of radius and time (Eq.3.24) [19]. Using the first hundred roots of the Bessel function to determine the D values at different swelling intervals, the initial linear portion of the mass uptake curve was plotted and a best fit curve showed that the D value is closest to $(2.16 \pm 0.56) \times 10^{-11}$ m^2 s^{-1} for the 90:10 VP/MMA (figure 3.35). This curve fit however does not apply to the latter stages of swelling where D is no longer constant – because of the change from Case I to anomalous diffusion. This has also been mentioned in previous studies where D was measured at swelling below 60% of maximum solvent uptake [24, 30]. This increase in D is expected due to changes in the physical structure of the gel. The chain relaxation of the polymer network creates larger chain to chain gaps for solvent penetration and the diffusion of free water. While this increases the rate of diffusion, the swollen gel will in theory act as a hydrophobic surrounding membrane.

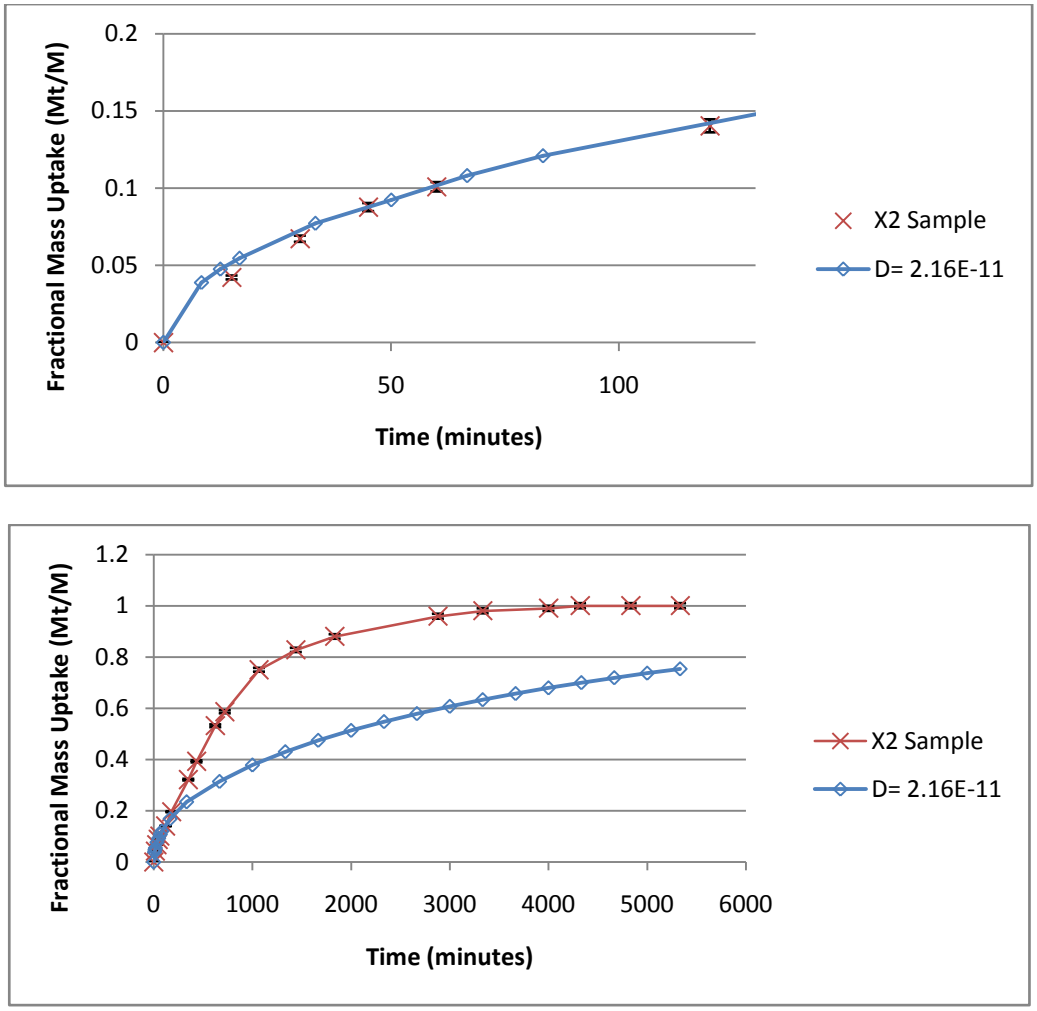

Figure 3.35: Mass uptake plot for 90:10 wt% VP/MMA at room temperature showing experimental points and the best fit curve for D= 2.16 x 10^{-11} m^2 s^{-1}. a) First two hours b) 3 days

The same method was used in calculation of the D for 95:5 and 99:1 VP/MMA samples. The calculated D values are (4.76 ± 0.64) x 10^{-11} m^2 s^{-1} and (1.23 ± 0.76) x 10^{-10} m^2 s^{-1} for 95:5 and 99:1 VP/MMA respectively. As shown in figure 3.36, the value of D increases with VP composition (C_{VP}). This behavior is expected since the hydrophilic component (VP) is the main driving force for water absorption; and consequently more amount of VP should promote faster diffusion.

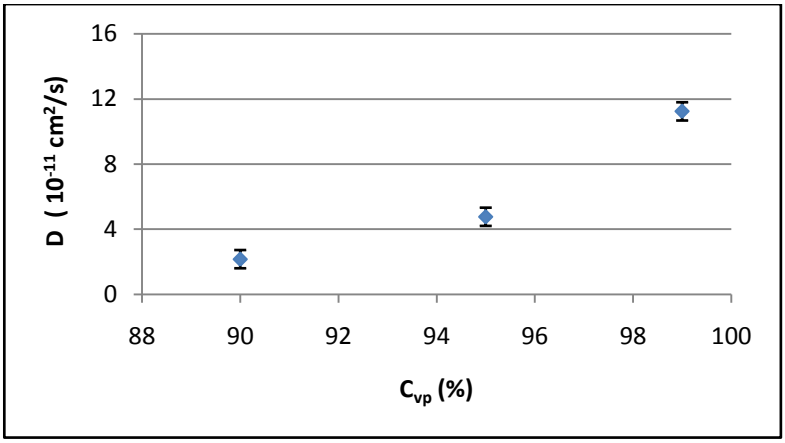

Figure 3.36: Effect of VP composition (C_{VP}) in VP/MMA gel on diffusion coefficient (D).

The mechanism of water transport with respect to pore size was investigated by Lowman [21]. Lowman described that the size of the pores within the structural network will affect the rate and type of water that the hydrogel holds. The porosity-related hydrogel kinetics is summarized in table 3.37. From physical observation of the gels and the result of the diffusion study, the VP/MMA gel system should be micro porous (pore size between 100-1000 Å). In other studies, the swelling behaviour of polymer gels was monitored by real-time visualization of dynamic deformation profiles [22] and by magnetic resonance imaging [23]. The results from these experiments showed that swelling is not a continual process but as mentioned; a balancing between thermodynamically favourable osmotic forces and opposing elastic force of polymer chains.

Table 3.37: The effect of pore size to swelling mechanism. Adopted form Ref[27]

Type	Morphology	Type of absorbed water	Major swelling mechanism	Swelling rate	Application
Non-porous	Without network porosity	Mostly bound	Diffusion through free volumes	Very slow, sample size-dependent	Various uses from contact lenses to artificial muscles, etc.
Micro-porous	Various porosity with closed-cell structure (100-1000 Å)	Mostly bound	Combination of molecular diffusion and convection in the water filled pores	Slow, sample size-dependent	Mainly in biomedical applications and controlled release technology
Macro-porous	Various porosity with closed-cell structure (0.1 -1 µm)	Mostly bound	Diffusion in the water filled pores	Fast, sample size-dependent	Mainly in form of superabsorbents in baby diapers, etc.
Super-porous	High porosity with interconnected open-cell structure	Mostly free	Capillary forces	Very fast, sample size-independent	DDS (particularly in the gastrointestinal tract), tissue engineering, etc.

3.3.3 Mechanical Properties

The moduli of 90:10, 95:5 and 99:1 VP/MMA gels of 5.77mm diameter and 6.00mm length were measured at different hydration periods under static compression using a dynamic mechanical analyser (DMA 7e Perkin Elmer). The stress-strain curves for 90:10 and 99:1 VP/MMA hydrogels were plotted for different times during hydration (figure 3.38). The stress-strain curve showed a rapid decrease in stiffness which is apparent between dry gel and a gel hydrated for 45 minutes. The modulus is then further decreased at a substantially slower rate until reaching equilibrium. The result showed expected non-linear behaviour for all non-hydrated and hydrated VP/MMA gels. The stress–strain curve of the dry gel plotted in both graphs showed a small error where the initially flat portion (<2.0% strain) is due to the gap between sample and compression plate. A 2.0% off-set is taken for modulus calculations.

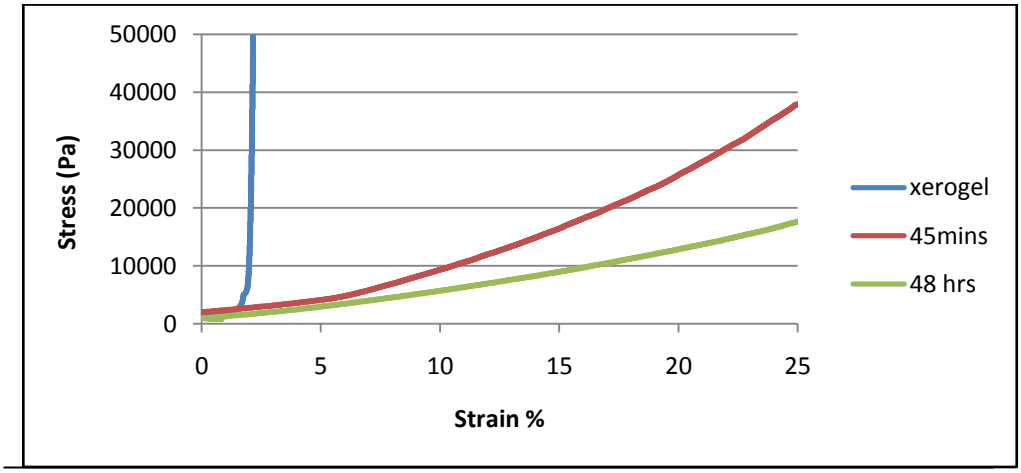

a)

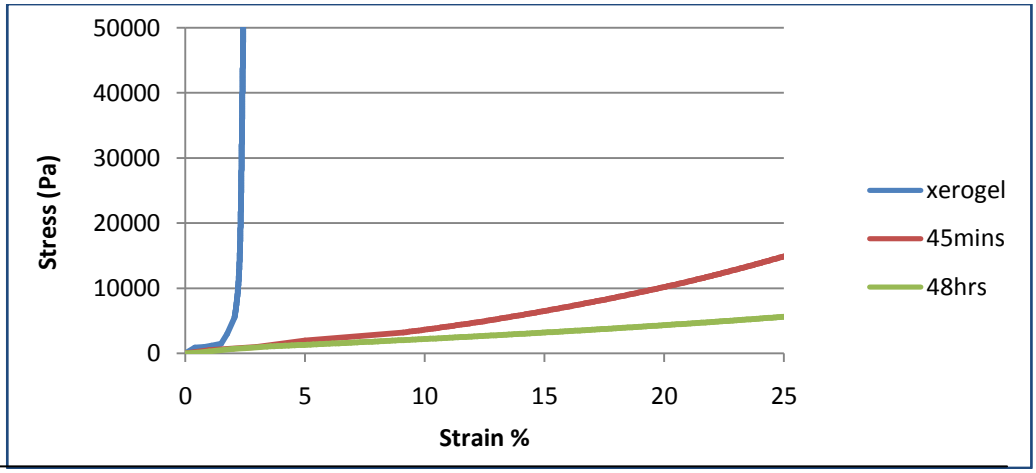

b)

Figure3.38: Compressive stress-stain curve of xerogel, 30mins hydrated, and fully swollen of a) 90:10 and b) 99:1 VP/MMA samples

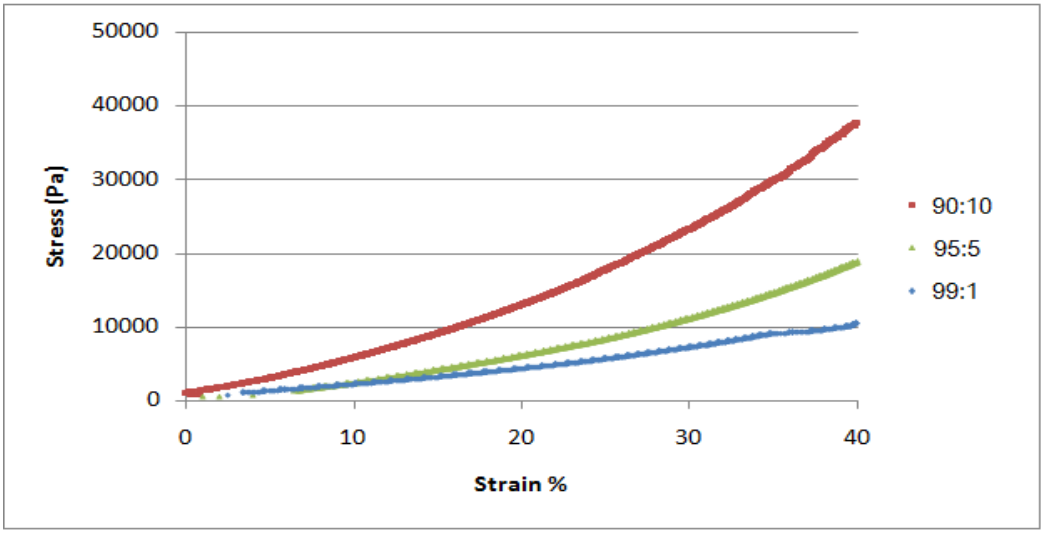

Figure3.39: Stress-strain curves for fully swollen 90:10, 95:5, and 99:1 VP/MMA gels under compression

Table 3.40: Compressive modulus for hydrated and non-hydrated VP/MMA

	(90:10 VP/MMA)			(95:5 VP/MMA)			(99:1 VP/MMA)		
	Dry gel	45mins	48hrs	Dry gel	45mins	48hrs	Dry gel	45mins	48hrs
$E_{2.5\%}$	56.2 MPa	40.5 kPa	40.3 kPa	37.5 MPa	20.2 kPa	22.5 kPa	32.8 MPa	35.3 kPa	14.8 kPa
$E_{10\%}$	-	121 kPa	60.6 kPa	-	95.5 kPa	36.7 kPa	-	49.8 kPa	18.0 kPa
$E_{15\%}$	-	165 kPa	70.3 KPa	-	120 kPa	43.7 kPa	-	67.4 kPa	20.6 kPa
$E_{20\%}$	-	242 kPa	89.8 KPa	-	149 kPa	52.7 kPa	-	81.1 kPa	31.4 kPa

Due to the non-linear stress-strain curve of rubber-like material, each modulus was measured at different strain values. Table 3.40 showed the calculated moduli at 2.5, 10, 15, and 20 % compressive strain of 90:10, 95:5 and 99:1 VP/MMA samples. The results showed a significant decrease in modulus over hydration times where the modulus is reduced by about a factor of 10^3 within the first 45 minutes. This was later followed by a much slower loss in stiffness until the gels are fully swollen at equilibrium. The large difference between the modulus of gels in contact with water for just 45 minutes and the modulus of dry gel marked the importance of device storage to maintain controlled properties.

Compression testing the material until failure showed that both hydrated and non-hydrated samples displayed brittle failure. Behaving like a rubber material once hydrated, the VP/MMA samples can go through high elastic strains but will go through minimal plastic strain before a catastrophic failure similar to one of a glassy material. The stress to failure for the hydrated VP/MMA is varied by composition, hydration period, and the mode of force applied. The failure can be explained through the Griffith concept of fracture in glassy materials.

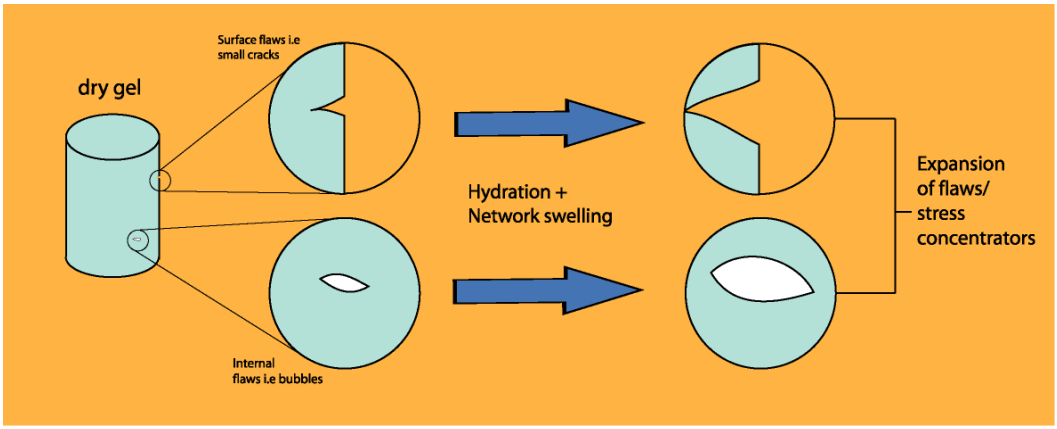

Table 3.41: A schematic diagram showing the expansion of surface cracks and internal flaws. The sharp edges of these flaws are 'stress concentrators' that will initiate cracking propagation at a critical stress.

Unlike materials that can plastically deform, the surface or internal flaws of glassy materials will act as 'stress concentrators' [31]. Flaws such as small cracks or scratches that were created during processing are most likely present in all samples. These flaws are leading pathways to propagated cracks and eventually failure when reaching a critical stress. With decreasing fracture toughness over hydration time for chemically cross-linked gels [32] and the exaggeration of flaws from structural expansion (see figure 3.41), the failure is more apparent in samples with higher swelling ratios. From the three fully hydrated samples tested, 90:10 and 95:5 VP/MMA gels showed good mechanical toughness while 99:1 VP/MMA samples were less predictable and showed proneness to brittle fracture. This is not favourable in terms of material criteria for tissue expanders as structural stability is needed to withstand both constant skin tension and various external pressures. For these reasons the hydrogel with 99:1 VP/MMA is not useful even though it showed great swelling capability. For the tougher gels with PMMA wt% > 5, surface polishing or any other forms of surface treatment could be an easy way of preventing premature failure.

As discussed in the literature, the equilibrium swelling degree and the elastic modulus of a hydrogel can be related to the cross-linking density [6, 25, 33]. In this study, this is calculated as the number of cross-links per unit volume. With an increase in cross-linking between network chains, the material tends to become stronger but at the expense of its expandability. The effective cross-linking density (v_e) and the average molecular weight between cross-links (M_c) are experimental quantities that can be calculated by using the elastic modus and the corresponding swelling ratio. These network parameters can be calculated using the following equations:

$$G = v_e RT Q_v^{\frac{1}{3}} \text{ and } \quad M_c = \rho / v_e \qquad \text{Eq. 3.41}$$

where ***G*** is the compressive modulus, ***ρ*** is the density of dry gel, and $\boldsymbol{Q_v}$ is the volume swelling ratio [6, 25]. Table 3.42 shows the calculated v_e and M_c for fully swollen 90:10, 95:5, and 99:1 VP/MMA samples at 294 K.

Table 3.42: Gel network parameters of fully swollen VP/MMA gels at 294 K.

VP:MMA	$E_{2.5\%}$ (kPa)	Equilibrium Q_v	$v_e \times 10^3$ (mol dm^{-3})	ρ - dry gel (kg dm^{-3})	M_c (kg mol^{-1})
90:10	40.3	8.7	33.9	1.09	0.0322
95:5	22.5	11.4	18.9	1.12	0.0595
99:1	14.8	14.1	12.5	1.16	0.0926

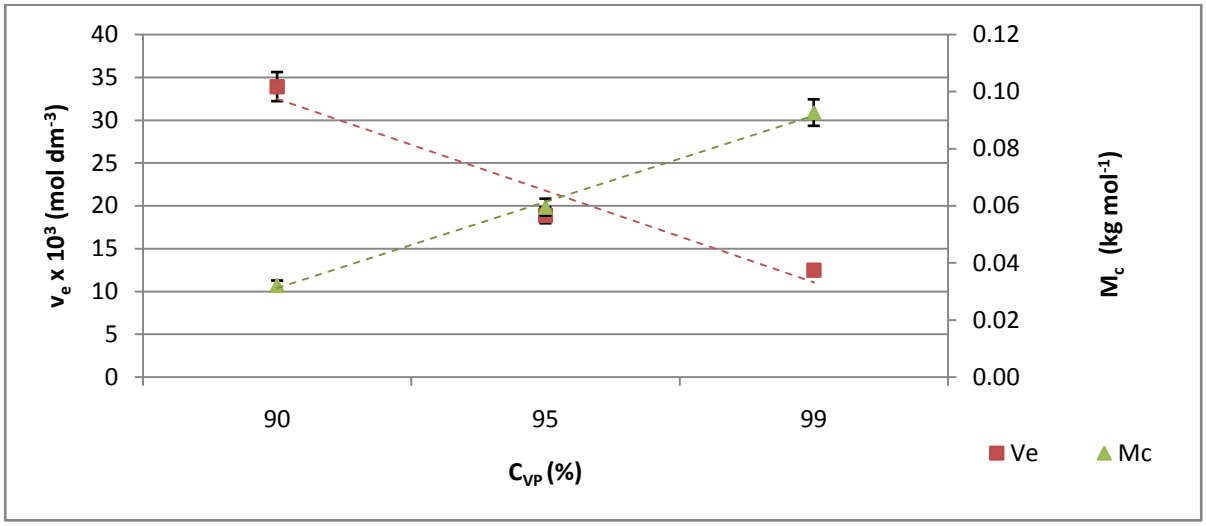

Figure 3.43: Plot of effective cross-linking density and molar mass per cross-link over change in wt% VP.

The two plots on figure 3.43 showed the changes in v_e and M_c with wt% of VP. A linear decrease is observed in cross-linking density as VP composition is increased from 90 to 99 wt%. This behaviour can be described by the increase in water uptake from having more hydrophilic material within the gel. The larger amount of water intake suggests that most volume is occupied by water molecules and hence the decrease in cross-linking density. This is supported with the increase of M_c. As suggested by $M_c = \frac{\rho}{v_e}$, this increase in mass between cross-links

has a reciprocal relationship with cross-linking density. The higher increment of M_c (fig. 3.33) showed us clearly the importance of cross-linking density as it can greatly affect the chain structure. With such a large deterioration in structure as the gel reaches a certain composition, it is important to have this information as a reference for material selection so that the desired behaviour is optimised. This relationship is depicted on figure 3.44 where the M_c is increased exponentially with linear decrease of cross-linking density. We can see that reducing the number of cross-links will result in higher molecular weight between cross-links. This is due to the length of cross-links being longer each time adjacent cross-links are removed.

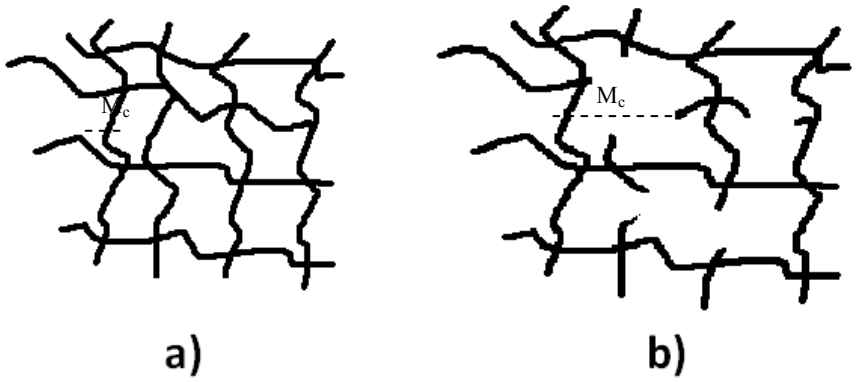

Figure 3.44: Schematic network of gel structure between a) a hydrogel with less hydrophilic composition b) a hydrogel with more hydrophilic composition

3.3.4 Force Measurements

90:10 and 99:1 VP/MMA samples were subjected to swelling force measurements under stationary plates attached to a load cell. Each sample was machined to cylinders with 5.77mm diameter and 6.00mm height and was tested at different plate gap starting from dry gel in full contact between the plates. The gel is hydrated in distilled water at 294 K where swelling force is measured until equilibrium. The plate is moved upwards in steps where a new dry sample is changed for every variation in plate displacement. The force is measured up to the maximum

swelling height where gel is barely in contact with the elevated plate. The measurement is described in figure 3.45.

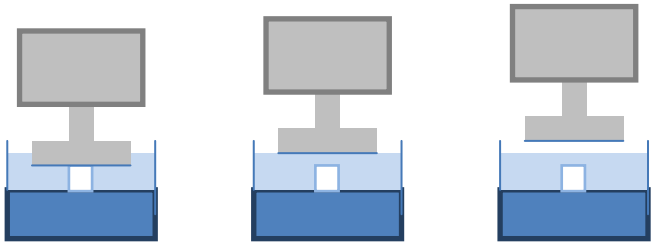

Figure 3.45: Schematic of force measurement set-up with change in plate height. Each gel sample will swell to press the compression plate giving force readings.

The final swelling stress at equilibrium at different swelling degree is shown in figure 3.46. The swelling force measured is decreased with each step increment of the plate height until no force is recorded. This result display that stress is highest when there is restriction to swelling. The maximum stress that can be created from water uptake is shown from the gel that is fully constrained between fixed plates. This is apparent for both compositions which have a maximum stress of 64.0 ± 3.2 kPa and 30.8± 1.5 kPa for 90:10 and 99:1 VP/MMA respectively.

a)

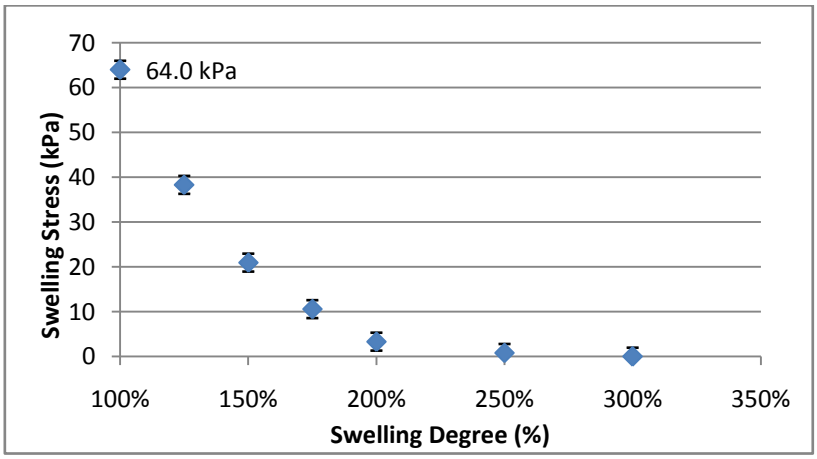

b)

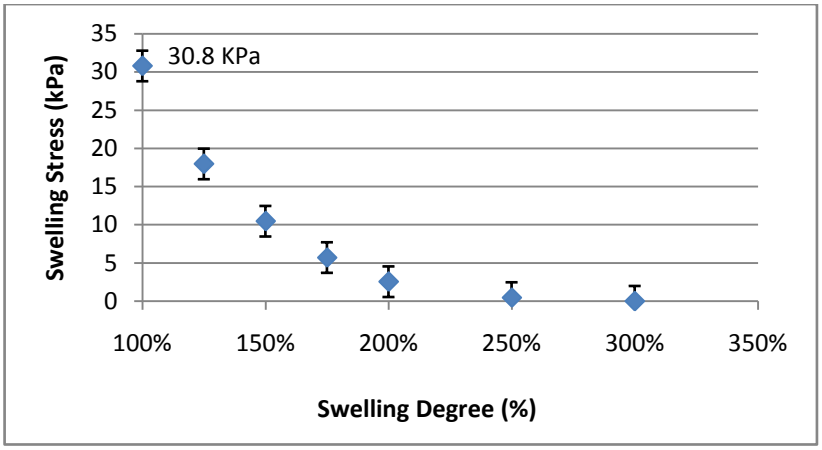

Figure 3.46: Experimental results of swelling stressover plate displacement for a) 90:10 and b) 99:1 VP/MMA hydrogels. At 100% plate displacement, the dry gel is in full contact between base and plate.

The values of the calculated swelling stress between 90:10 and 99:1 VP/MMA suggested that the 99:1 gel with higher swelling ratio does not exert more force but actually less force under the same initial conditions. With information from this force measurement, it can be said that between 90-99 wt% VP (10-1 wt% PMMA) the hydrogel with more VP composition will be the less effective material in terms of stress generation. This was shown by measuring the maximum swelling stress for intermediate compositions under the same experimental conditions. The change can be seen in figure 3.47 where the swelling stress is decreased with increasing VP ratio. This is due to increasing the water soluble VP content over the stiffer and hydrophobic PMMA. In addition to this reduction in structural strength, the higher swelling ratio of better swelling gels means a larger final surface area which will reduce the final stress ($\sigma=F/A$).

The swelling stress measured as the gel expands from dry to fully swollen can then be compared to the compressive stress that was measured from the stress-strain curve to confirm

if the swelling force of gel is completely elastic. The compression stress at swelling equilibrium was extrapolated from figure 3.39 to compare with force measurement results.

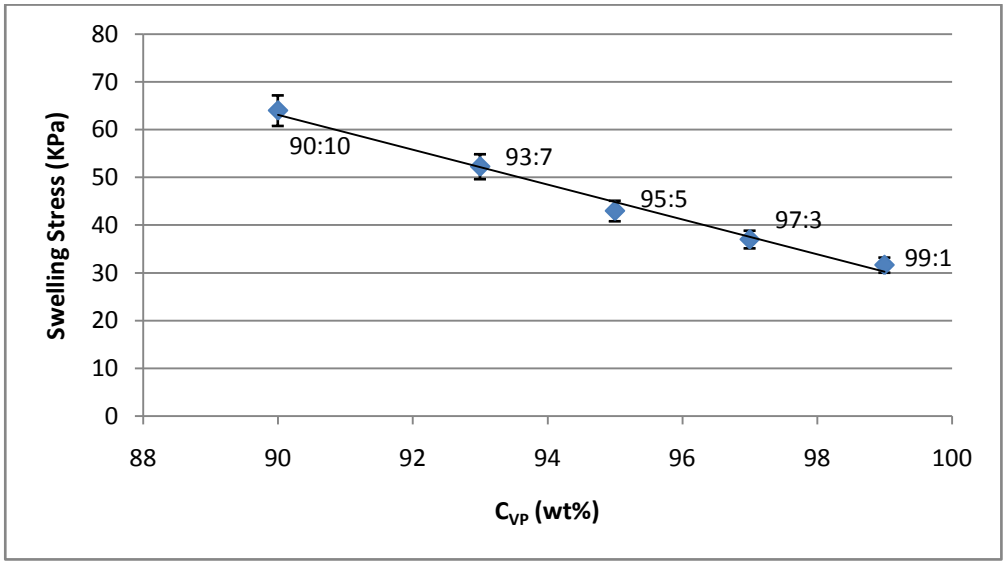

Figure 3.47: Graph of equilibrium swelling stress over changes in VP/MMA ratio (between 90-99 wt% VP).

Table 3.48: Swelling stress and compressive stress at same percent straining. The strain values were calculated from the equilibrium swelling height and the plate distance when fully in contact with the dry sample (6.00 ± 0.10 mm)

.

Sample (VP:MMA)	Percent strain at swelling stress (%)	Swelling stress (kPa)	Compression stress for same strain (kPa)
90:10	52.5	64.0 ± 3.2	64.7
95:5	55.6	43.0 ± 2.2	39.1
99:1	59.9	30.8 ± 1.5	16.2

One of the questions raised from the swelling force measurements is whether the mechanism behind generation of swelling force is totally elastic; i.e is the stress generated onto our loading plate equal to the stress required to compress the gel to the same strain. By comparing the swelling stress with the stress taken from an experimental stress-strain curve, we can see from table 3.48 that there is little difference between the two values for 90:10 and 95:5 VP/MMA samples but a notable difference in the 99:1 VP/MMA sample. The maximum stress generated

from 99:1 VP/MMA gel when left to self expand is 30.8 ± 1.5 kPa while the stress to compress a swollen gel to the same amount of strain is 16.2 kPa (table 3.48). This showed that there is at least one other form of swelling mechanism that can generate a measurable force apart from the elastic contribution. The result here brings the mechanism in generating swelling force to the mixture between diffusional and relaxational forces. This coincides with the results obtained from the mass transport investigation of our hydrogels.

As the hydrogel is being constrained and not allowed to swell freely, the chain is subjected to a different relaxation force which is now a balance between osmotic force and the force that the gel is pushing on the plate. This will limit the diffusion process resulting in reduced water transport. As this occurs, the material will have less amount of plasticizer and should have a greater stiffness than a fully swollen gel. This appeared to be more apparent in 99:1 VP/MMA samples with higher swelling properties and less so in hydrogels with more PMMA content.

99:1 VP/MMA hydrogels were used for investigating swelling pressure with respect to a change in volume. Samples were machined into cylinders of different size while maintaining the radius to height ratio. Volume of xerogel is increased up to 3 times and was fully constrained by the compression plate before being hydrated to measure the swelling force.

Table 3.49: Initial dry gel dimensions for measurement of swelling stress with change in volume

Volume (mm^3)	Initial Diameter (mm)	Initial Height (mm)
156.9	5.77	6.00
235.2	6.60	6.87
313.6	7.27	7.56
470.8	8.32	8.65

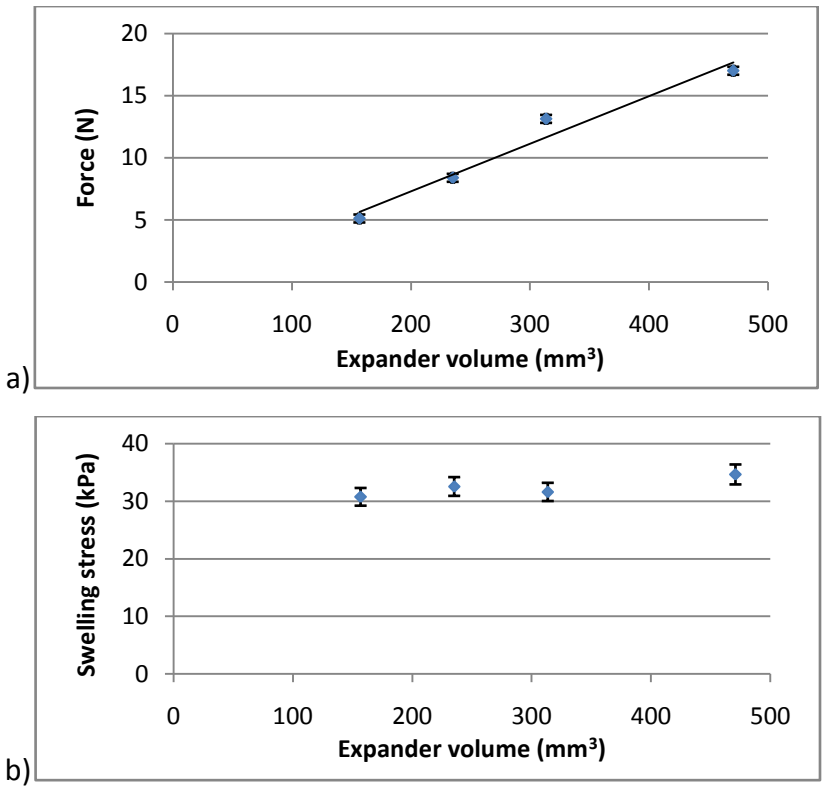

Figure 3.50: a) Equilibrium swelling force plotted against initial gel volume b) Equilibrium swelling stress plotted against initial gel volume.

The result showed a linear increase in swelling force with increasing volume (figure 3.38a). However, when the stress is calculated by force over the swollen area in contact with measuring plate, it is shown that the swelling stress at equilibrium does not significantly change and is between 30.7-34.7 kPa (figure 3.50b). This showed that the stress generation of the material is more or less volume independent and will generate a predictable swelling stress if composition and geometry is fixed. The main difference observed with volume variation is the rate of swelling. Although having the same surface area to volume ratio, equilibrium swelling state took longer to reach for larger gels due to thicker swollen gel region which acts as a semi-permeable membrane (fig 3.51).

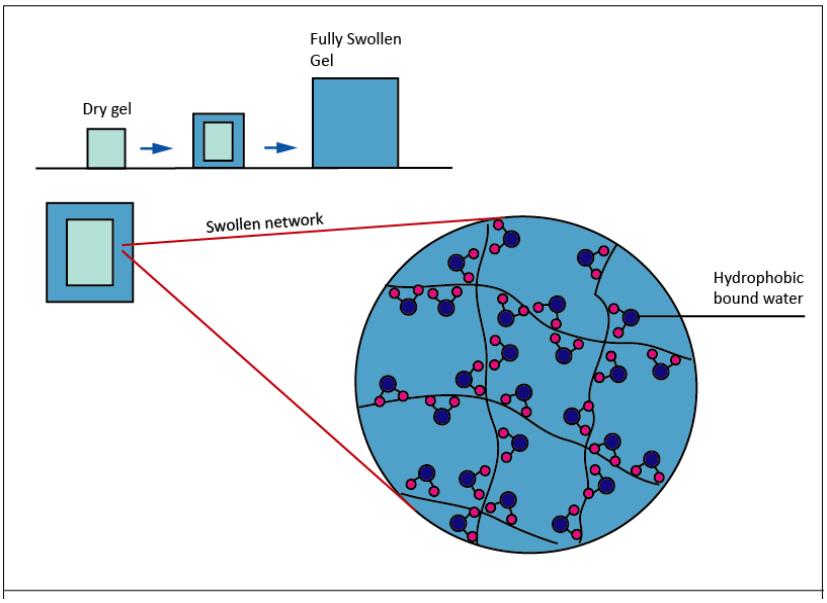

Figure 3.51: Schematic of swollen gel network with bound water

The swelling force developed by swelling of hydrogels has been studied by number of investigators using a similar technique [34-36]. Peppas and Colombo expressed their force measurements in terms of diffusion and relaxation controlled mechanics which is comparable to the Power Law (Eq. 3.22) [37]. However, the results they obtained are in agreement to the case of swelling force generation being totally diffusion controlled where the force is greater in a material that has higher diffusion coefficient. The swelling stress, *σ(t)*, was expressed by Dubroskii et al. showing relationship with diffusion coefficient through the equation [36]:

$$\sigma(t) \sim 1 - \exp\left(\frac{-t}{\tau}\right) \qquad \text{Eq. 3.52}$$

where τ is a characteristic swelling time using the radius (R) and diffusion coefficient (D) expressed as:

$$\tau = \frac{R^2}{2.05\pi^2 D}$$

By using Equation 3.52, the approximation of the swelling stress with time model showed the similar trend but does not predict the exact experimental swelling behaviour (figure 3.53). The

model expressed by Dubroskii et al. does not incorporate the stress relaxation properties of swelling which is present in anomalous diffusion. The VP/MMA samples in our case showed that the initial force generated is relaxation controlled. This is shown in graphs of swelling force against hydration time (figure 3.53a). Unlike the expected increase in force before gradually reaching equilibrium of such a typical diffusion curve, the plot of force against time shows an initial sharp peak in force before a noticeable decrease (0-2 hours). This force peak demonstrated that the swelling force cannot only be diffusion controlled but also controlled by notable softening of gel upon swelling. This decrease in force has not been observed in previous studies [34-37].

The peak observed was even more apparent when initial gel volume is increased 3 times. The force recorded for this peak is higher than force at equilibrium swelling (figure 3.53b). This is due to the larger surface area which gives more contact with water for faster initial swelling and a larger unhydrated core in which overall gel network is more slowly plasticised. This is different from the final stress of fully swollen gels where the magnitude of stress is independent of expander size (figure 3.50).

a)

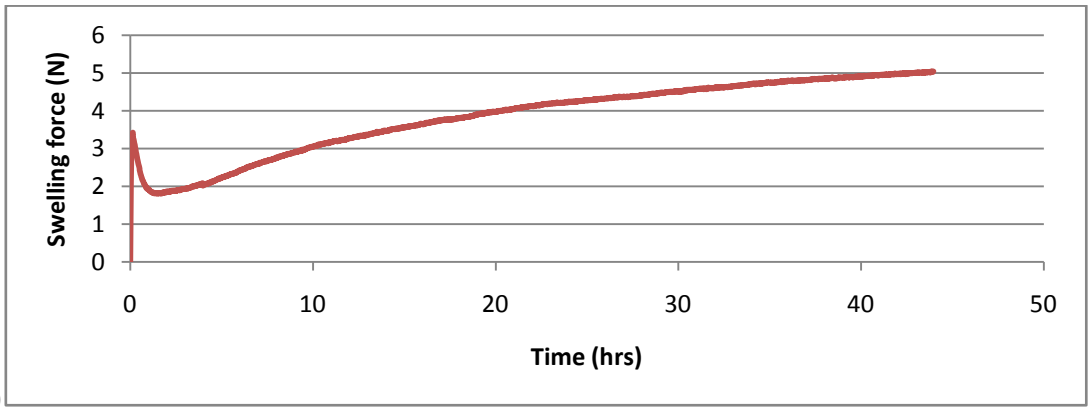

b)

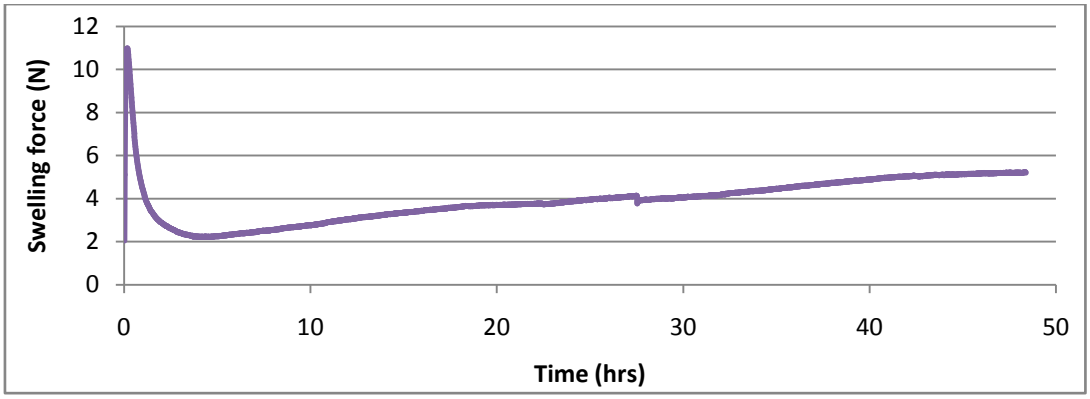

Figure3.53: Swelling force over hydration time of a) 90:10 hydrogel and b) in larger 90:10 hydrogel sample

It is shown from swelling force against time graphs (fig. 3.53a and 3.53b) that the swelling force of our hydrogel system is a function of diffusion and elastic modulus. This relationship is shown when the large and rapid decrease in modulus (E) discussed earlier is incorporated with the mass uptake (Q_m) curve. Figure 3.54 demonstrates the two key changes to the hydrogel material that effect the swelling force generation. The peak at the initial stage from the force vs. time graph is due to the high modulus where the hydrogel is still mostly glassy. Due to its greater stiffness, a small swelling degree is enough to generate high swelling force. However, as swelling continues, the gel is rapidly soften and hence more easily deformed. The force at this point is no longer greatly affected by the modulus change. At this point swelling force is dominantly controlled by water transport and the expansion of gel.

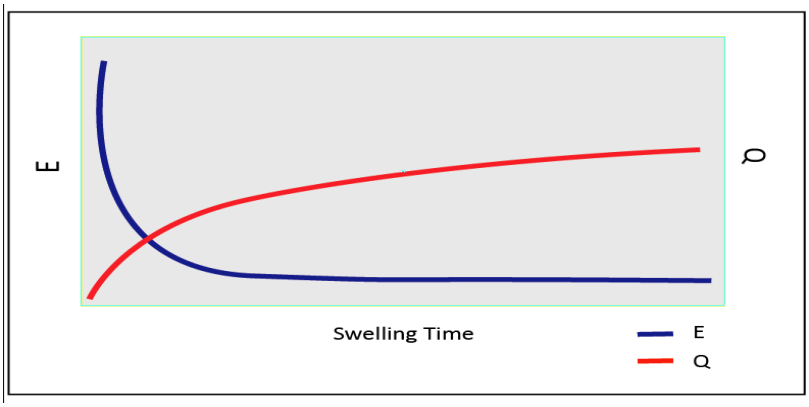

Figure 3.54: Comparison between modulus (E) and swelling ratio (Q) over hydration time.

The swelling stress due to elastic modulus (E) and compressive strain (ε) over swelling time can be added to the model derived by Dubroskii (Eq. 3.52) to fully represent the stress generation. The addition of material strain to this value incorporates the opposing factor to swelling and the effect it does to the equilibrium swelling degree. The total swelling stress (σ) is represented as:

$$\sigma(t) = \sigma_{\tau} + \sigma_{E} \qquad \text{Eq. 3.55}$$

where σ_E is the stress due to elastic modulus change and σ_τ is the stress obtained from solute diffusion.

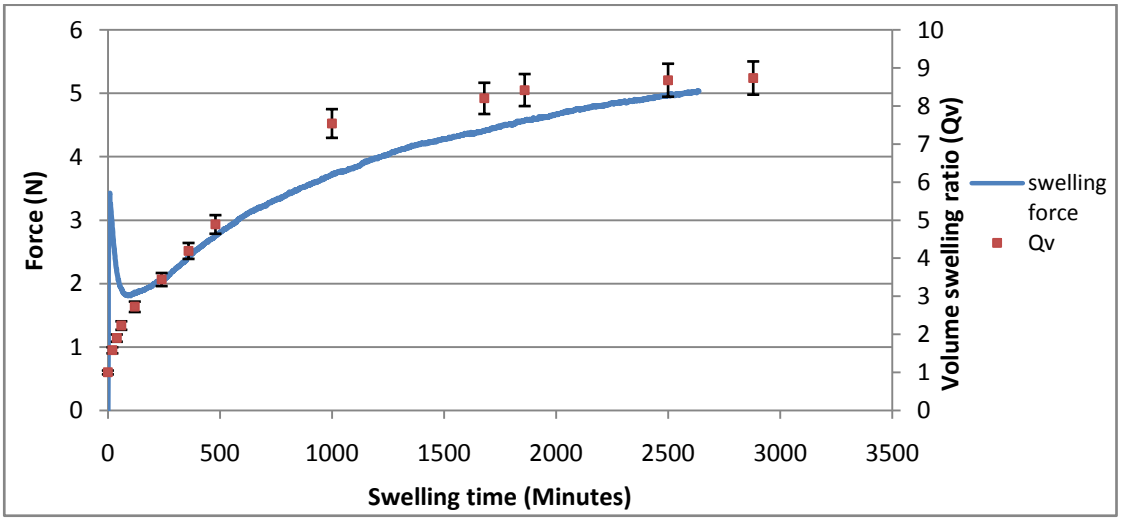

Figure 3.56: Swelling force and volume swelling ratio (Q_v) plotted against time.

With measurements of the swelling ratio at the corresponding times, the relationship between force and the volume swelling ratio can be seen in figure 3.56. The initial force peak is shown when the gel is swelling to 2-3 times the initial volume while the maximum swelling volume ratio is 8.7. This is at about 25% of the total swelling volume which may affect the device functionality for tissue expansion due to an initially high swelling pressure. This force peak can

be removed by slowly pre-hydrating the gel with very small amount of solvent. The result of this is a softer gel with reduced modulus and no glassy core. This is however in sacrifice of the swelling behaviour as gel is already partly swollen.

3.3.5 Thermal Properties of VP/MMA

A solution to avoid overly fast straining of the overlying skin is by creating an anisotropically swelling gel that has an initially disc-like shape. By having gels that can swell in one direction, the initial height of the implanted device can be made smaller due to significantly larger swelling capability. To introduce anisotropy, the gels will need to be compressed under heat treatment at temperature around its T_g. Prediction of the T_g can be made using the Flory-Fox and the Gordon-Taylor equation [18, 19, 20]. Using the Flory-fox equation (Eq. 3.28) and the known T_g of cross-linked PVP (T_g=185-190°C [43]) and atactic PMMA polymers (T_g=101-108°C [43]), the T_g of 90:10 VP/MMA is estimated to be between 171-177°C. An almost identical range of T_g was calculated using the Gordon-Taylor equation (Eq. 3.29). The T_g of different VP/MMA ratios were also calculated and shown in table 3.57. Due to the much higher weight ratio of the PVP polymer, the T_g of the hydrogel system is clearly closer to the T_g of pure PVP.

Table 3.57: Predicted glass transitional temperature (T_g) of VP/MMA hydrogels using the Flory-Fox and Gordon-Taylor equation.

VP/MMA Ratio	T_g^{FF} (°C)	T_g^{GT} (°C)
90:10	171-177	171-176
93:7	175-180	175-180
95:5	178-183	178-183
97:3	181-186	180-186
99:1	184-189	183-189

The thermal properties of VP/MMA dehydrated gels were characterised using thermogravimetric/differential thermal analyser (TG/DTA) and differential scanning calorimetry (DSC) to confirm the T_g. Figure 3.58 shows the TGA curve of 90:10 VP/MMA hydrogel heated from 20-600°C at 20°C/min. The data shows a continual decrease in mass until about 370°C where the gel begins to decompose. The broad range in weight loss shown on the mass spectrum is solely due to the evaporation of moisture and was not associated with material decomposition [44]. TGA spectra of other VP/MMA samples with more VP content were also tested and showed the same trend.

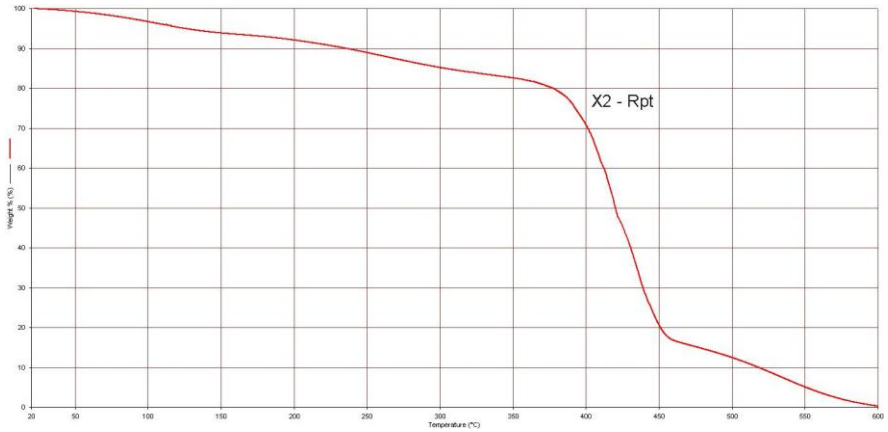

Figure 3.58: TGA mass spectrum of dry 90:10 VP/MMA gel.

DSC traces of 5 different gel compositions heated at 100°C/min were obtained. DSC trace of a 90:10 VP/MMA gel is shown in figure 3.59. The T_g can be assigned from the step in the baseline where the temperature was taken from the corresponding inflection point. The T_g for 90:10 was taken to be 150.31°C which is lower than the values predicted using the Flory-Fox and Gordon-Taylor equation (table 3.57). The experimental T_g acquired from DSC is summarised in table 3.60.

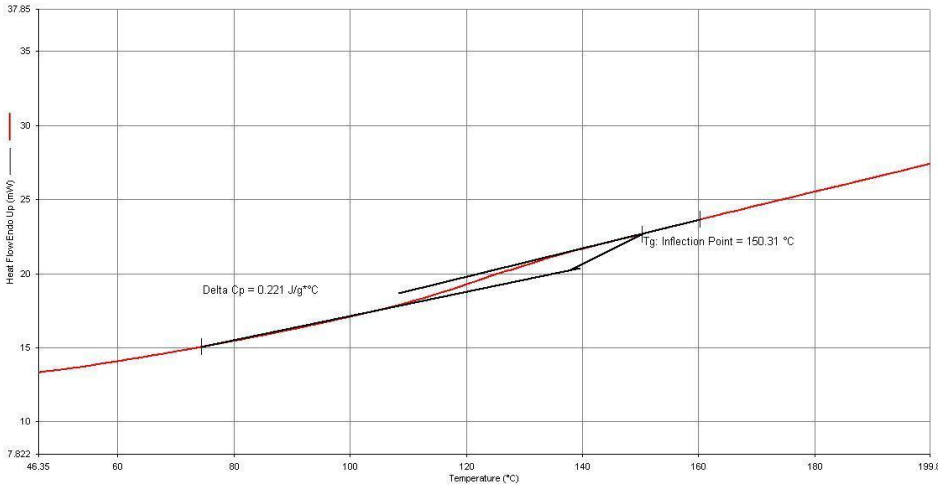

Figure 3.59: DSC trace of dry 90:10 VP/MMA gel heated at 100°C/min from 0-300°C

Table 3.60: Glass transitional temperature of VP/MMA gels

VP/MMA Ratio	T_g (°C)
90:10	150.31
93:7	150.35
95:5	160.34
97:3	142.13
99:1	149.81

By comparing the predicted T_g of the VP/MMA co-polymer which was calculated using T_g from literature [43] with the T_g that is taken from our DSC result, it is evident that the actual T_g of these hydrogels are significantly lower and extremely sensitive to the heating rate. When heated at a reduced rate of 50°C/min, the DSC trace becomes broad and smooth to an extent that the step in baseline used to calculate the T_g is no longer apparent.

An explanation to this irregularity is due to the presence of moisture content that was the cause of weight loss shown on the TGA spectrum (figure 3.58). The value of T_g is a function of water content where a small amount of moisture within the gel can greatly reduce the overall T_g [44]. As the gels were heated under the DSC, the T_g will shift higher as overall water content is

reduced due to evaporation. This is the reason why it was difficult to find T_g at slower heating rates. Due to this change in T_g with respect to the water content, the best T_g for our anisotropic modification of the gel is the intermediate between the experimental T_g and the T_g calculated from known references (150-175°C for 90:10 VP/MMA).

3.3.6 Anisotropic Swelling Modification

90:10 VP/MMA xerogels were heated to 164°C in a thermostatically controlled hydraulic press (Specac Ltd.) for 60mins before compressing at 100MPa. The compressed gels were held constrained at the temperature for further 60min before allowing the gel to cool to room temperature. The final hydrogel after this process is a gel that will restore most of its geometry once hydrated. This is shown in figure 3.61. Investigation on the swelling behaviour after heat treatment and compression was made by measuring the swelling force and varying the compression ratio.

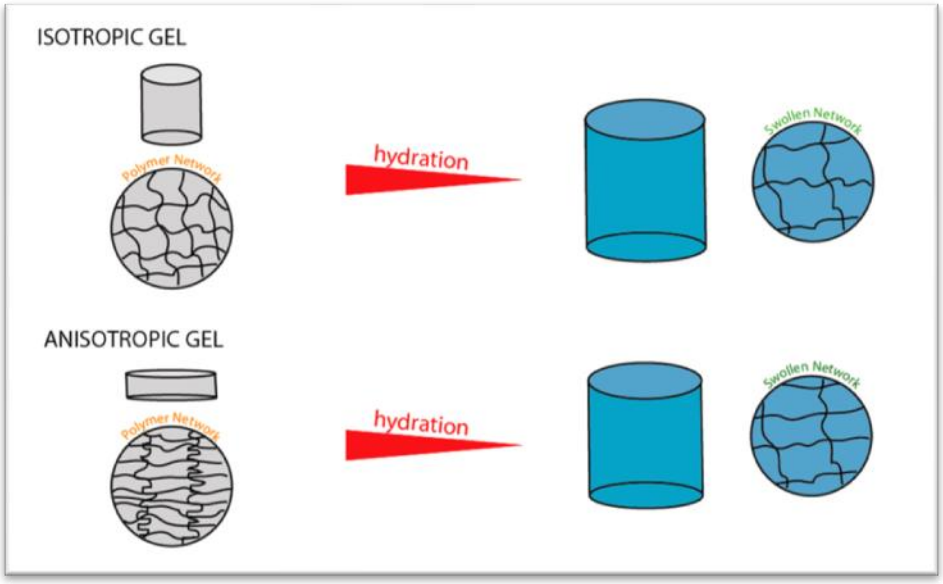

Figure 3.61: Schematic comparing the network of isotropic swelling and anisotropic swelling gels.

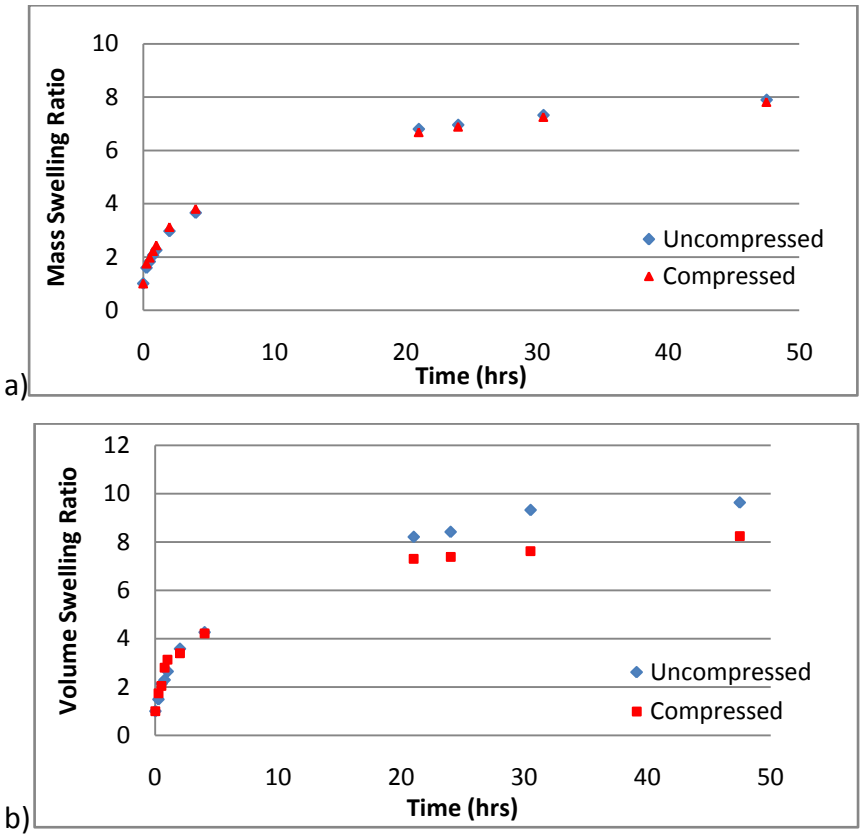

Figure 3.62: a) Mass and b) volume swelling ratio of compressed and uncompressed hydrogels.

The rate of swelling and diffusion was investigated by comparing the swelling ratio (Q) between compressed and uncompressed gels. Figure 3.62a showed that there was no significant difference in mass uptake between the two gels; hence a similar diffusion mechanism is likely to be occurring. However, it is shown in figure 3.62b that the overall volume swelling ratio is decreased when the dimensions were measured over the hydrating process. This shows that there were some permanent structural changes during anisotropic modification.

While soft and rubbery at $T_{g,}$ the gels were slowly cooled to room temperature and will return to its glassy state. The strain energy stored during this cooling process is the main mechanism of anisotropic swelling. As this internal stress gets higher, it is evident that the gel network,

which was stretched in radial directions, can be permanently deformed. This is why the compressed gels did not expand to the same Q_v compared to its unmodified counterpart.

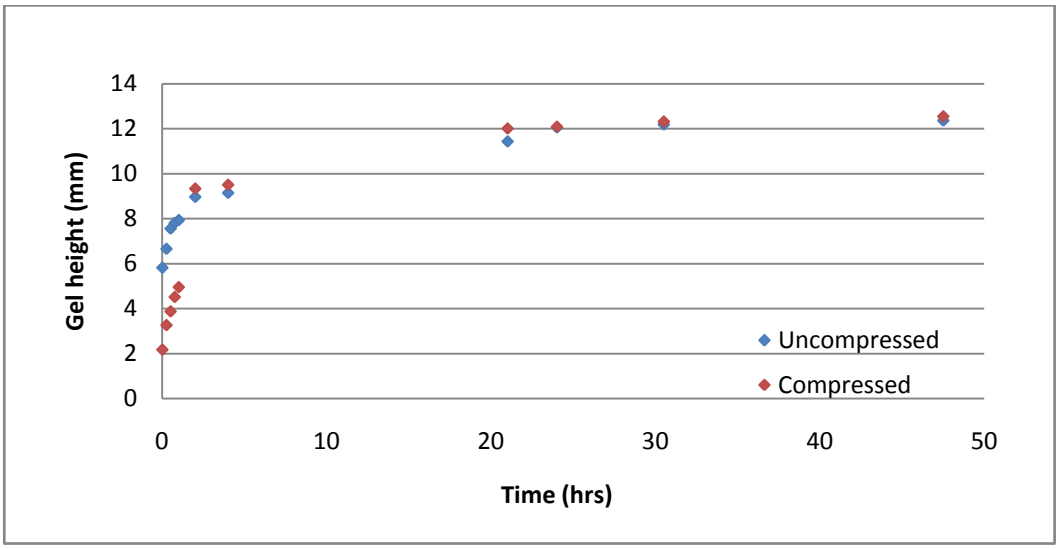

Figure 3.63: height of compressed and uncompressed gels over hydration period.

The advantage of anisotropic gel is the ability to swell in one direction. The height of the initial gel is smaller with a thicker base as a result of compression. The expander height measurement over swelling process is shown in figure 3.63 (note that the compressed gel started expansion from 2.0 mm thickness). Depending also on the co-polymeric composition, VP/MMA isotropic gels can expand 2-3 times its initial dimension while anisotropic gels showed expansion up to 6-8 times in the desired direction.

The change in compression ratio was investigated by compressing the gel from different heights as shown in table 3.64. The diameters of the compressed samples were then later polished to the same diameter for comparison. The 'compression ratio' is calculated as the ratio between the initial gel height and the compressed height.

Table 3.64: Samples for testing effect of heat treatment and compression

Samples	Compression Ratio	Height pre-compression	% compressed strain
1	1.00	6.00	0
2	1.18	7.00	15
3	1.43	8.57	30
4	1.82	10.91	45
5	2.50	15.00	60

Although the dry gels were initially cut into same sized cylinders, the magnitude of compression during modification showed that the vertical expansion is much greater for gels that were deformed at higher compression ratio. Due to higher strains experienced from the expansion onto the load cell and the reduced radial expansion due to anisotropy, the force record from the anisotropic gels was measured to be higher than the isotropic gels. This increase in swelling stress is shown in the first three points in figure 3.65.

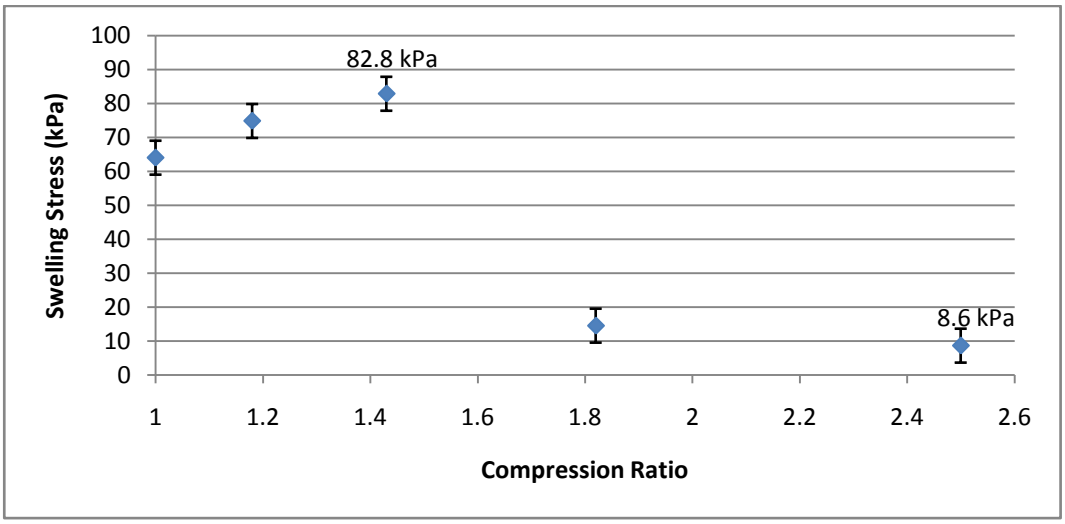

Figure 3.65: Swelling stress versus compression ratio of modification. The first three points showed stress increment with compression ratio while samples with greater compression ratios resulted in buckling of the gels cylinders.

As the diffusion rate of gels with the same composition is independent of the compression ratio (figure 3.62a), the swelling force increment observed must be due to chain relaxation and the stored stress during modification. The increase in swelling force is however limited by high

internal stresses after the compression process. These residual stresses may be high enough to cause fracture of the hydrogels either pre-or post- hydration.

Another limitation that was observed in using anisotropic gels is the buckling of gel cylinders. This was observed in the two samples with higher compression ratios (figure 3.65). The occurrence of buckling means that there is a limit to the shape of swelling gels under the force it generates. This is important for maintaining structural stability of gels. For cylindrical shape materials, this geometrical consideration is called the 'slenderness ratio' [38]. This is the ratio between the length and radius.

Euler (1757) derived a formula that predicts the maximum axial load that an ideal column can withstand without buckling [38].

$$\sigma_{\text{crit}} = \frac{F}{A} = \frac{\pi^2 E}{(l/r)^2} \qquad \text{Eq. 3.28}$$

where $\boldsymbol{\sigma_{crit}}$ is the critical stress, $\boldsymbol{E}$ is the Young's modulus, and ($\boldsymbol{l/r}$) is the slenderness ratio.
From Eq. 3.28 and the measured gel modulus, the theoretical stress before buckling for fully swollen gels can be plotted over a series of slenderness ratios (figure 3.66). With the known amount of swelling stress generated it is possible to predict if the gels will self-buckle during the swelling process. The maximum slenderness ratio for 90:10 VP/MMA gels is predicted to be around 6 while for the softer 99:1 VP/MMA gels the maximum slenderness ratio is about 4. Beyond these respective values the gels are considered theoretically unstable and could fail due to buckling [38].

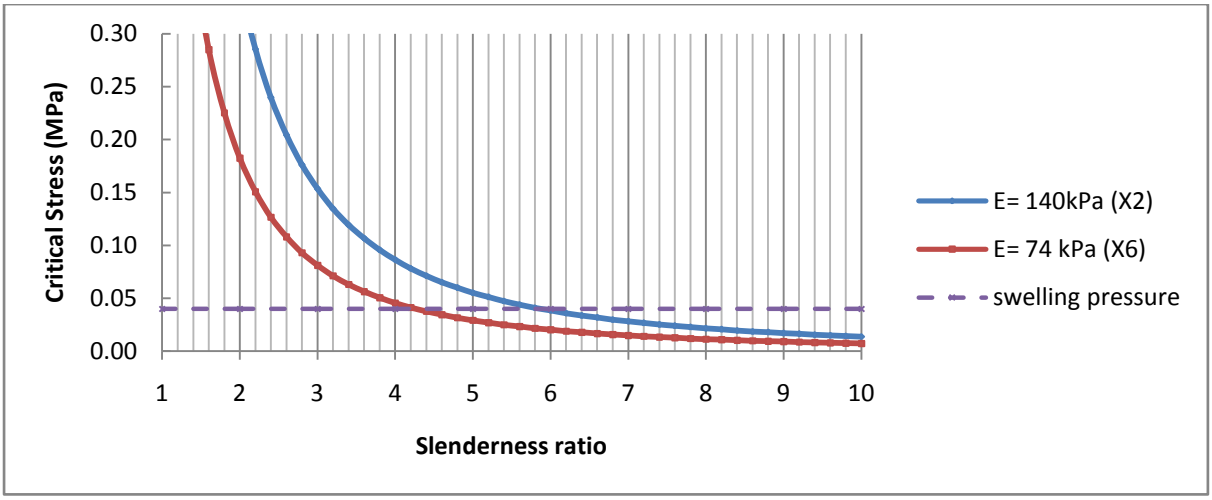

Figure 3.66: Euler's approximation curve for fully swollen 90:10 and 99:1 VP/MMA gels

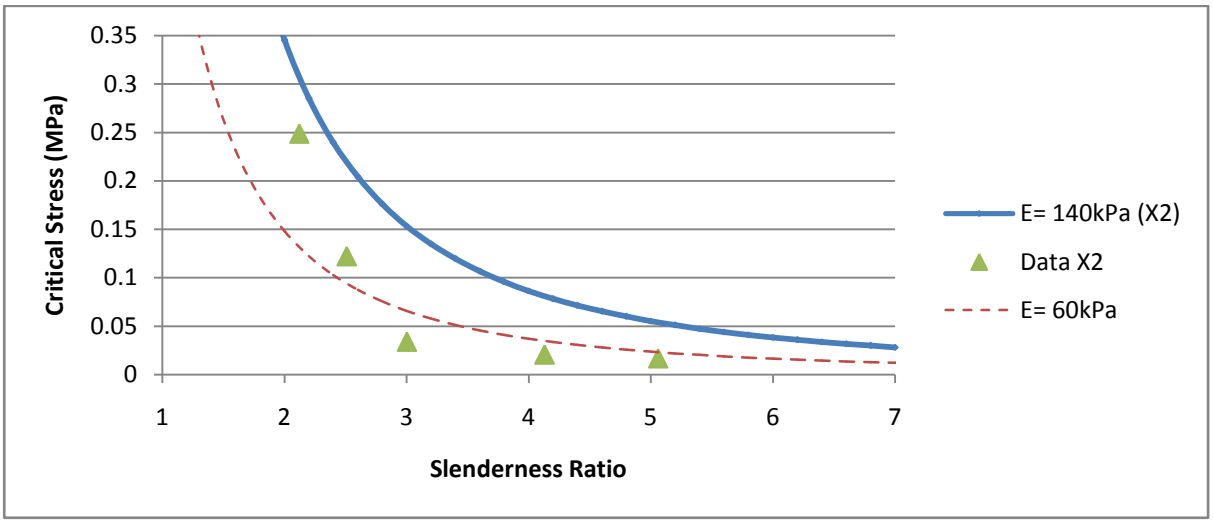

Figure 3.67: Euler's approximation curve and plotted experimental data for fully swollen 90:10 VP/MMA gels

The model derived by Euler is compared to experimental data where 90:10 VP/MMA gels were tested for buckling by varying the slenderness ratio (figure 3.67). The result shows a large difference between the model and the experimental result as the critical stress is much overestimated with the Euler's approximation. This is due to the following factors:

1) The model is derived for an ideal column of perfect geometry whereas the samples made will always have imperfections.
2) The model is derived for samples with linear stress-strain behaviour while the formula does not consider the non-linear stress-strain behaviour of such hydrogels.

3) There is no consideration of material's own weight.
4) The hydrogel surface has low friction in water where slippage may occur before buckling.

Due to these factors the experimental data is in fact more matched to the approximation when modulus is reduced to about 60kPa (figure 3.45). This is less than half the measured modulus of 90:10 VP/MMA hydrogel. Due to this uncertainty, there are safety factors or design considerations in which can be introduced. One of these safety considerations is the Rankine Gordon formula which gives a conservative value for the maximum stress (σ_{max}) [39].

$$\frac{1}{\sigma_{max}} = \frac{1}{\sigma_e} + \frac{1}{\sigma_c} \quad \text{Eq. 3.29}$$

where σ_e is the experimental critical stress and σ_c is the maximum compressive stress.

While the safety factor is incorporated, it is also necessary to think about the external forces that may be present when a tissue expander is in use. These forces may vary on different body areas and also the daily activities of patients.

3.4 Chapter summary

The use of hydrogels as tissue expanders is a new method in acquiring extra skin in reconstructive surgery. It is a method which can promote new skin that is grown from an adjacent area by using expanding pressure as a skin-growing stimulus. The newly formed skin will be a skin of natural tone and texture where these qualities were not made possible from typical skin grafting. The swelling behaviour and the measurement of swelling stress of various

VP/MMA hydrogel compositions were investigated in this chapter as it is important to quantify the mechanical function of such a medical device to see how it would fit its potential use.

The mass transport between VP/MMA hydrogels and the swelling solvent proves to be the key explanation to the mechanism of swelling where gel swelling is the balance between two main driving forces; the relaxation of the gel network and the osmotic diffusion of solvent due to gel hydrophilicity. By applying the Power Law (Eq 3.22) to mass uptake data, it was clear from the diffusion exponent that diffusion is 'anomalous' at most times until an equilibrium is reached. The diffusion coefficients of 90:10, 95:5 and 99:1 VP/MMA gel compositions were extrapolated from linear portion of the mass uptake.

Different compositions of VP/MMA were used in the range of 90-99wt% VP. The swelling ratios were increased and the moduli were decreased for gels with more VP composition. The increased in swelling ratio is due to more hydrophilic groups which can absorb more solvent. The increase in water content leads to a softer material due to greater chain to chain distance which is also observed as reduced cross-linking density.

The uniaxial swelling force was measured in gels of different compositions and volume. The results show that gels with a higher modulus will generate more swelling stress than gels that are softer even when the swell ratio is less. This contradicts with previous literature that suggested that the swelling pressure is more diffusion controlled and hence always higher in gels with larger swelling capability. This was not observed from our gels where gel stiffness is also greatly important in force generation. However, it is also evident that for samples with a high swelling ratio, the swelling force is beyond the value of normal elastic considerations. The

force generation from a swelling gel can be summarized in terms of decreasing modulus and increasing solvent uptake.

While the natural property of hydrogels is to swell in an isotropic fashion, anisotropic swelling can be modified into these gels by heat treatment and compression. The swelling force of these modified gels was measured which showed larger force generation due to a higher amount swelling and straining in the measured direction. The anisotropic gels also showed less volumetric expansion compared to isotropic gels. This is because of some plastic deformation and alignment in structure as gels were cooled from a highly deformed state. This marked the limit to gel processing where the maximum amount of anisotropy that can be induced is related to dry gel elasticity.

The buckling of VP/MMA was investigated as a safety measure. The experimental buckling showed that the critical stress calculated from Euler's approximation is highly overestimated mainly due to the non-ideal shape and low friction surfaces of gels. A safe shape for tissue expander is a short cylinder with slenderness ratio below 2.5.

3.5 Chapter 3 references

1) Refojo MF. Hydrophobic Interaction in Poly(2-hydroxyethyl Methacrylate) Homogeneous Hydrogel. J. Polym. Sci., 5:3103-3113, 1967

2) Weise KG. Osmotically induced tissue expansion with hydrogels: a new dimension in tissue expansion? A preliminary report. *J of Craniomaxillofac Surg*, 21:309-313, 1993

3) Peppas NA and Franson NM. The swelling interface number as a criterion for prediction of diffusional solute release mechanisms in swellable polymers, J. Polym. Sci., Polym. Phys. 21: 983-987, 1983

4) Khare AR and Peppas NA. Dynamic and equilibrium swelling characteristics of hydrophilic copolymers with carboxylic functional groups. Absorbant polymer Technology pp. 223-232, Elsevier, New York, 1990

5) Swan MC, Bucknall DG, Goodacre TEE, and Czernuszka JT. Synthesis and properties of a novel anisotropic self inflating hydrogel tissue expander. Acta Biomaterialia, 7:1127-1132, 2011

6) Lee JH, Bucknall DG. Swelling behaviour and network structure of hydrogels synthesized using controlled UV-initiated free radical polymerization. J. Polym. Sci., Polym Phys, 48:1450-1462, 2008

7) Peppas NA. Hydrogels in Biomaterial Science 2nd ed. Academic Press, 2004

8) Downes R, Lanvin M, Collin R. Hydrophillic expanders for the congenital anophthalmic socket. Adv Ophthalm Plast Reconstr Surg 1992;9:57-61

9) Volker B. Excipients for Pharmaceuticals - Povidone, Crospovidone and Copovidone. Springer. 1–254, 2005

10) Kaufmann TJ, Jensen ME, Ford G, Gill LL, Marx WF, Kallmes DF. Cardiovascular Effects of Polymethylmethacrylate Use in Percutaneous Vertebroplasty. American Journal of Neuroradiology 23: 601–604, 2002

11) Li H. Smart Hydrogel Modelling1st Edition. XIII, 356 p. 288 illus., Springer 2009

12) Astarita G. Thermodynamics: An Advanced Textbook for Chemical Engineers. Springer 1989

13) Brazel CS and Peppas NA. Synthesis and Characterization of Thermo- and Chemomechanically Responsive Poly(N-isopropylacrylamide-co-methacrylic acid) Hydrogels. *Macromolecules*, 28: 8016–8020, 1995

14) Phillip LR and Peppas NA. A Simple equation for description of solute release I. Fickian and non-fickian release from non-swellable devices in the form of slabs, spheres cylinders or discs. Journal of Controlled Release, 5; 23-36 1987

15) Crank J. The Mathematics of Diffusion. Oxford University Press ,U.K., Chapter 5, 1964

16) Zainuddin, Strounina E V, Hill DJT, and Whittaker AK. Magnetization-prepared NMR imaging of water penetration into poly(vinylalcohol)-poly(N-vinyl-2-pyrrolidone) hydrogels. Polym Int 59:1520-1525, 2010

17) Ghi PY, Hill PY, and Whittaker AK. NMR imaging of water sorption into poly(hydroxyethylmethacrylate –co-tetrahydrofurfuryl methacrylate). Biomacromolecules 2: 504-510, 2010

18) Al-Issa MA, Davis TP, Huglin MB and Yip DCF. Copolymerizations involving *N*-vinyl-2-pyrrolidone. Polymer, 26:1869-1974, 1985

19) Rodriguez F. Principles of Polymer Systems, 4th edition, Taylor & Francis: Washington DC; 1996.

20) Malak MD, Hill JT, and Whittaker AK. Water sorption into poly [(2-hydroxyethyl methacrylate)-co-(1-vinyl-2-pyrrolidone)] at 310 K, Polym Int, 52: 1740–1748, 2003

21) Lowman AM, Dziubia TD, Bures P, and Peppas NA. Structural and dynamic response of neutral and intelligent networks in biomedical enviromants. Advances in Chem Eng, 29:75-130, 2004

22) Achilloes EC, Prud'hommr RK, Christodoulou KN, Gee KR, Kevrekidis IG. Dynamic deformation visualization in swelling of polymer gels. Chem Eng Sci, 55: 3335-3340, 2000

23) Kojima M, Ando S, Kataoka K, Hirota T, Aoyagi K, Nakagami H. Magnetic resonance imaging (MRI) study of swelling and water mobility in micronized low-substituted hydroxypropylcellulose matrix tablets. Chem Pharm Bull, 46: 324-328, 1998

24) Lee JH. Development of an anisotropic swelling hydrogel for tissue expansion: Control over the degree, rate and direction of hydrogel swelling. PhD Thesis, Georgia Institute of Technology, Atlanta, GA, United States, 2008

25) Davis TP, Huglin MB, Yip DCF. Properties of poly(N-vinyl-2-pyrrolidone) hydrogels crosslinked with ethylene glycol dimethacryalte, Polymer, 29:701-706, 1988

26) Chung JT, Vlugt-Wensink KDF, Hennink we, Zhang Z. Effect of polymerization conditions on the network properties of dex-HEMA microspheres and macro-hydrogels. int J Pharm, 288: 51-61, 2005

27) Ganji F, Vasheghani-Farahani S, and Vasheghani-Farahani E. Theoretical description of hydrogel swelling: a review. Iranian Polym J, 19, 375-398, 2010

28) Rossi G, Mazich KA. Kinetics of swelling for a cross-linked elsatomer or gel in the presence of a good solvent. Phys Rev A, 44:4793-4796, 1991

29) Gerhke SH, Biren D, Hopkins JJ. Evidence for Fickian water transport in initially glassy poly(2-hydroxyethyl methacrylate). J Biomater Sci Polym, 6:375–390, 1994

30) Brazel CS and Peppas NA. Dimensionless analysis of swelling of hydrophilic glassy polymers with subsequent drug release from relaxing structures. Biomaterials, 20:721-732, 1999

31) Lawn BR. Fracture of Brittle Solids Second Edition. Cambridge University Press ,U.K., 1975

32) Tominaga T, Tirumala VR, Lin EK, Gong JP, Furukawa H, Osada Y, and Wu W. The molecular origin of enhanced toughness in double-network hydrogels: A neutron scattering study. Polymer, 48: 7449-7454, 2007

33) Okay O. General Properties of Hydrogels. Hydrogel Sensors and Actuators; 1st ed. Springer: Berlin, Germany, 1–14, 2009

34) Khare AR, Peppas NA, Massimo G and Colombo P. Measurement of the swelling force in ionic polymeric networks. I. Effect of pH and ionic content. J. of Controlled Release. 22:239-244, 1992

35) Bell CL and Peppas NA. Measurement of the swelling force in ionic polymeric networks.III. Swelling force of interpolymer complexes. J. of Controlled Release. 37:277-280, 1995

36) Dubrovskii SA, Lagutina MA, and Kazanskii KS. Method of measuring swelling pressure of superabsorbent gels. J. Chem. Phys, 70;1214-1218, 1979

37) Peppas NA and Colombo P, Development of disintegration forces during water penetration in porous pharmaceutical systems. J. Control Release, 10;245-250, 1989

38) Marks R, Berg DM, Eckmann D. General Structures. Kaplan Education, Chicago, IL, Chapter 2, 2006

39) Case J, Chilver H, Ross CTF. Strength of materials and structures. Butterworth-Heinemann. Linacre House, Oxford. Chapter 18, 1999

40) Radzi Z. Development of Self-Inflating Anisotropic Tissue Expanders for Clinical Applications. PhD Thesis, University of Oxford, (to be submitted 2012)

41) Quinn FX, Kampff E, Smyth G, and McBrierty VJ. Water in Hydrogels 1. A Study of water in Poly(N-vinyl-2-pyrrolidone/methyl methacrylate) copolymer. Macromolecules, 21:3193-3198, 1988

42) Qu X, Wirsen A, and Albertsson AC. Novel pH-sensitive chitosan hydrogels: swelling behavior and state of water. Polymer, 41:4589-4598, 2000

43) Mark JE. Polymer Data Handbook. Oxford University Press, p.656, 1999

44) Meakin JR and Hukins DWL. Thermal analysis of poly(2-hydroxyethyl methacrylate) (pHEMA) hydrogels. J. Material Sci.: Materials in Medicine, 14: 9-15, 2003

45) Mark JE. Polymer Data Handbook. Oxford University Press, p.963, 1999

Chapter 4: Tissue expansion in skin mimicking apparatus

4.1 Introduction

In previous chapters we have discussed the mechanical properties of skin tissue and the swelling properties of poly(vinyl-pyrrolidone)/methyl-methacrylate (VP/MMA) hydrogels. The main function of the skin is to act as a protective cover for the body and its internal organs [1]. The body's ability to adapt to an external stimulus is a natural phenomenon. Examples of these changes are the darkening in the skin tone when exposed to sunlight and the improvement in skin complexity from the use of cosmetic products. Similarly, the expansion of the skin area to reduce excessive tension is a natural response to protect our body.

Our interest is that the skin will stretch to a point where the growth of new tissue is stimulated. This same kind of growth is naturally present in the women's abdominal wall during pregnancy while the stretching of the skin area is also used for aesthetic and religious purposes in some primitive cultures [2]. All these manipulations of the skin area require some form of stretching mechanism that can create skin tension large enough for a bodily response.

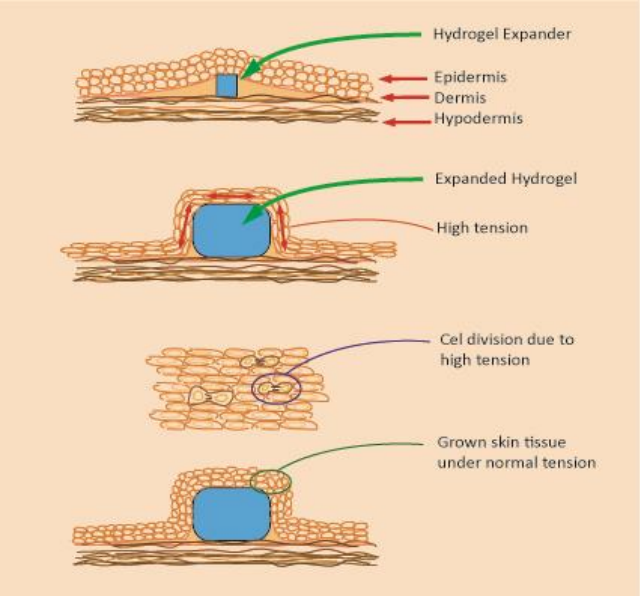

F ıders

By holding this stress long enough, new skin cells will proliferate along the stress axis until the skin is grown to a relaxed state (figure 4.01). Changes of the skin during skin expansion include [2]:

1) Hyperpigmentation due to increase in melanocyte activity along the epidermis.
2) Compression but not degradation of hair follicles.
3) Separation of hair follicles but no new hair follicles formation.
4) Decreasing thickness of the dermis with observed activated fibroblasts throughout expanded area.
5) Compact alignment and stretching of collagen in parallel orientation to the expander surface.
6) Mitosis of the fibroblast with maximum activity during initial expanding period.

The implant is usually left in place for 6-8 weeks after the desired expansion is reached. Once the reconstruction process is completed by the growth of new cells and the reduction in tension, the skin will return to normal tone and thickness [7]. No visual sign of hair thinning was observed at expansion of twice the initial skin area [2]. Upon removal, the extra skin flap can be used to perform the wanted reconstruction. The expansion of skin is a reversible process. The skin expanded will return to its initial condition over the course of 4-6 weeks if the given tension is removed [4].

The main criterion for a device to exploit this natural skin growth is to have a material that can expand with appropriate swelling pressure and swelling rate to avoid cellular necrosis or even dermis rupture [4]. Hydrogels are materials of choice due to their highly versatile properties. As investigated in Chapter 3, the swelling stress generated from hydrogels is driven by the

combination of diffusion and chain relaxation. The swelling pressure is controlled through balancing between the rapid softening of gel and the increasing volume. The VP/MMA hydrogel tissue expander is capable of expanding up to 8-14 times its initial volume while maintaining good structural stability. Although the swelling stresses and the swelling ratios are known, these parameters are insufficient to justify the working condition of the device once under the human skin.

Surgeon William Grabb predicted that "tissue expansion will have a major impact in reconstructive surgery" [5]. Today, this prediction has become a reality with the balloon tissue expander being an essential device for most plastic, reconstructive, and aesthetic surgeons. With the success over skin expansion, the idea of tissue expansion has developed into the expansion of other soft tissues.

Expansion of the artery and vein was observed by Stark et al. which showed capability of rapid expansion without causing disruption of blood vessels or other complication [6]. Manders et al. attempted the expansion of median nerve to treat neuroma while they also tried enlarging the bowel and bladder [7]. Martini et al. used intraoperative expansion of facial nerve as a method to repair nerve defect [8]. Expansion of the ureter to use the tissue for augmentation of pig's urinary bladder was tested by Ikeguch et al. [9]. The method of expanding tissue was also used to expand the bony orbit around the eye area in case of congenital anophthalmos in which the method supports bone growth and enlargement of the eye socket [10]. The expansion of bileral labia majora was used by Chudacoff et al. for treating vaginal agenesis [11]. Recently, the Oxford University Biomaterial group have developed an anisoropically swelling hydrogel device to stretch the mucosal tissue. This provides the surgeon with addition tissue for connecting upper

gum of cleft palate patients [12]. These innovative approaches demonstrate that the tissue expansion is a powerful surgical method with numerous potential applications.

Although revolutionizing in the medical field, the way to get a new medical device clinically approved requires a long process which involves passing the regulatory framework made to protect the safety of its users. The U.S. Food and Drug Administration (FDA) have classified the traditional balloon tissue expander as a Class II device which in the clinical studies section stated:

"… accordance with the act, the agency (FDA) will rely upon well-designed bench and/or animal testing rather than requiring clinical studies for new devices unless there is a specific justification for asking for clinical information to support a determination of substantial equivalence. While, in general, clinical studies will not be needed for most tissue expanders, FDA may recommend that you collect clinical data for a tissue expander with any one of the following:

- *indications for use dissimilar from legally marketed devices of the same type*
- *designs dissimilar from legally marketed designs*
- *new technology (i.e., technology different from that used in legally marketed devices of the same type).*

FDA will always consider alternatives to clinical testing when the proposed alternatives are supported by an adequate scientific rationale."[3]

The use of hydrogels for temporary (less than 6 months) implantation is however a different case in fulfilling the regulations of the FDA and other national administrations. Hydrogels are new and less evaluated material compared to silicone based material which is abundantly used in the medical field. The use of innovative materials especially when in exposure to the body will require significant amount of assessments. The directives of introducing a medical device often require risk assessment of design and manufacturing, possible animal testing, and finally using the device on clinical trials. As the design of hydrogel device for tissue expansion is always

changing in which new innovative approaches often arise, it will be most useful to have a testing method to simulate how the device will perform before proceeding to *in vivo* studies.

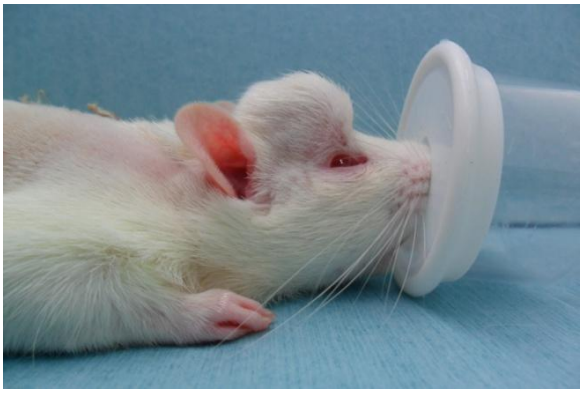

Figure 4.02: Test of hydrogel tissue expander on rats. Taken from Ref. [18]

In this chapter, VP/MMA self-expanding tissue expanders were tested on a newly designed apparatus which goal is to mimic the *in vivo* conditions of the skin. The expansion of skin was observed to see how the expander can stretch a skin-like material. Stress and strain contours can be plotted for further studies especially for the improvement of new tissue expanding devices. With the mechanical function that mimics the skin's response to such expanding pressure, we can use such acquired information as an alternative to results taken from animal testing. With the possibility to reduce the cruel but yet necessary animal testing, this testing apparatus is designed in hope of building a new trend in the biomedical field.

4.2 Materials and Methods

The main design criterion of this apparatus is to mimic the mechanical property of skin when stretched by a hydrogel tissue expander. To create a similar condition to when expander device is subjected under the skin, the apparatus must be able to hold a skin-like sheet while also

capable of containing a source of flowing fluid. The amount, type, temperature of swelling solvent can be changed to *in vivo* conditions. The straining of skin once hydrogel sample is placed can be measured by contour mapping the skin sheet area and by direct measurements using a digital caliper (Mitutoyo Absolute Digimatic, Japan). The apparatus was designed according to these main considerations.

4.2.1 Apparatus design

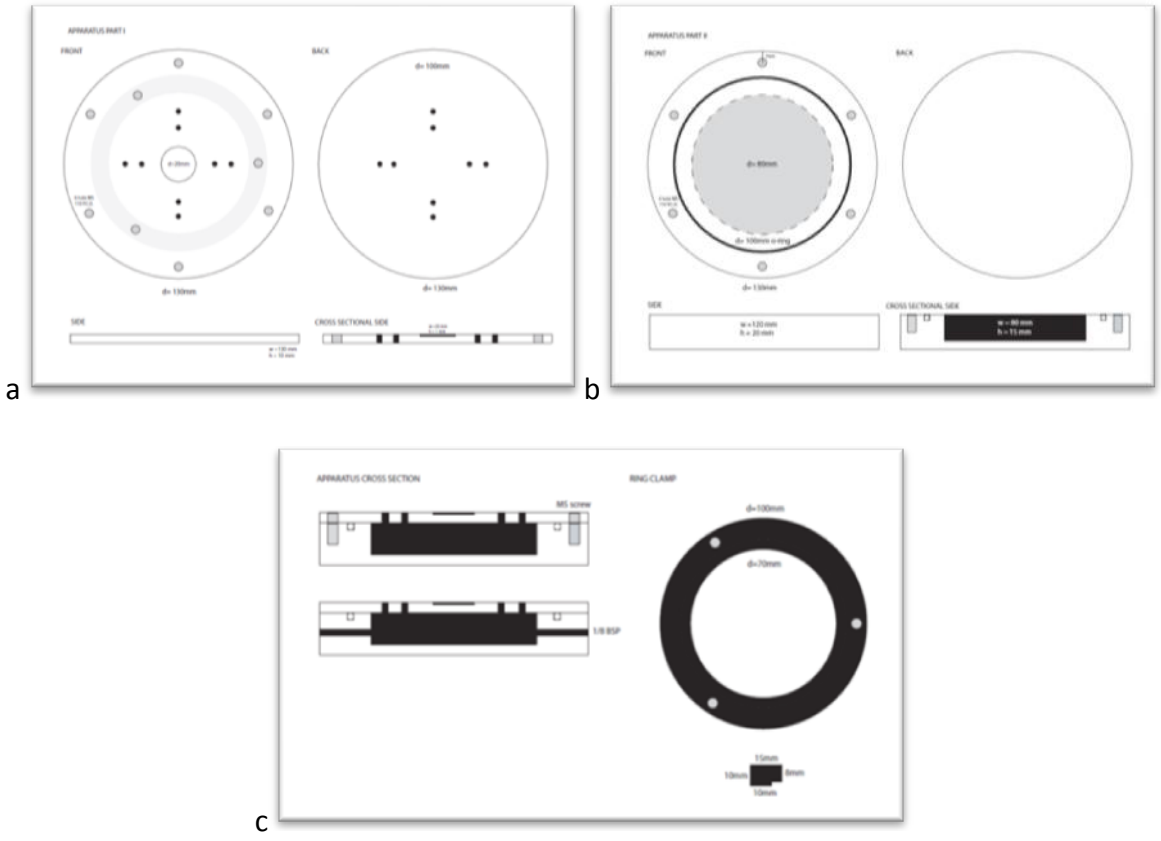

Figure 4.03: Design of a) sample holding piece b) solvent reservoir piece and c) a ring clamp.

The final design of the apparatus is shown in figure 4.03. The design consists of three disc shaped pieces (view appendix A for full size images):

1. The sample holder (fig. 4.03a)
2. The solvent reservoir (fig. 4.03b)
3. A ring clamp (fig. 4.03c)

The sample holder is designed to prevent sample slipping by a circular indentation at the centre of the piece and holes were made around the plate area for entry of solvent from the reservoir. The skin-like material of choice will be placed over and fixed with a metallic ring clamp. Once the sample and the skin-like material are in place, the wanted solvent can be added through the reservoir from two side channels . During addition of solvent the other channel is open such that no pressure build-up is present. Once the apparatus is filled, the channels are closed.

The material used for the frame is brass. This is due to the ease in shaping the alloy and its reasonable resistance to corrosion within the experimental time. From the blueprints shown in figure 4.03, brass alloy was made into the parts using lathe (XYZ 1440, XYZ Machine Tools, UK), milling (Bridgeport Milling Machine, Adcock & Shipley, UK), and drilling (Pillar Drill, Arboga Maskiner, Sweden) machines. A rubber O-ring was inserted between the reservoir and sample holder to prevent solvent leakage. The frame parts were tightly assembled with screws for completion.

Figure 4.04: Images of the apparatus rig.

4.2.2 Skin Mimicking Sheet

Selection of the material that can replicate the skin's elastic properties is the main area of importance for making such a testing system. The methods of characterising the mechanical

properties of the human skin were discussed in section 2.3.3. The moduli of the skin taken from various literatures were summarised in table 2.19. The material of choice for our skin-like material is an elastic and waterproof material with modulus of approximately 0.11-1.32 MPa and sheet thickness between 1.50-2.50 mm [16].

The material selected is a 2mm thick Shore 10A hardness polyurethane sheet (Provincial Rubber Agencies Ltd, Bristol, UK). The selection of polyurethane (PU) materials as the skin-mimicking sheet is due to the wide range of modulus that can be tailored (1-10 MPa [13]). Unlike real skin grafts or processed skin such as Demagraft®, PU is more reliable in terms of data reproduction while being much more cost efficient. In addition, the use of real skin grafts will not initiate cell proliferation when used *in vitro*. This makes natural skin no different from synthetic materials in terms of mechanical characteristics.

To confirm if the modulus of our PU material is between 0.11-1.32 MPa, the 2.0mm thick sheet was cut to a strip of 20mm x 35mm and tensile tested under 300N load cell (SMA miniature S-type, Interface Measurements Ltd.) at constant strain rate of 0.5 mm/s. The PU sheet was cut into circular discs of 80.0mm diameter. Each of the circular sheets was marked with graphing grid of 1 x 1 cm using fine tip permanent marker. The grid was used for indicating magnitude of mechanical strains in x- and y-axis.

4.2.3 Geometric assumption of skin area

Assuming that the skin area is fixed inside a circular ring with no initial tension, the expansion of skin can be measured using basic geometry calculations [18]:

1) Once dry gel is inserted under the skin. The skin is under a small tension with cross-sectional shape of a flat trapezoid. The surface area of the skin is equal to the surface area of a truncated cone without the inclusion of the lower base (shaded grey).

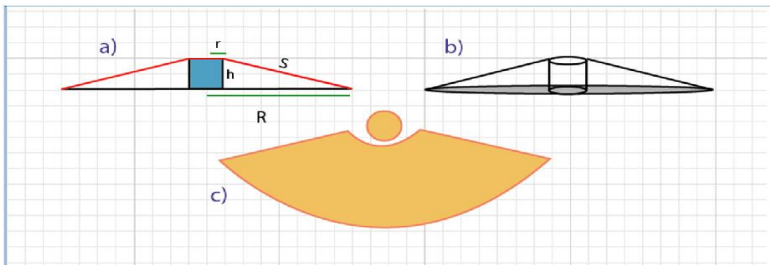

Figure 4.06: Schematic representation of a) cross-section of a dry cylindrical expander under skin (red), b) truncated cone with underlying expander, and c) the approximate surface area of skin.

The surface area of a truncated cone is calculated using the two radii (R and r), the height (h), and the shortest length between the edges of the two radii (S).

The lateral area of the cone is:

$$A_l = \pi(R + r)S$$

Adding the upper circle area (πr^2) to the lateral area gives the approximate area of the skin.

$$A_{skin} = \pi[S(R + r) + r^2]$$

2) After it is fully swollen, the gel becomes a soft material and is expected to be slightly pushed down by the skin tension. Naturally, the skin will enfold around the shape of the expanded hydrogel due to the localization of solvent into the gel. This is approximately the shape of truncated cone and a flat surrounding skin area (figure 4.07a).

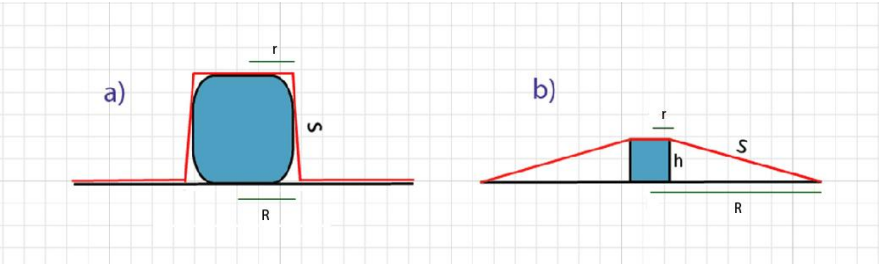

Figure 4.07: Schematic representation for the cross-section of a) expanded gel under skin b) dry gel under skin.

The surface area of the skin once expanded is:

$$A_{skin\ over\ expander} = \pi[S(R + r) + r^2]$$

$$+$$

$$A_{surrounding\ skin} = \pi(r_o^2 - R^2)$$

where r_o is the ring radius (*note that the skin-like material is constrained within a circular ring clamp).

The geometrical dimensions of the skin and gel on apparatus can be measured using a digital caliper. Diameters of the circular bases were measured where each diameter was measured twice perpendicularly. The difference in skin area between pre- and post-expansion is the estimation of newly acquired skin. The surface area of synthetic skin is measured at different intervals during total hydration period of 5 days. Differences between expansion from isotropic swelling gels and modified anisotropic swelling gels were also observed on the apparatus.

4.2.4 Surface topography and strain contour plots

Dry 90:10 VP/MMA hydrogels of 14.00mm diameter and 14.55mm height were used for testing the designed apparatus. A sample is placed on the centre of the frame before covering the gel over with grid marked PU sheet. Once the gel and sheet are place centrally over the apparatus, the sheet is fixed using a ring clamp and screws. Distilled water is injected through side channels of the reservoir where only the reservoir is filled. To prevent straining of the synthetic sheet due to water pressure and to avoid air bubbles within the testing area, the water channels were open and the skin area was pressed tightly using paper towels during solvent filling. Once the solvent is filled the hydration period is initiated by turning the device over to allow solvent to come in full contact with the inserted gel. The change in synthetic skin area was measured over the course of expansion (5 days).

The surface topography is mapped using the end of a digital caliper (±0.05 mm) where the height at each point of the circular sheet is plotted on a 19 x 19 matrix where the position of each point is fixed. The height contour can then be extrapolated into a 3D surface plot. Surface areas of the expanded polymer sheet at different hydration intervals were calculated through surface analysis software (OriginPro v.8.1, OriginLab). The surface area outputs can be compared to the results calculated using the area of a truncated cone. The skin expansion rate is taken as the change in surface area over time.

The surface strain contour was measured with a similar technique. The skin mimicking PU sheet was marked with 10 x 10 mm grid under no applied stress. As the hydrogel tissue expander swells, the grid marks will be strained together with the PU skin. The strain on each marked

block can be measured during swelling process using copper wire (diameter = 0.25mm) and a digital caliper. The strain was measured in both x- and y- axes and the principle strain is plotted onto an 8 x 8 matrix. The stress contour can also be plotted using pre-measured tensile modulus of the PU rubber.

The height and strain contour plots were taken for both the isotropic gels and the compressed anisotropic gels. The two sample types were initially of the same size and geometry (cylinders of 14.00 mm diameter and 14.55 mm height) before modification of the anisotropic swelling gels. Anisotropic gels were heat treated and axially compressed from 14.55mm to 4.85mm in sample thickness (detailed method in section 3.24).The compression ratio of the anisotropic swelling gel is 2.89. Comparison was made between the unmodified and modified gels through surface topography and skin expansion rate.

4.3 Results and Discussion

The stress-strain curve of the selected polyurethane (PU) sheet under tensile loading is shown in figure 4.08. The calculated engineering stress is converted into true stress to adjust with the significant reduction of sample's cross-sectional area. This was done by multiplying the engineering stress by the 1.0 + the strain.

The plotted graph showed a J-shaped curve which is the same stress-strain relationship that soft tissues such as the skin exhibit [15]. The curve shows that initially, the increment of stress is small over large extensions, however, over larger strains the material becomes stiffer and more difficult to extend. This is due to the initially random coiling of polymer chains that would later

be aligned in tensile direction to enhance the overall stiffness (figure 4.09). In the case of dermal tissue, this is the arrangements of collagen fibres.

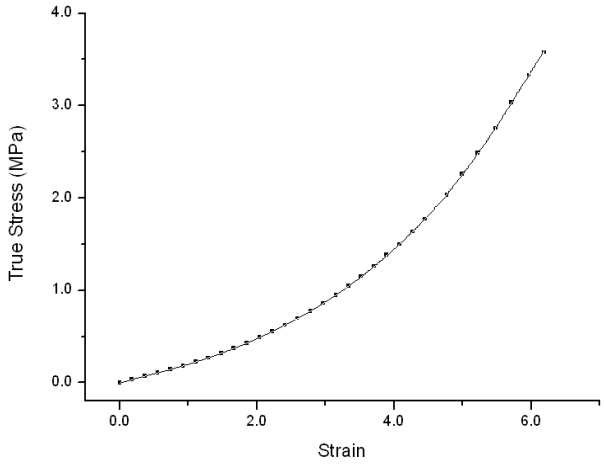

Figure 4.08: Stress-strain curve of Shore 10A polyurethane under tensile loading.

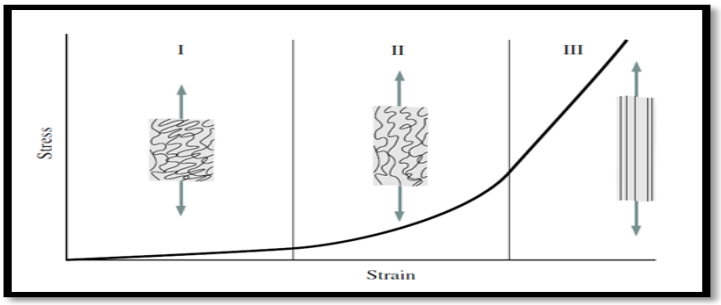

Figure 4.09: Typical stress-strain curve of elastic polymer showing alignments of fibres at three different straining stages. Adopted from Ref. [15]

Due to the always increasing stiffness of the PU sheet, the elastic moduli of the sheet were taken between three straining intervals. The elastic moduli were taken at 1.0, 3.0 and 5.0 strains where the calculated moduli are 0.23 ± 0.11 MPa, 0.48 ± 0.12 MPa, and 0.99 ± 0.08 MPa respectively. This confirmed that the selected PU sheet does have comparable mechanical properties to human skin in terms of elastic modulus (E_{skin}= 0.11-1.32 MPa).

4.32 Skin Expansion

The stretching of skin was monitored for 5 days where the shape of expanding skin was assumed to be comparable to a truncated cone. The increase in expanded area over time is

shown in figure 4.10. The expanded area was taken as the difference in sheet area when gel is dry to the area at each hydrated state. The final height from base is 24.60 ± 2.4 mm. The final increase in surface area of the skin is about 800 ± 25 mm^2 for isotropic swelling gels (figure 4.10). These measured parameters are relative to the composition, size, and geometry of the initial gel.

Figure 4.10 shows that the expansion of skin is linear for the first 3 days before showing a reduced rate until near saturation at day 5. This linear increase in skin area is an unexpected behaviour as we had expected the hydrogel to rapidly swell within the first 24 hours similarly to how the gels were observed to expand inside a solvent-filled beaker.

The reason to this slow skin expansion is due to the already stretched skin prior to expansion. The initial height of the dry cylindrical sample (14.55 mm) is large enough to slightly stretch the PU skin. Because the calculation of expanded skin is the final surface area subtracted by the area of skin over the unhydrated gel, the more stretched skin prior to expansion means a reduction in efficiency of the device. As skin area is already under pre-tension due to the geometry of the expander, the gel is subjected to an opposing force before being hydrated. In addition, the gel was also set under a controlled amount of water supply with less area of contact due to both circular bases being pressed by the overlying skin. The equilibrium swelling is reached when the driving force of swelling is balanced with the restoration force of the PU sheet.

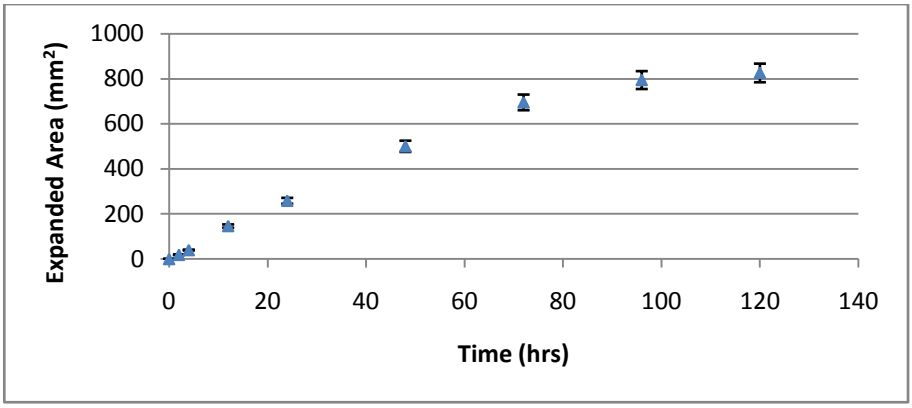

Figure 4.10: The amount of expanded skin over time using isotropic gel

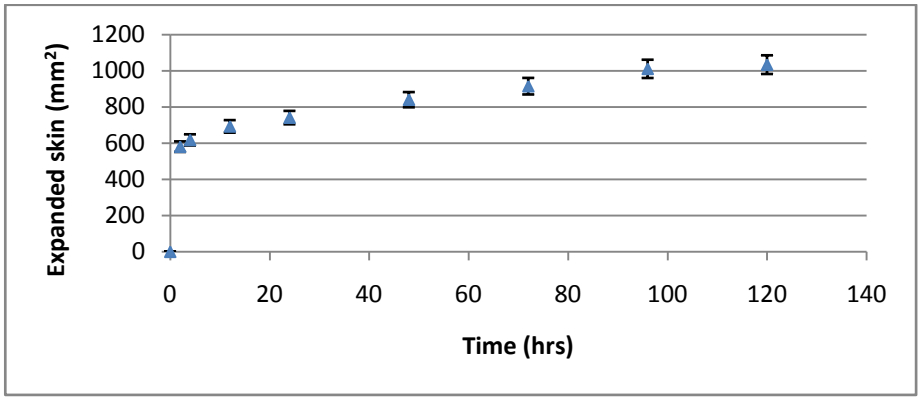

Figure 4.11: The amount of expanded skin over time using anisotropic gel

In contrast when the expansion of the synthetic skin was observed using modified anisotropically swelling hydrogel (figure 4.11), it is clear that most of the skin expansion occurred during the first day of device implantation. This showed a significant difference with the skin expanded using isotropic swelling gels.

The final height of the skin over expander is 23.22 ± 2.2 mm, which is marginally lower than the expansion of unmodified gel. This was expected as explained in Chapter 3 that the compressed gels will not recover a hundred percent of their geometry because of internal changes to the chain alignment.

Although both the anisotropic and isotropic devices swell to approximately the same shape, the initial shape of the gels prior to swelling was not the same. The dry anisotropic gels could be placed under the skin without inducing much tension due to their flatter shape. This means that the skin was less strained from the moment of implant which may help to explain the abrupt expansion during the initial stages.

The shape shifting of the anisotropic swelling gels from disc to cylinder clearly showed the greater potential in expanding an overlying skin. The advantages these modified gels have in terms of tissue expansion are the small amount of skin tension needed to insert the device and the greater amount of expansion in the desired direction. With this modified swelling behaviour, it is clear that the initial amount of skin needed can be reduced and the expansion of skin area is greater by about 20%.

This enhancement of the gel however comes with a drawback of speeding the already rapid skin expansion. As shown in figure 4.11, the skin has already expanded by about 60% of the overall expansion within the first 4 hours. This expansion rate from the hydrogel tissue expander was demonstrated to be too fast for healthy skin growth in two animal studies [17, 18]. Rapid swelling of the hydrogel was observed by Varga et al. where gels made of acrylamide (AAm), acrylic acid (AAc) and N-isopropylacryamide (NIPAAm) were implanted under dorsal regions of wistar rats for 18 days [17]. The results from Varga et al. showed that the maximum skin expansion took less than one week to reach while histological analysis of rapid skin expansion by AAc gel revealed serious tissue damage [17].

A more direct comparison with our results is the animal studies performed by Radzi using the same hydrogel material (VP/MMA) on the foreheads of 67 wistar rats. The rats were monitored for any symptoms and signs of device complication. The fast straining of skin was proved to cause major complications around the expanded skin area [18]. The observation made in the experiment showed that both expanders, especially the anisotropically swelling type, will cause significant pain and irritation shown by stiffness and reluctance in movement of the animal [18]. Tissue necrosis was observed and the experiment was terminated before the expander reaching full expansion [18]. Bone resorption under the implant was also shown in post-mortem investigations due to the hardness of the initial gel [18]. This coincides with the force generation over time data shown in Chapter 3 where the measured force is substantially high when the hydrogel is still glassy. Due this undesirable rate of expansion, researchers have been working on different types of coatings and the use of biodegradable inter-penetrating networks (IPN) to reduce the rate of hydrogel swelling [18,24].

Radzi also showed that the expansion rate of gel disc (diameter= 10 mm, thickness= 2.0 mm) is significantly high in the first 1.5 days while overall expansion takes 5 ± 0.5 days inside the rats. The implanted gels took 2.5 ± 0.5 days longer to reach maximum swelling *in vivo* compared to expansion in a petri dish [18]. This showed that the swelling behaviour of the hydrogel inside a living rat and the hydrogel inside our apparatus proved to have positive similarities. The controlled amount of fluid within the apparatus also showed an increase in the overall swelling time while the amount of solvent is still enough to initiate rapid swelling. Although our gels were larger than the ones used by Radzi, the expansion process seemed to have the same time frame (5 days) which mimicked the *in vivo* of rats quite naturally.

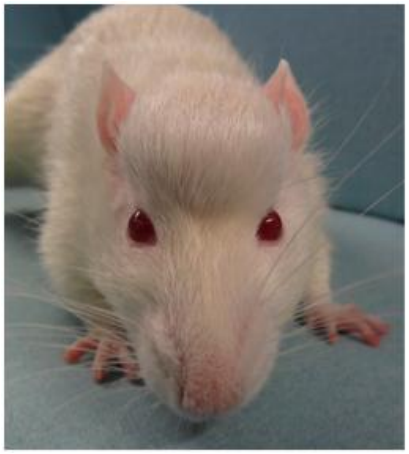

Figure 4.12: Fully expanded VP/MMA gel implanted on a wistar rat by Radzi [18]. This image was taken after 5 weeks of expansion. Skin encapsulates shape of a slightly deformed cylinder.

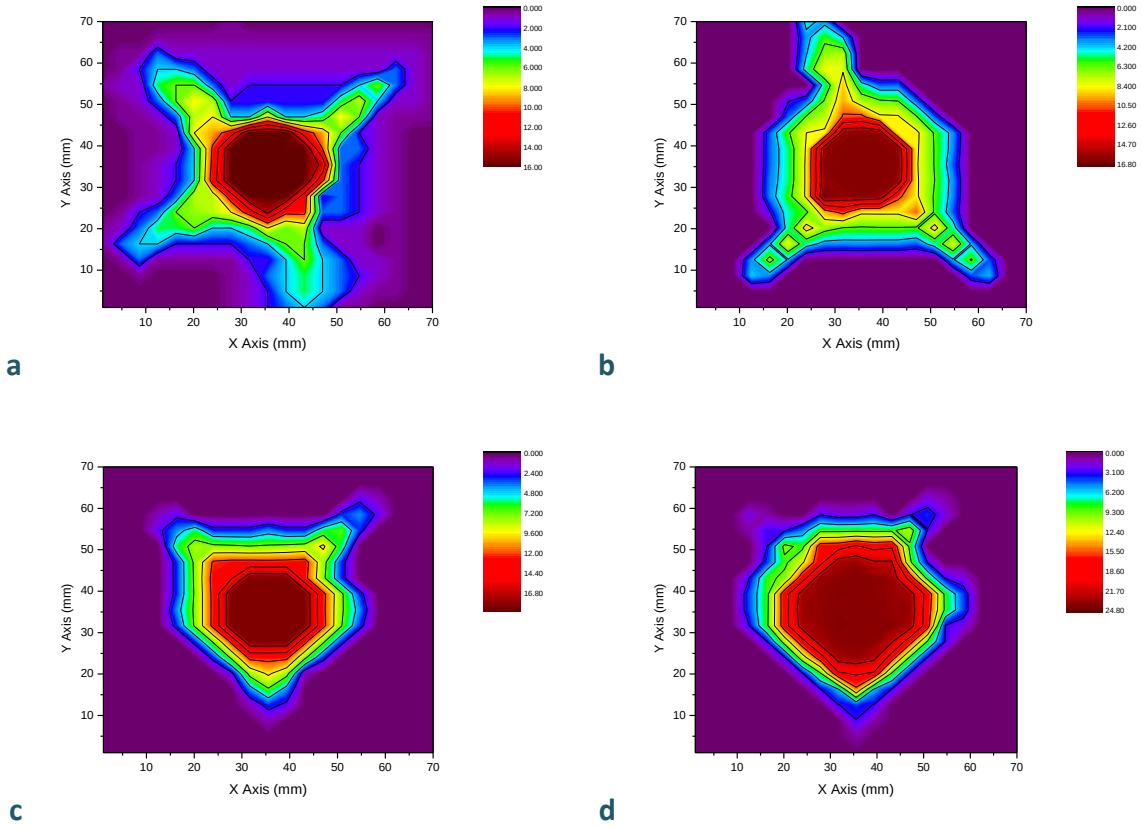

Figure 4.13: Projection of height contour of PU sheet over isotropic swelling hydrogel. a) 0 hrs, b) 24 hrs, c) 48 hrs, d) 120 hrs hydration.

Another way to calculate the change in surface area of the PU skin is by plotting the height contour of the skin area. The height contours of the gels were plotted at different intervals of hydration. The projected contour plots are shown in figure 4.13.

The contour plots display the transition of skin over the expansion period of 5 days. With the dry expander under the skin, the shape of the skin shows noticeable folds in radial directions from the expander while the majority of the PU skin is not in contact with the base plate. These folds showed that there are water filled spaces under the skin which had been created due to the stiffness of the implant. As seen from how the contours change shape with time, the folds began to widen out and the surrounding skin area started to come into more contact with expander surface. This is due to the reduction of space occupied by free water due to water uptake of the hydrophilic hydrogel. This localization of water caused the skin to be pulled in to direct contact to the gel surface. This was also observed from *in vivo* studies by Radzi on rat skin (figure 4.12). The result is that the final expanded skin will cover to the shape of the swollen expander. This coming together of the skin and gel may also affect the gel expansion due to the reduced surface contact with the solvent.

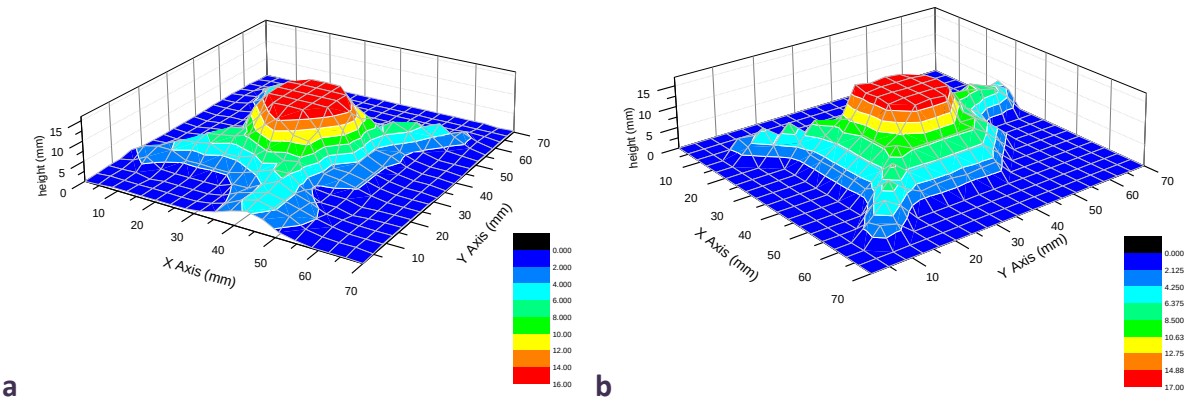

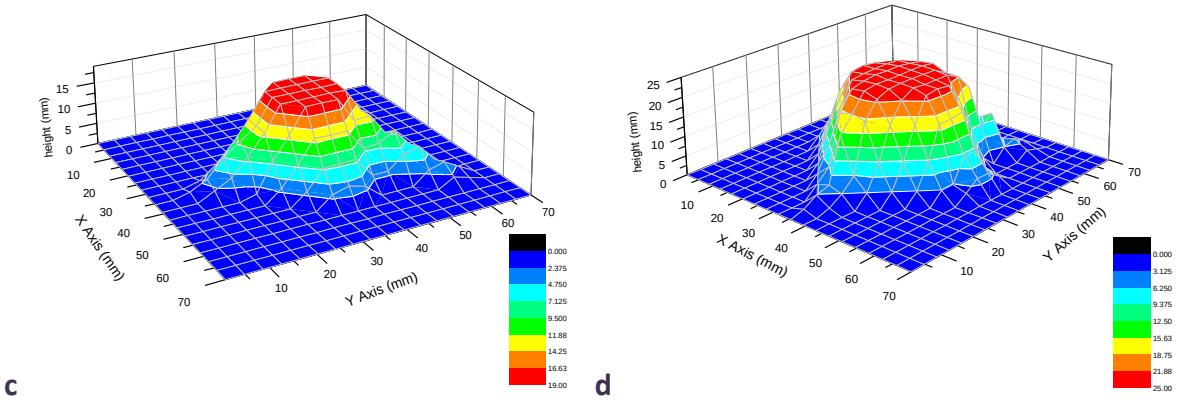

Figure 4.14: Skin topography maps at a) 0 hrs, b) 24 hrs, c) 48 hrs, and 120 hrs. (Isotropic swelling gels)

Figure 4.14 displays the transition of the skin's topography over time. The shape of skin can be viewed at many angles and the surface area can be computed with the input of matrix properties using 3D plotting software (OriginPro v.8.1). The area of the skin is calculated using the 'calculate matrix surface area' function of the program. Because the dimension of matrix was set at 70 mm x 70 mm while the actual PU sheet is circular with diameter of 70mm, the extra area of the matrix square has to be taken out by the amount of:

$$70^2 - \pi\left(\frac{70}{2}\right)^2 = 1053.5\ mm$$

This will correct the matrix surface area to the same area of the fitted PU sheet. The surface area of skin over isotropically swelling hydrogel is summarized in table 4.15. The table shows the calculation of skin area using the height contour matrix and the area taken from assuming that the expanded skin is a truncated cone. The results showed both methods of measuring the area comes to a comparable expansion trend where calculated skin area is within the same range.

Table 4.15: Summary of the measured surface area of skin over isotropically swelling gel.

Hydration time (hours)	Matrix area (mm^2)	Matrix area – 1053.5 (mm^2)	Area using truncated cone (mm^2)
0	5690 ± 94	4637 ± 94	4448 ± 54
2	5740 ± 78	4687 ± 78	4467 ± 58
4	5766 ± 77	4712 ± 77	4488 ± 56
24	5823 ± 67	4769 ± 67	4707 ± 63
48	5968 ± 68	4914 ± 68	4948 ± 65
120	6495 ± 88	5442 ± 88	5274 ± 66

The small difference in area that can be seen between the two methods is mainly due to flaws that each of the methods has. For the truncated cone assumption, the deviation of the skin's geometry from a truncated cone will always be present. The skin will not have sharp edges, a straight slant heightor perfect symmetry (figure 4.16). This is due to the sample preparation flaws and the softness of the swollen gel which will not maintain cylindrical shape under the stretched skin. As for the measured height contour, although the 19 x 19 matrices may contain a fair amount data to show a good representational image, the quality of the image so produced is still limited. Steps and sharp edges on the 3D projection (figure 4.14 and figure 4.18) are present which does not match the smooth surfaces of the actual PU skin. Due to these deformities, the acquired surface areas are only close estimates. More sophisticated measuring devices such as 3D surface scanning tools can be used in the future when more accuracy is required.

Figure 4.16: Isotropic swelling gel after 24 hrs of hydration under apparatus.

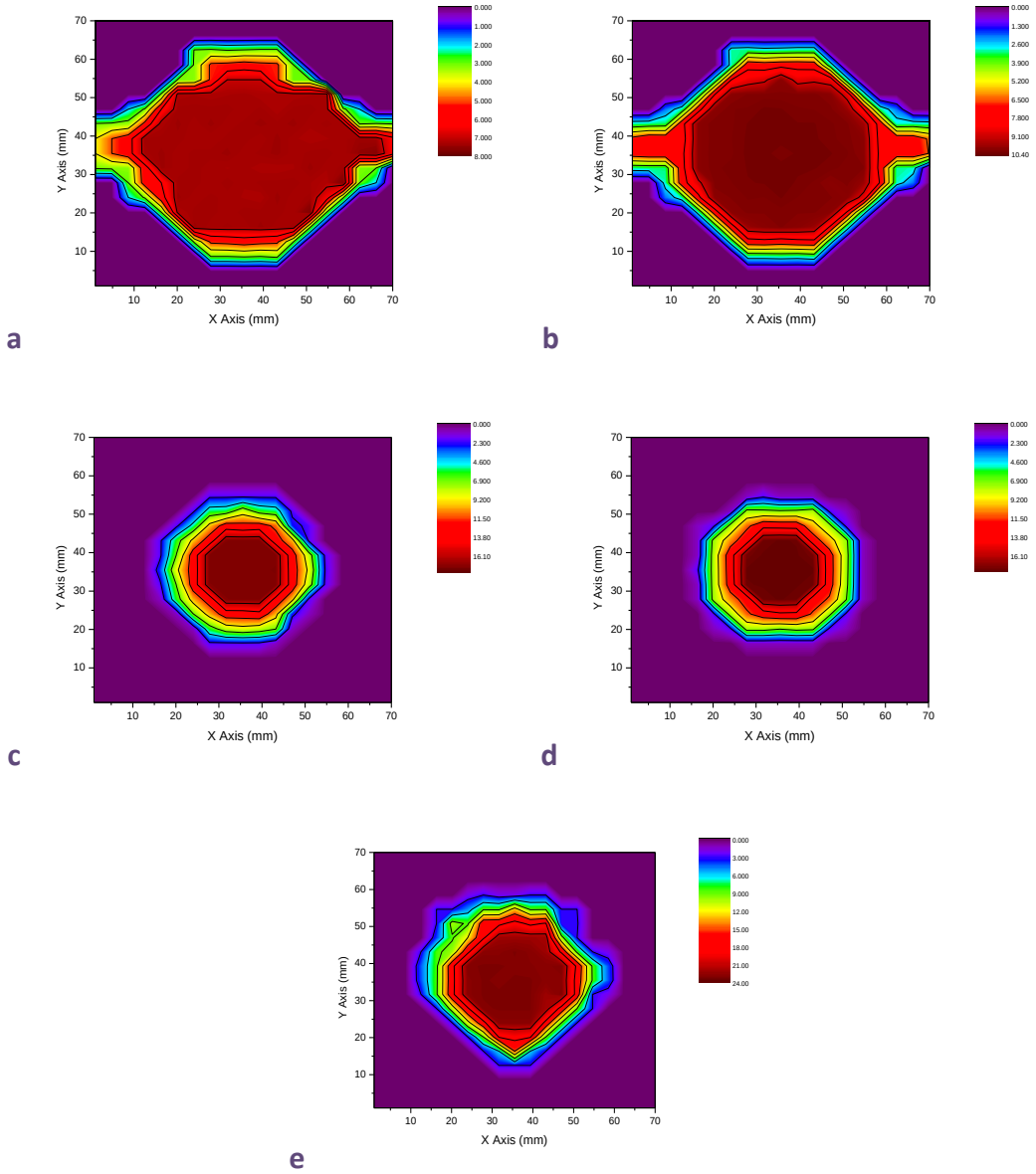

Figure 4.17: Projection of height contour of PU sheet over anisotropic swelling hydrogel. a) 0 hrs, b) 2 hrs, c) 24 hrs, d) 48 hrs, and e) 120 hrs. Height is measured in millimetres.

The same method of plotting the surface contour was also made on the PU skin over anisotropically swelling hydrogels. Once again, the 2D and 3D images of the height contour were plotted in figure 4.17 and figure 4.18 respectively. The transition of skin area was modelled as the expander swelled from a glassy disc to a cylinder gel. One of the differences observed on the surface was the reduction in number of skin folds throughout the expansion period. The shape of the skin surface was more defined by the implanted gel and the change in

the diameter of the expander was apparent as seen from figures 4.17 a, b, and c. From the moment of hydration, the gels anisotropically swelled upwards and shrank in radial directions. This change in shape was due to the modification process of heating and compressing the gels which created a shape-memory gel. The returning of the shape was induced by the reduction of glass transition temperature from solvent uptake.

As the gels became softer, the once compressed polymer network began to relax. This anisotropic swelling process was present only at hydration times up to 24 hours. Beyond 24 hours the swelling of the modified gels became isotropic until reaching maximum swelling capacity. Both the modified and unmodified gels showed to have stretched the skin to almost the same surface area and shape. This was shown in skin area calculations (tables 4.15 and 4.19) and 3D plots (figures 4.14d and 4.18e). From this observation it can be said that the main differences between the swelling characteristic of the two gel types will only be displayed within the first 24 hours of expansion. The desired anisotropic swelling property is present when the ratio between height and radius is constantly changing.

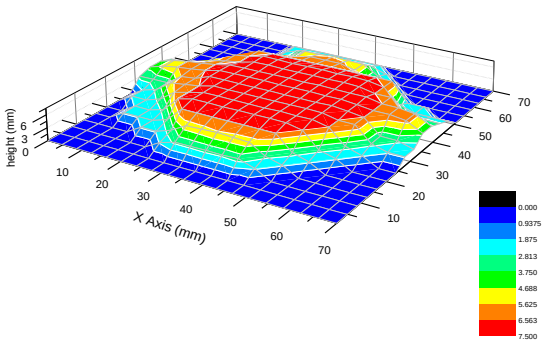

a

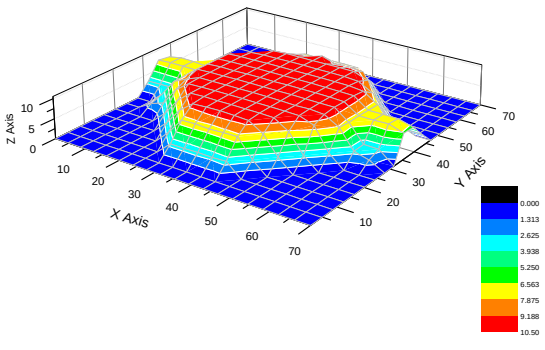

b

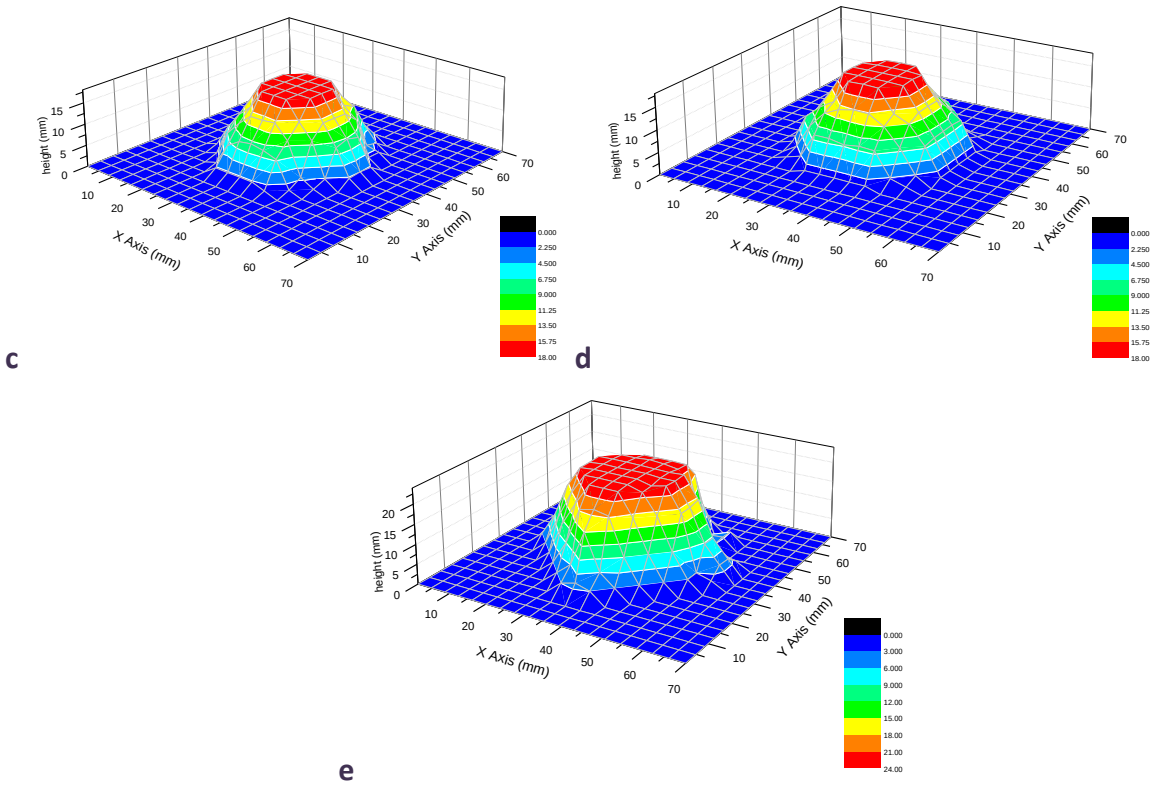

Figure 4.18: Skin topography maps at a) 0 hrs, b) 24 hrs, c) 48 hrs, and 120 hrs. (anisotropic swelling gels)

Table 4.19: Summary on the measured surface area of skin over anisotropically swelling gel.

Hydration time (hours)	Matrix area (mm^2)	Matrix area – 1053.5 (mm^2)	Area using truncated cone (mm^2)
0	5139 ± 87	4086 ± 87	4001 ± 44
2	5513 ± 102	4460 ± 102	4581 ± 55
4	5534 ± 76	4481 ± 76	4618 ± 63
24	5586 ± 72	4533 ± 72	4742 ± 57
48	5631 ± 76	4577 ± 76	4841 ± 64
120	6442 ± 83	5389 ± 83	5034 ± 62

4.3.3 Strain Contour

The strain contours of PU skin over isotropic swelling gels and anisotropic swelling gels are shown in figures 4.20 and 4.21 respectively. The contour maps were plotted by measuring the strains in both the x- and y- axes on the grids marks of the PU sheet. The resulting strains at each hydration time were calculated and plotted onto 8 x 8 matrixes.

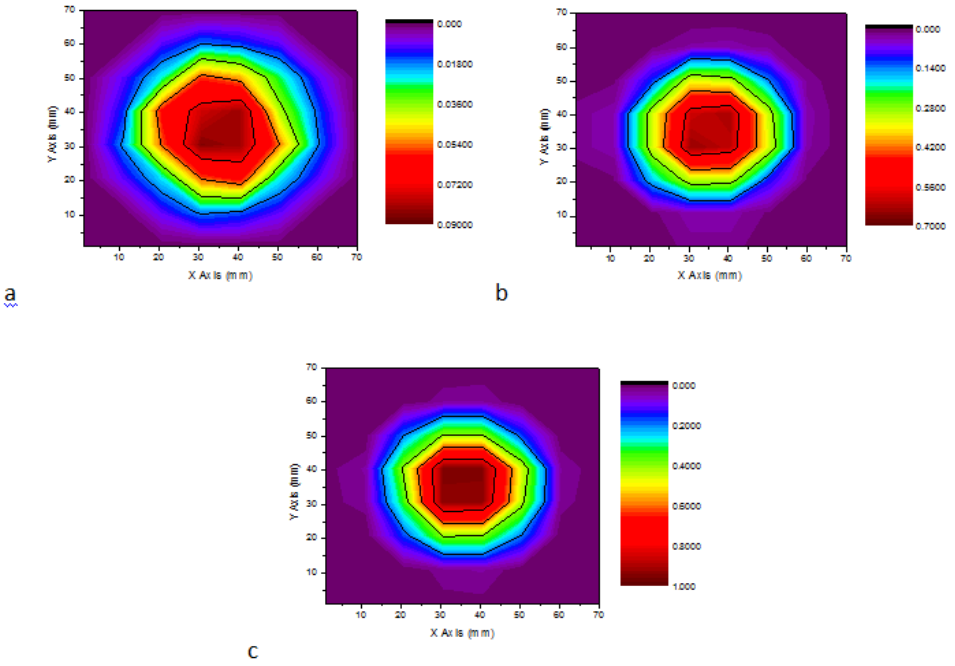

Figure 4.20: Stain contour plots of PU skin over a) dry gel, b) 1-day hydrated gel, and c) 4-days hydrated gel. (Isotropic swelling gels)

From the start of the expansion we can see that the maximum strain on the PU sheet is significantly larger over the isotropically swelling gel compared to the compressed anisotropically swelling gel. Before the addition of solvent, the maximum strain on the sheet over isotropically swelling gel is measured to be 32.7 ± 2.3 % while the maximum strain induced by the dry anisotropic gel is 8.5 ± 2.1 %. The observed and measured strains suggested that overall tension from the more slender-shape gel is higher. The amount of tension on the skin will create a similar magnitude of opposing force which presses down on the expander. As this occurs, the driving force for expansion is reduced and hence a smaller equilibrium swelling ratio.

The straining of our synthetic skin observed after 24 hours showed that the modified and unmodified expanders were identical once the anisotropic swelling behaviour of the

modified gels is lost. The strain rates from expansion of the two different gels were comparable from this point until the end of the swelling process. The maximum strain after 5 days of device implantation was 97.6 ± 3.4 % and 98.7 ± 3.6 % when isotropic gels and anisotropic gels were used respectively. The skin area of maximum strain can be seen centrally and on the circular edges of the cylindrical expander. The swollen gel will however soften during hydration which will allow the encapsulating skin to deform sharp corners of the gel cylinder into more rounded corners. This was the reason why the stress concentration on the edges was not as high as we would expect. In terms of a tissue expander, this is a good property as it is important to have a more evenly distributed tension. Sharp edges of the dry cylinder gel can additionally be blunted during manufacturing process to reduce any potential stress concentrations further.

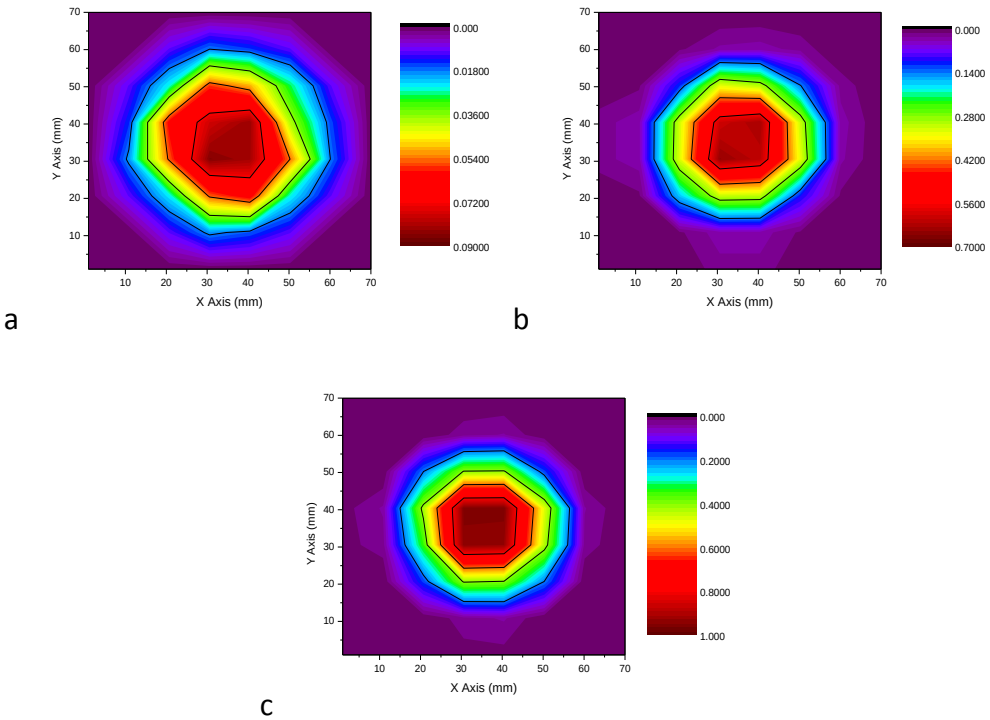

Figure 4.21: Stain contour plots of PU skin over a) dry gel, b) 1-day hydrated gel, and c) 4-days hydrated gel. (Anisotropic swelling gels)

The strain distribution on the skin can be compared using strain maps on figures 4.19 and 4.20. Although the strain was low prior to expansion, it was apparent that the strain was more evenly spread around the tested area when the hydrogel material was dry. This was observed for both cylindrical and disc-shaped gels. As the swelling process proceeds, the straining of skin increased centrally above the hydrogel but the distribution of strain was decreased to a narrower region around the expander. At equilibrium, the straining of skin around the edges was measured to be zero. This showed that skin expansion is high only at specific areas while at some distance away from the expander, the surrounding skin will not be stretched (figure 4.21).

This localization of strain may be due to the suctioning pressure cause by water absorption of the hydrogel which prevented the movement of the surrounding skin while another possibility is due to creep deformation of the skin mimicking material. Due to this characteristic of the hydrogel expander, the simulation showed that there is a possibility for reconstructive surgeons to insert multiple gels into adjacent areas rather than implanting one large gel for more skin expansion. The optimum distance between each gel will need to be further investigated where it is clearly relative to the hydrogel composition and size. The use of one-sized gel is advantageous in terms of ease in manufacturing, setting a universal standard, and quality control. Having multiple gels for expansion also mean larger expanded surface area compared to a single gel of same volume.

Figure 4.21: Image of swollen hydrogel expander under polyurethane skin.

The apparatus made for testing self-inflating hydrogel tissue expander showed us that it is possible to mimic the conditions under the human skin down to a good estimation. The accuracy of our result is highly dependent on the accuracy of the presumed values of the thickness and modulus of selected skin area. The drawback to this is the limited number of investigations on the biomechanics of skin and all the soft tissues. The mechanical property of skin, like most biological material, is commonly understood to be difficult to generalise due to variations across anatomical sites, age and gender, and other external factors. However, the advantage of our device is the ease in data reproduction in which *in vivo* studies cannot provide.

Another limitation to the simulation of skin expansion is the inability to emulate skin growth. While elastic properties were met and the maximum skin expansion is known, the viscous behaviour of skin during the creep loading was not fully investigated in this study. The permanent deformation that arises from creep loading and the mitotic stimulation of fibroblasts which support growth are the two main contributions to the expansion of skin. This

gap in our apparatus showed that there is still a continuing challenge in replicating the key mechanisms that happen inside a human body. One possible advancing path for our apparatus is to incorporate tissue engineering and real life biological functions into the synthetic skin sheet. An example of such material is the commercially selling synthetic skin with living cell culture and wound healing mechanism (Labskin^{TM}, Evocutis plc., UK). The man made skin from Evocutis plc. is a novel skin equivalent material which showed great potential for the future of testing skin tissue expansion.

4.4 Chapter summary

The experimental apparatus set to simulate the expansion of skin is a useful method for understanding the mechanics of tissue expanders. The aim of this apparatus was to create an *in vitro* test that can mimic *in vivo* conditions of the human skin. The design of the testing rig consists of a solvent reservoir with channels for solvent entry into the hydrogel sample. VP/MMA hydorgel cylinders of 90:10 wt% ratio were used and each was sealed under a sheet of synthetic skin before distilled water is passed into the frame. The skin mimicking material of choice was Shore 10A hardness polyurethane with elastic properties comparable to skin. The polymer sheet was tensile tested to have a modulus between 0.23-0.99 MPa. This modulus range matches the modulus of human skin shown in the literature [25-30].

The use of the designed testing method showed that we can quantify the amount of skin expansion, analyze surface topography, and understand the stress and strain distribution of the skin. These measurements are crucial when it comes to designing a new tissue expander where the swelling behaviour *in vivo* is unknown. The use of the apparatus showed that gel swelling is

delayed under the synthetic skin compare to a gel freely swollen in a beaker with excess solvent. This increase in overall expansion time is due a number of possible factors:

1) Amount of solvent is limited within the designed apparatus.
2) Fluid flow is restricted around the hydrogel due to diffusion of surrounding free water into the hydrogel matrix. The volume transfer created movement of the PU skin to come in more contact to the gel surface.
3) Osmotic expansion is opposed by the downward pressure due to skin tension.

By comparing the effectiveness in skin expansion between isotropically swelling gels and anisotropically swelling gels, the results showed that the initial strain on the skin is much lower if the gel is flat. As the gels come to approximately the same size at equilibrium swelling, the difference in skin area from start to finish showed that anisotropically swelling gel can expand the skin 20% more than isotropic swelling gels. The skin expansion rate of anisotropic swelling gels showed that anisotropy is present only in the first day of expansion. The rapid expansion observed from these gels could cause severe skin necrosis in animal studies. Methods of rate control are being developed to prevent medical complications [18, 24].

The main goal of this design is for the results to show that it is possible to simulate the same skin expansion with the experiments which were done through animal studies. Although the use of synthetic material to mimic the skin may not be able to show its full biomechanical properties, the rate of expanded area and the topography of skin over hydrogel can be fit into the animal model developed by Zamri due to use of the same hydrogel material [18].

While we focus on the expansion of skin, the apparatus is also capable of replicating the expansion of any other soft tissue. The elastic modulus and thickness of the polymer sheet can be tailored to match the desired living tissue. With this possibility, the swelling behaviour and the tissue expansion can be observed before proceeding into animal testing.

4.5 Chapter 4 references

1) Madison K. Barrier function of the skin: "la raison d'être" of the epidermis. J Invest Dermatol. 121(2):231-41,2003

2) Agrawal K and Agrawal S. Tissue regeneration during tissue expansion ad choosing an expander. Indian J Plast Surg. 45(1):7-15, 2012

3) U.S Department of Health and Human Services. Draft Guidance for Industry and FDA Staff: Class II Special Controls Guidance Document: Tissue Expander. Food and Drug Administration, Center for Devices and Radiological Health, 2008

4) Argenta LC. Controlled tissue expansion in reconstructive surgery. Br J Plast Surg. 37:520–9, 1984

5) Radovan C. Breast reconstruction after mastectomy using the temporary expander. Plast Reconstr Surg. 69:195–208, 1982

6) Stark GB, Hong C, Futrell JW. Rapid elongation of arteries and veins in rats with a tissue expander. Plast Reconstr Surg. 80:567–78, 1987

7) Manders E, Sasaki G, Austad E. Tissue expansion today. A symposium sponsored by the Plastic Surgery Educational foundation, Hershey. Plast Reconstr Surg. 80:579-81, 1987

8) Martini DV, Har-el G, Mcphee J, Lucente F. Rapid intraoperative facial nerve expansion.Otolaryngol Head Neck Surg. 114:602–12, 1996

9) Ikeguch EF, Stifelman MD, Hensle TW. Ureteral tissue expansion for bladder augmentation. J Urol. 159:1665–8, 1998

10) Tse DT, Abdulhafez M, Orozco MA, Tse JD, Azab AO, Pinchuk L. Evaluation of an integrated orbital tissue expander in congenital anophthalmos: report of preliminary clinical experience. Am J Ophthalmol. 151:470–82, 2011

11) Chudacoff RM, Alexander J, Alvero R, Segars JH. Tissue expansion vaginoplasty for treatment of congenital vaginal agenesis. Obstet Gynecol. 87:865–8, 1996

12) Swan MC, Bucknall DG, Goodacre TEE, and Czernuszka JT. Synthesis and properties of a novel anisotropic self inflating hydrogel tissue expander. Acta Biomaterialia, 7:1127-1132, 2011

13) Urethane Rubber Polymer Database. 2009 Matbase.com. http://www.matbase.com/material/polymers/elastomers/urethane-rubber/properties, accessed on: 12 June 2013.

14) Diridollou S, Patat F, and Gens F. In vivo model of the mechanical properties of the human skin under suction. Skin Research and Technology; 6; 214-221, 2000

15) Holzapfel GA. Biomechanics of soft tissue. Biomech Preprint Series. 7:12-15, 2000

16) Laurent A, Mistretta F, Bottigioli D, Dahel K, Goujon C, Nicolas JF, Hennin A, and Laurent PE. Graphic measurement of skin thickness in adults by high frequency ultrasound to assess the appropriate microoneedle length for intradermal delivery of vaccines. Vaccine 25:6423-6430, 2007

17) Varga J, Janovak L, Varga E, Eros G, Dekany I, and Kemeny L. Acrylamide, Acrylic Acid and N-Isopropylacrylamide Hydrogels as Osmotic Tissue Expanders. Skin Pharmacology and Physiology, 22; 305-312, 2009

18) Radzi Z. Development of Self-Inflating Anisotropic Tissue Expanders for Clinical Applications. PhD Thesis, University of Oxford, Oxfordshire, UK, 2012

19) Abrahamsson P, Isaksson S, Andersson G. Guided bone generation in a rabbit mandible model after periosteal expansion with an osmotic tissue expander. Clin Oral Implants Res, 22(11): 1282-8, 2011

20) Manschot JFM and Brakkee AJM. The Measurement and Modelling of the Mechanical Properties of Human Skin In Vivo – I The Measurement. J. Biomechanics, 19(7): 511-515, 1986

21) Dunn MG and Silver FH. Viscoelastic Behavior of Human Connective Tissue: Relative Contribution of Viscous and Elastic Components. Connective Tissue Res. 12:59-70, 1983

22) Wilkes GL, Brown IA, and Wildnauer RH. The biomechanical properties of skin. Critical Reviews in Bioengineering. 453-495, 1973

23) Wildnauer RH, Bothwell JW, and Douglass AH. Stratum Corneum biomechanical properties – influence of relative humidity on normal and extracted human stratum corneum. The journal of Investigative Dermatology, 56: 72-78, 1971

24) Lee JH, Radzi Z, Swan MC, Bucknall MD, and Czernuszka J. Interpenetrating Polymer Network Hydrogel Based on VP/MMA Gel and PLGA Diacrylate Macromers. Americal Physical Society, APS March Meeting 2010

25) Agache PG, Monneur C, Leveque JL, and De Rigal J. Mechanical Properties and Young's Modulus of Human Skin In Vivo. Arch Dermatol Res 269, 221-231, 1980

26) Manschot JFM and Brakkee AJM. The Measurement and Modelling of the Mechanical Properties of Human Skin In Vivo – I The Measurement. J. Biomechanics 19(7)511-515, 1986

27) Escoffier C, Pharm M, de Rigal J. Age-Related Mechanical Properties of Human Skin: An In Vivo Study. J Invest Dermato, 93(3):353-7, 1989

28) Diridollou S, Patat F, and Gens F. In vivo model of the mechanical properties of the human skin under suction. Skin Research and Technology, 6:214-221, 2000

29) Leveque JL, de Regal J, Agache PG, and Monneur C. Influence of Ageing on the in Vivo Extensibility of Human Skin at a Low Stress. Arch Dermatol Res, 269:127-135 1980

30) Barel AO, Courage W, and Clary P. Suction method for measurement of skin mechanical properties: The Cutometer. Handbook of Non-Invasive Methods and the skin. Boca Raton, CRC Press, 1995

Chapter 5: Thesis Summary

and Future Work

5.1 Thesis Summary

Tissue expansion is a standard treatment of skin defects, severe scarring and deformed skin. To date, surgeons have the choice between manually inflated silicone balloon expander and the self-inflating hydrogel tissue expander. The use of self-inflating tissue expander is however a more promising device as the reconstructive procedure is less complicated and also more economical. Potentially the expander can be used in many other applications. This includes the expansion of different skin sites and the expansion of other soft tissues.

The aim of this study is to design a testing apparatus which can replicate the use of animal models. In order to achieve this goal, the mechanical behaviour of skin and the swelling mechanics of the poly(vinylpyrrolidone)/poly(methyl-methacrylate) (VP/MMA) hydrogel expanders were investigated. With considerations to this information, the apparatus was designed to simulate *in vivo* conditions and for observation of the expanding skin area through the use of synthetic polyurethane material. The result from this apparatus has proved to be comparable to a related study using animal subject [1].

One key area of interest is the stress-strain relationship of skin under tension as the stretching of the skin is the known stimulus to tissue growth. The available methods in testing the mechanical properties of skin are by tensile, torsional, suction, and indentation tests [2-6].By compilation of these different methods, it can be said that it is still a challenge to find quantitative understanding on the mechanical properties of the tissue. The Young's modulus of skin is suggested to be around 0.10 – 1.32 MPa. Due to identified errors in the tensile and indentation testing methods, this range of modulus is taken from the more accurately measured torsional and suction method [3,6].

Through investigation of water transport, the swelling of hydrogels can be simplified as the balance between two main driving forces; the relaxation of the gel network and the osmotic diffusion of solvent due to gel hydrophilicity. This is supported by the diffusion exponent which showed that the overall diffusion is 'anomalous'. In this study, different compositions of VP/MMA were used ranging from 90-99 wt% PVP. The main observed properties of the gels with more PVP content was the increase in swelling ratio and the decrease in gel stiffness, i.e., the more hydrophilic polymers showed greater water absorption capacity in the exchange of reduced cross-linking density.

The uniaxial swelling force was measured in gels of different compositions and volume. The general force versus time plot of these gels displayed a sharp force increase which comes from rapid expansion during the initial stages. While previous experiments suggested that swelling stress is totally diffusion controlled and hence always higher in gels with larger swelling capability [7-10], the swelling force from VP/MMA gels in this study does not increase with higher swelling ratio but on the contrary; decreases in more hydrophilic gel systems. This is due to the large decrease in the modulus due to water uptake. Although the increase in size of the gels will support higher force generation, the softening of gel will decrease the swelling force per unit area. The swelling force generation is summarized as the mixture of two mechanisms: the mass uptake through diffusion, and the reduced chain-chain stiffness.

Anisotropic swelling behaviour can be introduced into VP/MMA gels by heat treatment and compression. The swelling stress of these modified gels was measured and showed a larger force generation due to a higher amount swelling and straining in the vertical axis. The anisotropic gels also showed less volumetric expansion compared to isotropic gels. This is

because of some plastic deformation when the gels were cooled from a deformed state. This marked the limit to the modification as gels become permanently deformed rather than maintaining shape memory characteristics.

The buckling of VP/MMA gels was also investigated as another limitation to the design of tissue expanders as slipping of gel under the skin is unwanted. The experimental buckling of the gel cylinders showed that the critical stress calculated from Euler's approximation is highly overestimated mainly due to the non-ideal shape and low friction surfaces of these gels. A safe shape for VP/MMA tissue expander is a short cylinder with slenderness ratio below 2.5.

A skin-mimicking testing method was designed to measure the amount of skin expansion, analyze surface topography, and understand the strain distribution of the skin. These measurements are important when it comes to designing a new tissue expander where the *in vivo* swelling behaviour is unknown. An apparatus was made where Shore 10A polyurethane (PU) was used as the skin mimicking material. The hydrogel cylinders were inserted under this PU sheet with limited flow of solvent as an attempt to match *in vivo* conditions.

The use of the skin-mimicking apparatus showed that gel swelling ratio is decreased under the synthetic skin compared to a gel freely swollen in a beaker with excess solvent. This is due to the reduced solvent contact and the opposition of swelling due to skin tension. Analysis of the strain contour showed that the stretched area of skin becomes more local to the gel during expansion. This is due to contraction between the PU sheet and hydrogel resulting from reduced solvent volume. Because of this localised straining of the skin, surgeons may be able to insert multiple gels adjacent to one another to increase the effect of a single procedure.

At full expansion, the size and shape of the anisotropic and isotropic gel samples are almost identical. The advantage of the anisotropic gels was clearly shown when compared with the isotropic gels under the testing apparatus. Once inserted, the anisotropic gels did not give rise to high skin tension due to its initially disc-like shape. As the skin is stretched less from the start, the final change in area after full expansion is greater (~20%) than from using isotropic gels. The lower induced tension from insertion of the anisotropic gels is also favourable for the healing of surgical wounds.

5.2 Future Work

The experiments done in this research was focused on the VP/MMA with compositions of interest (90-99 wt% VP). While this is the range of which the gels have enough structural stability to function as a tissue expander, the general scope of some experiments might be more comprehensive if more variety of gel samples were tested. This might be the use of gels at lower wt% VP or other similar hydrogel systems such as the commonly used poly(2-hydroxyethyl methacrylate) (pHEMA). The effect of diffusion/ gel relaxation to force generation of different gel systems would provide a good comparison to the results of this research.

The skin mimicking apparatus designed in this research was made such that the synthetic skin sheet and the type of solvent can be changed. The thickness and stiffness of polyurethane sheet was fixed for the experiments using the designed apparatus while it is possible to change the thickness or the stiffness of the sheet material to see the effect of this variation. The specification of polyurethane sheet can be changed to replicate characteristics of the tissue

that the inserted expander is for. This is for the newer generations of self-inflating devices where swelling behaviour is unknown.

As discussed in Chapter 2, understanding the correlation between mechanical behaviour and cell proliferation of the human skin is crucial for the design and control considerations of the tissue expander. As this is the basis of tissue expansion, future work should be focused on how to quantitatively measure the amount of cellular growth with regard to a unit amount of increased tension. This might proved to be a challenging task as shown in the many attempts to characterise the mechanical behaviour of the skin [2-6].

The research provided in this thesis has posed the beginning of how we can test tissue expanders *in vitro* under *in vivo* conditions. With more sophisticated methods in replicating the human body such that it is close enough to simulate clinical trials, the use of animal test subjects might not be necessary or even be surpassed by well-designed tests. Numerous possibilities are still waiting as the idea of self-inflating device, together with the understanding of tissue engineering, has become an alternative way in promoting newly formed tissue. The ability to create extra skin may be adopted into the growing of a whole organ without the extraction of stem cells. This is an exciting prospect for the future and a big milestone in regenerative medicine as we are living in the age driven by biotechnology.

5.3 Chapter 5 Reference

1) Radzi Z. Development of Self-Inflating Anisotropic Tissue Expanders for Clinical Applications. PhD Thesis, University of Oxford, (to be submitted 2013)

2) Manschot JFM and Brakkee AJM. The Measurement and Modelling of the Mechanical Properties of Human Skin In Vivo – II The Model. J. Biomechanics. 19(7):517-521, 1986

3) Diridollou S, Patat F, and Gens F. In vivo model of the mechanical properties of the human skin under suction. Skin Research and Technology. 6; 214-221, 2000

4) Escoffier C, Pharm M, De Rigal J. Age-Related Mechanical Properties of Human Skin: An In Vivo Study. Investigative Dermatology, 1989

5) Bader DL and Bowker P. Mechanical characteristics of skin and underlying tissues in vivo. Biomaterials. 4:1-8, 1983

6) Agache PG, Monneur C, Leveque JL, and De Rigal J. Mechanical Properties and Young's Modulus of Human Skin in Vivo. Arch Dermatol Res. 269:221-231, 1980

7) Khare AR, Peppas NA, Massimo G and Colombo P. Measurement of the swelling force in ionic polymeric networks. I. Effect of pH and ionic content. J. of Controlled Release. 22:239-244, 1992

8) Bell CL and Peppas NA. Measurement of the swelling force in ionic polymeric networks.III. Swelling force of interpolymer complexes. J. of Controlled Release. 37:277-280, 1995

9) Dubrovskii SA, Lagutina MA, and Kazanskii KS. Method of measuring swelling pressure of superabsorbent gels. J. Chem. Phys, 70;1214-1218, 1979

10) Peppas NA and Colombo P, Development of disintegration forces during water penetration in porous pharmaceutical systems. J. Control Release, 10;245-250, 1989

Appendix A

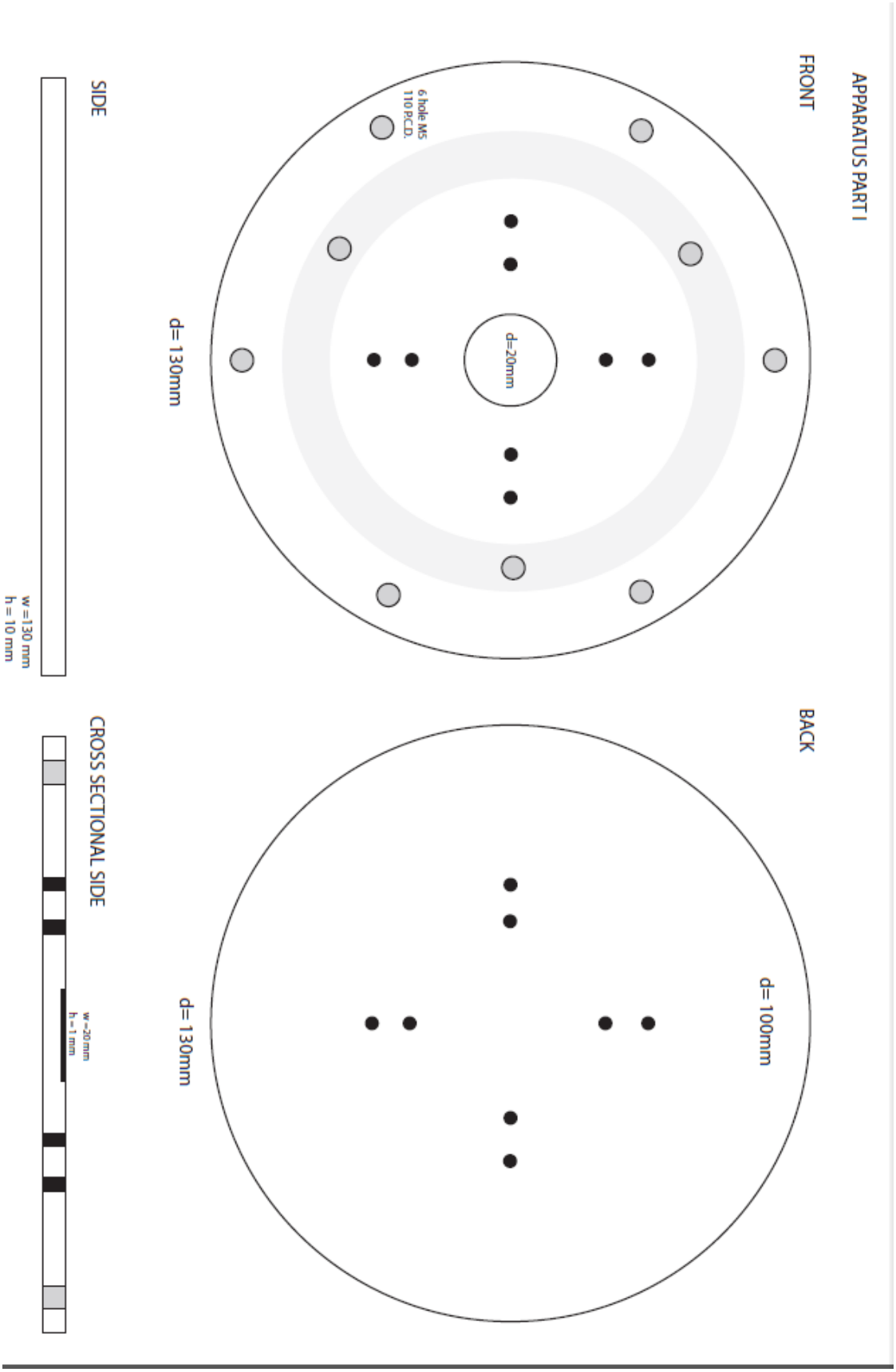
APPARATUS PART I
FRONT
6 hole M5
110 PCD.
d=20mm
d= 130mm
BACK
d= 100mm
d= 130mm
SIDE
w = 130 mm
h = 10 mm
CROSS SECTIONAL SIDE
w =20 mm
h = 1 mm

APPARATUS PART II

FRONT

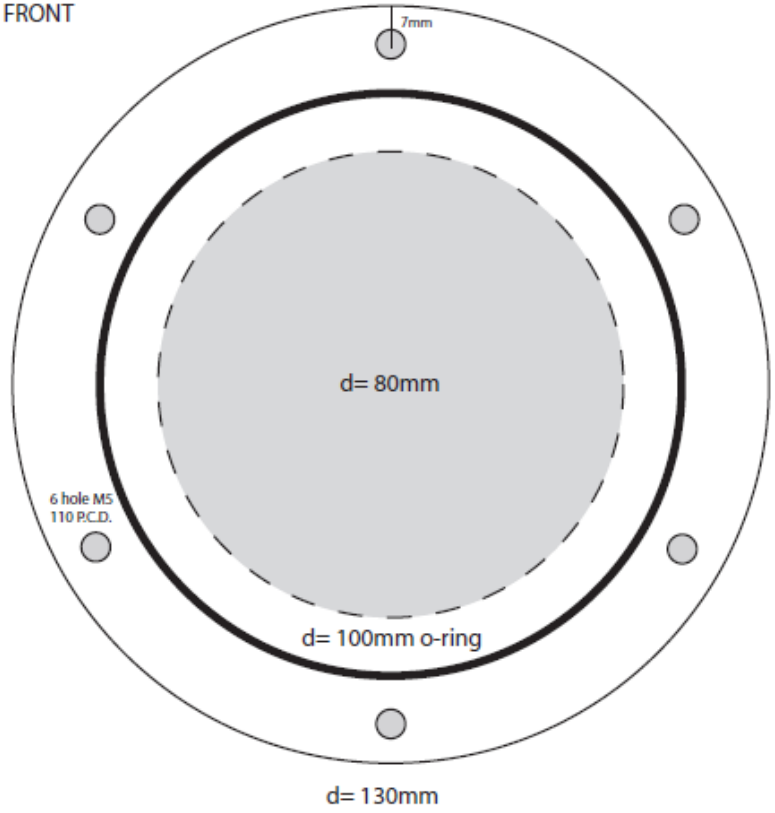

BACK

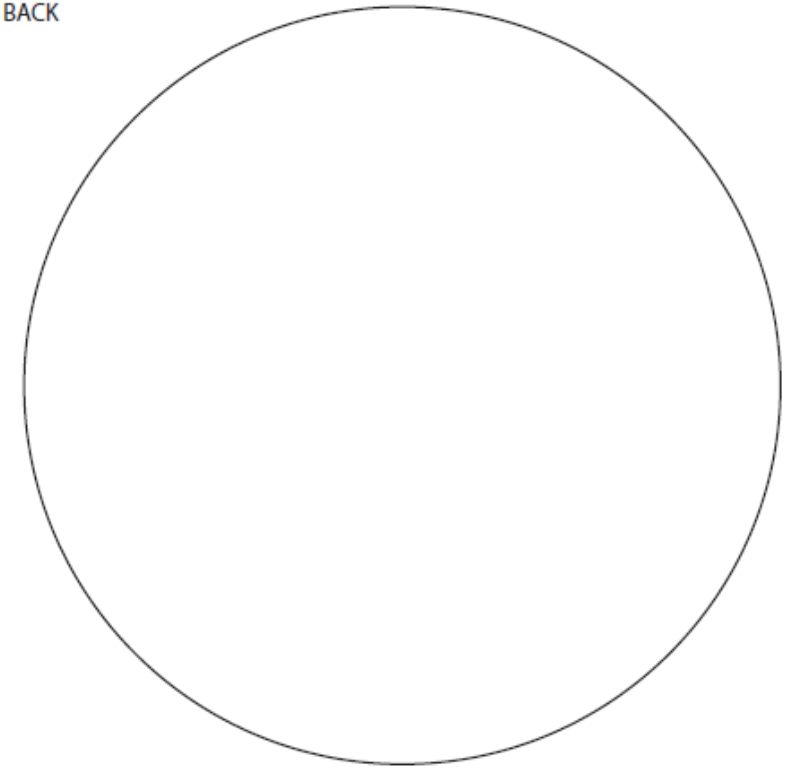

SIDE

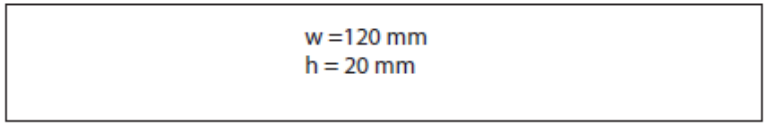

CROSS SECTIONAL SIDE

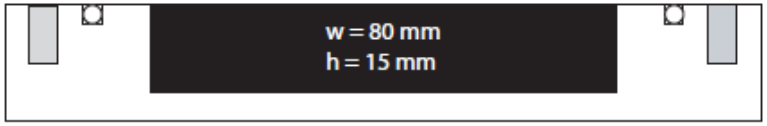

APPARATUS CROSS SECTION

RING CLAMP